UNIVERSIDAD REGIONAL AMAZÓNICA IKIAM

FACULTAD DE CIENCIAS DE LA TIERRA Y AGUA

CARRERA DE GEOCIENCIAS

ESTUDIO PALEOSISMOLÓGICO DE LA FALLA POROTOYACU EN EL BARRIO LAS VERÓNICAS, ZONA SUBANDINA DEL ECUADOR

Proyecto de investigación previo a la obtención de Título de:

Ingeniero en Geociencias

AUTORES: Henry Patricio Conteron Moreta

Samira Mishell Lluno Zambrano

Tena - Ecuador

2025

UNIVERSIDAD REGIONAL AMAZÓNICA IKIAM

FACULTAD DE CIENCIAS DE LA TIERRA Y AGUA

CARRERA DE GEOCIENCIAS

ESTUDIO PALEOSISMOLÓGICO DE LA FALLA POROTOYACU EN EL BARRIO LAS VERÓNICAS, ZONA SUBANDINA DEL ECUADOR

Proyecto de investigación previo a la obtención de Título de:

Ingeniero en Geociencias

AUTORES: Henry Patricio Conteron Moreta

Samira Mishell Lluno Zambrano

TUTOR: Corina Campos Serrano

COTUTOR: Oswaldo José Guzman Gutierrez

Tena - Ecuador

2025

Unidad de Titulación

Carrera de Geociencias

Autorización de publicación en el repositorio institucional

Tena, 07 de Marzo de 2025

Yo, Samira Mishell Lluno Zambrano, con documento de identidad 1725501348 en calidad de autor/a y titular de los derechos morales y patrimoniales del trabajo de titulación "Estudio Paleosismológico de la Falla Porotoyacu en el barrio Las Verónicas, Subandino del Ecuador", de conformidad con el Art. 114 del CÓDIGO ORGÁNICO DE LA ECONOMÍA SOCIAL DE LOS CONOCIMIENTOS, CREATIVIDAD E INNOVACIÓN, reconozco a favor de la Universidad Regional Amazónica Ikiam una licencia gratuita, intransferible y no exclusiva para el uso no comercial de la obra, con fines estrictamente académicos.

Así mismo autorizo a la Universidad Regional Amazónica Ikiam para que realice la publicación de este trabajo de titulación en el Repositorio Institucional de conformidad a lo dispuesto en el Art. 144 de la Ley Orgánica de Educación Superior.

Atentamente,

Samira Mishell Lluno Zambrano
CI: 1725501348

Unidad de Titulación

Carrera de Geociencias

Autorización de publicación en el repositorio institucional

Tena, 07 de Marzo de 2025

Yo, Henry Patricio Conteron Moreta, con documento de identidad 1550177578 en calidad de autor/a y titular de los derechos morales y patrimoniales del trabajo de titulación "Estudio Paleosismológico de la Falla Porotoyacu en el barrio Las Verónicas, Subandino del Ecuador", de conformidad con el Art. 114 del CÓDIGO ORGÁNICO DE LA ECONOMÍA SOCIAL DE LOS CONOCIMIENTOS, CREATIVIDAD E INNOVACIÓN, reconozco a favor de la Universidad Regional Amazónica Ikiam una licencia gratuita, intransferible y no exclusiva para el uso no comercial de la obra, con fines estrictamente académicos.

Así mismo autorizo a la Universidad Regional Amazónica Ikiam para que realice la publicación de este trabajo de titulación en el Repositorio Institucional de conformidad a lo dispuesto en el Art. 144 de la Ley Orgánica de Educación Superior.

Atentamente,

Henry Patricio Conteron Moreta

CI: 1550177578

Unidad de Titulación

Carrera de Geociencias

Declaración de derecho de autor, autenticidad y responsabilidad

Tena, 07 de Marzo de 2025

De mi consideración:

Yo, Samira Mishell Lluno Zambrano_con documento de identidad 1725501348, declaró que los resultados obtenidos en la investigación que presento en este documento final, previo a la obtención del título de Ingeniera en Geociencias son absolutamente inéditos, originales, auténticos y personales.

En virtud de lo cual, el contenido, criterios, opiniones, resultados, análisis, interpretaciones, conclusiones, recomendaciones y todos los demás aspectos vertidos en el presente documento, son de mi autoría y de mi absoluta responsabilidad.

Por la favorable atención a la presente, suscribo de usted,



Atentamente,

Samira Mishell Lluno Zambrano

CI: 1725501348

Unidad de Titulación

Carrera de Geociencias

Declaración de derecho de autor, autenticidad y responsabilidad

Tena, 07 de Marzo de 2025

De mi consideración:

Yo, Henry Patricio Conteron Moreta con documento de identidad 1550177578, declaró que los resultados obtenidos en la investigación que presento en este documento final, previo a la obtención del título de Ingeniero en Geociencias son absolutamente inéditos, originales, auténticos y personales.

En virtud de lo cual, el contenido, criterios, opiniones, resultados, análisis, interpretaciones, conclusiones, recomendaciones y todos los demás aspectos vertidos en el presente documento, son de mi autoría y de mi absoluta responsabilidad.

Por la favorable atención a la presente, suscribo de usted,

Atentamente,

Henry Patricio Conteron Moreta

CI: 1550177578

Unidad de Titulación

Carrera de Geociencias

Certificado de dirección de trabajo de titulación

Tena, 07 de Marzo de 2025

Certifico que el trabajo de titulación: "Estudio Paleosismológico de la Falla Porotoyacu en el barrio Las Verónicas, Subandino del Ecuador aprobado bajo el mecanismo de titulación de: artículo, fue realizado por Henry Patricio Conteron Moreta y Samira Mishell Lluno Zambrano, bajo nuestra dirección. El mismo ha sido revisado en su totalidad y analizado por la herramienta de verificación de similitud de contenido; por lo tanto, cumple con los requisitos teóricos, científicos, técnicos, metodológicos y legales establecidos por la Universidad Regional Amazónica Ikiam, para su entrega y defensa.

Ph. D. Corina Campos Serrano
C.I: 1759458670
Tutora

Ph. D. Oswaldo Guzmán Gutiérrez
C.I: 1759458613
Cotutor

AGRADECIMIENTOS

Nunca imaginas lo que encontrarás en este capítulo de tu vida, pero incluso en la incertidumbre puedes lograr grandes cosas. Descubres que los caminos no siempre se recorren solos, sino que te encuentras con personas que te impulsan y te acompañan. Agradezco al Dr. Oswaldo Guzmán y a la Dra. Corina Campos, por permitirme tenerlos de mentores y amigos, que me han apoyado y ayudado a forjar mis conocimientos. A mis abuelos, que con sus enseñanzas me mostraron el valor de la vida, del trabajo y de la naturaleza. A quienes ya no están físicamente, pero los llevo mis recuerdos y en cada logro. A quienes se encuentran lejos, pero sus acciones determinaron mi carácter y perspectiva. A mis padres, quienes me han sacado adelante brindándome su confianza, comprensión y paciencia. A mis hermanos que siempre me han a acompañado. A los Ing. Anderson Guamán y Carolina Cornejo, grandes académicos, que más que amigos, los considero mis hermanos. A cada compañero de clase, a los que compartieron conmigo largas jornadas de estudio, de campo y de risas interminables, que hoy son parte de una historia que quedara atrás. A mi compañera de vida, que me devolvió la confianza en mí mismo, recordándome que un gran poder conlleva una gran responsabilidad. A la vida misma, por hacerme reír hasta llorar y llorar hasta reír. Y hacerme entender de varias formas que se debe de seguir a pesar de las cosas que dejes atrás. Por último, a mí mismo. Porque, a pesar de todo, siempre voy por más. En fin, gracias a todos. Me han dado mucho y nunca han dudado de mí. Los quiero.

Henry Patricio Conteron Moreta

AGRADECIMIENTOS

Agradezco a Dios por mantenerme aquí a pesar de todo, a mi familia por su apoyo incondicional, a mi amada hermana Gaby y mi prima Tiguer que siempre han estado a mi lado apoyándome y consolándome en mis peores momentos. Mis queridos tutores Cortinas Campos y Oswaldo Guzman, por ser otras figuras parentales para mí, por ver mi potencial, por su paciencia y apoyo en toda la carrera. A cada profesor que conforma nuestra carrera, todos son increíbles y hacen una labor increíble. Agradezco a mi gatito Amaru por estar conmigo en los momentos difíciles de desveladas. A Henry Conteron, por todo el apoyo, amor y consideración hacia mi persona en los momentos divertidos, tristes y estresantes de toda la Universidad. A todas las personas que conocí inclusive hasta el último semestre, mis compañeros y amigos Karlita, Jordy, Cristian, Jhonny, Anthony, Pancho y Carolina por su cariño, apoyo, conocimiento y ayuda. Anderson y Daya (Nuestros hermanos mayores y técnicos de laboratorio) y todas las demás personas que ellos me permitieron conocer, con los compañeros que empezamos y compartimos grandes momentos, por las divertidas salidas, las comidas, reuniones, por todo. Gracias a todos porque incluso cuando me equivoque, cuando era doloroso seguir…… todos ustedes me motivaron. Gracias por permitirme conocerlos y estar a su lado creciendo como persona y profesional.

Samira Mishell Lluno Zambrano

TABLA DE CONTENIDO

Declaración de derecho de autor, autenticidad y responsabilidad ii

Autorización de publicación en el repositorio institucional iv

Certificado de dirección de trabajo de titulación vi

AGRADECIMIENTOS vii

TABLA DE CONTENIDO ix

ÍNDICE DE TABLAS xii

ÍNDICE DE FIGURAS xiii

ÍNDICE DE ANEXOS xiv

RESUMEN…… xv

ABSTRACT….. xvi

CAPÍTULO 1. INTRODUCCIÓN GENERAL 1

1.0 INTRODUCCIÓN 1

1.1 RESUMEN DE CAPÍTULOS Y RESULTADOS 1

CAPÍTULO 2 CARTOGRAFÍA MORFOTECTÓNICA DE LA FALLA POROTOYACU EN LA ZONA SUBANDINA DEL ECUADOR 3

RESUMEN…… 4

2.0 INTRODUCCIÓN 5

2.1 METODOLOGÍA 9

2.1.1 Fotointerpretación de indicadores morfotectónicos 9

2.1.2 Identificación y validación en campo de indicadores morfotectónicos … 10

2.2 RESULTADOS 14

2.2.1 Escarpes 15

2.2.2 Contraescarpes 22

2.2.3 Drenaje Semi Rectilíneo 23

2.2.4 Drenaje Ortogonal 24

2.2.5 Terrazas Colgadas … 26

2.3 Discusion 27

2.3.1 Análisis de indicadores morfotectónicos 27

2.3.2 Relocalización de la Falla Porotoyacu basada en evidencias morfotectónicas 29

2.4 CONCLUSIONES 30

Agradecimientos 31

REFERENCIAS

CAPÍTULO 3. FAULT ACTIVE MAPPING BASED ON PHOTOGRAMMETRY AND SEISMIC REFRACTION TOMOGRAPHY: A CASE STUDY OF THE SOUTHERN SECTION OF THE POROTOYACU FAULT, ECUADORIAN AMAZON. 36

ABSTRACT 37

3.0 INTRODUCTION 38

3.0.1. Geodynamics and Seismicity of the Study Área 41

3.1 METHODOLOGY 42

3.1.1 Photogrammetry 43

3.1.2 Seismic Tomography of Refraction 45

3.1.3. Regularization strategy 47

3.2 RESULTS 51

3.2.1. Local Cartography 51

3.2.2. Refraction Seismic Tomography 53

3.2.2.1 Regularization 53

3.3 DISCUSSION 58

3.3.1. Porotoyacu Fault extensión 58

3.3.2. Subsurface Fault Geometry 59

3.3.3. Fault Classification 60

3.4 CONCLUSIONS 60

Acknowledgments 61

REFERENCES

CAPÍTULO 4. DETERMINATION OF THE ACTIVE TECTONIC ACTIVITY OF THE POROTOYACU FAULT, SUB-ANDINE OF ECUADOR APPLY MORPHOTECTONIC, MORPHOLOGIC, AND PALEOSEISMOLOGY ANALYSIS 66

ABSTRACT 67

4.0 INTRODUCTION 68

4.0.1 Tectonic and seismic setting of study área 71

4.0.2 ***Geological context*** 72
4.1 METHODOLOGY 73
4.1.1 ***Selection of Study Área*** 73
4.2 RESULTS 75
4.2.1 ***Morphotectonic in the south of the Porotoyacu Fault*** 75
4.2.2 ***Stratigraphic and paleoseismic analysis*** 78
4.2.3 ***Characteristics and paleo magnitude obtained from the outcrop*** 81
4.2.4 ***Soft sediment deformation (SSDS) in the outcrop*** 84
4.3 DISCUSSION 86
4.3.1 ***Morphotectonic indicators and fault length*** 86
4.3.2 ***Superficial deformation of the outcrop-Pedogenesis process*** 86
4.3.3 ***Dykes, mechanisms, and tectonic feature*** 87
4.3.3.1 Trigger mechanisms of seismites 88
4.3.3.2 Triggering Mechanisms of dykes 88
4.4 CONCLUSIONS 90
Acknowledgments 91
REFERENCES .....
ANEXOS .....

ÍNDICE DE TABLAS

Tabla 1-2: Parámetros para caracterizar indicadores morfotectónicos en campo 13

Tabla 2-2: Características de los escarpes identificados a lo largo de la Falla Porotoyacu 21

Tabla 3-2: Características de los contraescarpes identificadas al norte de la traza de la Falla Porotoyacu 23

Tabla 4-2: Características de los drenajes semi rectilíneos y ortogonales identificados en el sector sur de la Falla Porotoyacu. 26

Tabla 5-2: Características de la terraza colgada en el Sitio 6, ubicada en el sector norte de la Falla Porotoyacu 27

Table 1-3: Characteristics of the morphotectonic scarp. 52

Table 1-4: Summary of ruptures and vertical displacements caused by paleo-seismic events in the affected units of the outcrop 83

Table 2-4: The summary of magnitudes calculated for each rupture used the empirical equations 84

ÍNDICE DE FIGURAS

Figura 1-2: Ubicación del área de estudio y la Falla Porotoyacu 8

Figura 2-2: Identificación de indicadores morfotectónicos asociados a la Falla Porotoyacu 11

Figura 3-2: Traza propuesta de la Falla Porotoyacu basada en el análisis de indicadores morfotectónicos 14

Figura 4-2: Escarpes de falla en la zona sur 16

Figura 5-2: Escarpes de falla en la zona sur transicionando al norte 18

Figura 6-2. Escarpes de falla en la zona norte 20

Figura 7-2. Contraescarpes de falla en la zona norte 22

Figura 8-2. Mapa de los drenajes semi rectilíneos y ortogonales..... 25

Figure 1-3. Location of the study area 40

Figure 2-3. Proposed fault segmentation and associated topographic profiles.... 44

Figure 3-3: Examples for the seismic line of the experiment 47

Figure 4-3: Travel time curves for seismic tomography inversion 50

Figure 5-3: Regularization 55

Figure 6-3: A priori model 56

Figure 7-3: Seismostratigraphic and structural interpretation of the line 58

Figure 1-4: Ubication of the study area 69

Figure 2-4: Morphotectonic Indicators in the South of Porotoyacu Fault 76

Figure 3-4: Sedimentary Column of the outcrop 79

Figure 4-4: The outcrop profile 82

Figure 5-4: Dykes observed at the top of the outcrop 85

ÍNDICE DE ANEXOS

ANEXO A: Resúmenes extendidos presentados en el Congreso Internacional REDU, desarrollado en Universidad Regional Amazónica IKIAM

ANEXO B: Resúmenes extendidos presentados en el Congreso Internacional PATAdays desarrollado en Chile

RESUMEN

Este trabajo investiga la actividad tectónica de la Falla Porotoyacu en la Zona Subandina del Ecuador, combinando técnicas a escala regional y local. Esta estructura, previamente estimada con 15 km de longitud, se extiende a través de Tena y Archidona, en la provincia de Napo. A escala regional, se emplearon imágenes satelitales junto con verificaciones de campo para identificar indicadores morfotectónicos, lo que permitió relocalizar su traza y extenderla a 19 km. A nivel local, se utilizó fotogrametría aérea con dron para cartografiar un segmento detallado de 0.36 km², definiendo una traza con un desplazamiento hacia el este y una prolongación de 684.9 m hacia el sur. Asimismo, se utilizó tomografía sísmica en esta zona para visualizar la geometría de la falla en el subsuelo, obteniendo una configuración de retroempuje. Paralelamente, se realizó un estudio paleosismológico en un afloramiento revelando dos rupturas principales, denominadas R1 y R2. R1 registró dos eventos sísmicos, con magnitudes de 6.68 ≤ Mw ≤ 6.70 y 6.88 ≤ Ms ≤ 6.91, mientras que R2 mostró un solo evento con 6.13 ≤ Mw ≤ 6.51 y Ms = 6.24. Entre las sismitas identificadas se encuentran huellas de carga, estructuras de flama, pseudonódulos y diques, todas originadas por sismos de magnitud Mw > 5. Finalmente, se determinó que los eventos afectaron unidades Cretácicas y deformaron depósitos superficiales recientes, confirmando que la Falla Porotoyacu es tectónicamente activa en esta sección estudiada.

Palabras claves: Falla Porotoyacu, Fotogrametría, Indicadores morfotectónicos, Zona Subandina, Tomografía sísmica, Paleosismológia.

ABSTRACT

This work investigates the tectonic activity of the Porotoyacu Fault in the Sub-Andean Zone of Ecuador, using techniques at both regional and local scales. This structure, previously estimated to be 15 km long, extends through Tena and Archidona, in the Napo province. At the regional scale, satellite images and field verifications were used to identify morphotectonic indicators, allowing the fault's trace to be relocated and extended to 19 km. At the local scale, drone-based aerial photogrammetry was used to map a detailed segment of 0.36 km², defining a trace that shifts eastward and extends 684.9 m to the south. Additionally, seismic tomography was applied in this área to visualize the fault's subsurface geometry, revealing a backthrust configuration. In parallel, a paleoseismological study in an outcrop identified two main ruptures, named R1 and R2. R1 recorded two seismic events with magnitudes of 6.68 ≤ Mw ≤ 6.70 and 6.88 ≤ Ms ≤ 6.91, while R2 showed one event with 6.13 ≤ Mw ≤ 6.51 and Ms = 6.24. Among the identified seismites were load casts, flame structures, pseudonodules, and dikes, all formed by earthquakes with Mw > 5. Finally, it was determined that these events affected Cretaceous units and deformed recent surface deposits, confirming that the Porotoyacu Fault is tectonically active in this studied section.

Keywords: Porotoyacu Fault, Photogrammetry, Morphotectonic Indicators, Sub-Andean zone, Seismic tomography, Paleoseismology.

CAPÍTULO 1. INTRODUCCIÓN GENERAL

1.0 INTRODUCCIÓN

La identificación y caracterización de fallas activas son fundamentales para comprender los procesos que modelan la corteza terrestre y para evaluar el riesgo sísmico asociado. Estas fallas, que representan zonas de debilidad en la corteza, acumulan y liberan energía durante eventos sísmicos, generando deformaciones superficiales y subterráneas (McCalpin & Nelson, 2009; Papanikolaou *et al.,* 2015). La integración de herramientas modernas como el análisis de imágenes satelitales, la fotogrametría aérea, la tomografía sísmica de reflexión y los estudios paleosismológicos ha permitido avanzar significativamente en la caracterización de estas estructuras en las últimas décadas (Wu & Hu, 2019; Vasuki *et al.,* 2014; Bemis *et al.,* 2014).

En las zonas tectónicamente activas, como la región Subandina de Ecuador, la interacción entre el levantamiento y la erosión preserva y borra la evidencia de la actividad sísmica pasada, por lo que es esencial emplear enfoques multidisciplinarios para estudiar estos paisajes (Keller & Pinter, 2002; Audemard, 1999; Scheidegger, 2004). La región Subandina del Ecuador situada en la Amazonía, es una de las áreas tectónicamente más activas del país debido a la subducción de la placa de Nazca bajo la placa Sudamericana a una velocidad promedio de 55 ± 1~56 mm/año a $1°N$ y 60 mm/año a 6°S (Trenkamp *et al.,* 2002; Kendrick *et al.,* 2003; Nocquet *et al.*, 2014).

El proceso de subducción ha dado lugar a varios sistemas de fallas activos, como el sistema Cutucú-Napo, que forma parte del cinturón de deformación Subandino (Alvarado *et al.,* 2016) y se le asocia eventos sísmicos significativos, como el terremoto de Macas en 1995 (Mw 7.0), el más reciente ocurrido a 13.30 Km de la ciudad de Tena en el 2009 a la 1 pm (Mw 5.4) y otro a las 18:11 pm a -0.962,-77.817, de profundidad 35.2 km ,(Mw 5.2) (Legrand *et al.,* 2005; Font *et al.,* 2013; El comercio, 200

Entre las estructuras destacadas del sistema Cutucú-Napo se encuentra la Falla Porotoyacu, una falla transcurrente-inversa localizada en la provincia de Napo, cuya extensión inicial se estimó en 15 km mediante fotointerpretación (Costa et al., 2020). Estudios recientes han propuesto una extensión hacia el sur de la Falla Porotoyacu (Cornejo *et al.,* 2024). A pesar de su relevancia, persisten interrogantes sobre su longitud exacta, geometría subsuperficial y actividad tectónica actual.

El presente trabajo tiene como objetivo abordar estas interrogantes mediante la integración de metodologías a escalas regional y local. Para ello, se analizaron imágenes satelitales y se llevó a cabo trabajo de campo con el fin de identificar indicadores morfotectónicos que permitieron relocalizar la traza. Adicionalmente, se empleó fotogrametría aérea con drones para determinar su prolongación hacia el sur, y tomografía sísmica para analizar su estructura en profundidad. Asimismo, se aplicaron análisis paleosismológicos para estudiar un corte antropogénico que revela evidencias de actividad sísmica pasada, junto con la identificación de sismitas como parte del análisis integral.

1.1 RESUMEN DE CAPÍTULOS Y RESULTADOS

Esta tesis se organiza en un capítulo introductorio (Capítulo 1), un capítulo de libro y dos artículos (listos para ser enviados a revistas especializadas), los cuales contienen los resultados principales y conclusiones. El capítulo 2, titulado "Cartografía morfotectónica de la Falla Porotoyacu en la Zona Subandina del ecuador", presenta los indicadores morfotectónicos que evidencian la traza de la Falla Porotoyacu relocalizada regionalmente. El capítulo 3, titulado "Integrated Drone-Based Photogrammetry and Seismic Tomography for Fault Characterization: A Case Study of the Southern Section of the Porotoyacu Fault, Ecuadorian Amazon", será sometido a la revista "Applied Geophysics". Este artículo aborda la identificación de la estructura superficial y subsuperficial de la falla mediante técnicas fotogramétricas y sísmicas. El capítulo 4, titulado "determination of the active tectonic activity of the Porotoyacu Fault, sub-andine of Ecuador apply morphotectonic, morphologic, and paleoseismology analysis ",

será sometido a la revista "Quaternary International". Este artículo evalúa la Falla Porotoyacu como una fuente sismogénica activa, centrándose en la identificación de paleo-sismos, paleo-magnitudes y estructuras de deformación en el afloramiento Las Verónicas. Los hallazgos de los manuscritos reflejan la relevancia de la Falla Porotoyacu como una estructura tectónica activa. A través de un enfoque multidisciplinario que combina fotogrametría, tomografía sísmica, análisis morfotectónicos y paleosismológicos, aportando datos clave para el entendimiento de los riesgos geológicos y sísmicos en la región Subandina del Ecuador.

1.2 OTROS APORTES CIENTÍFICOS

Durante el desarrollo de la presente tesis, los resultados fueron presentados en dos congresos internacionales: uno enfocado en Paleosismología, Tectónica Activa y Arqueosismología, y otro dedicado a la Biodiversidad, el Cambio Climático y la Sostenibilidad, abarcando su pasado, presente y futuro.

REFERENCIAS BIBLIOGRAFICAS

Conteron, H., Lluno, S., Guzmán, O., Araujo, S., Campos, C., Valencia, B., Guamán, A., & Villacrés, J. (2024). Cartography of the Porotoyacu Fault in a Southern Section of the Ecuadorian Amazon. PATA Chile 2024: Paleoseismology, Active Tectonics, and Archaeoseismology Conference.

Lluno, S., Conteron, H., Guzmán, O., Campos, C., & Cornejo, C. (2024). Paleoseismological study of the Porotoyacu Fault in the Amazon Ecuadorian Piedmont. PATA Chile 2024: Paleoseismology, Active Tectonics, and Archaeoseismology Conference.

Conteron, H., Lluno, S., Campos, C., Guzmán, O., & Guamán, A. (2024). Cartografía de la Falla Porotoyacu en el barrio Las Verónicas: Resultados preliminares. Congreso REDU (Red Ecuatoriana de Universidades y Escuelas Politécnicas para la Investigación y Posgrados).

Lluno, S., Conteron, H., Guzmán, O., Campos, C., & Guamán, A. (2024). Estudio paleosismológico de la Falla Porotoyacu en un afloramiento del barrio "Las Verónicas": Resultados preliminares. Congreso REDU (Red Ecuatoriana de Universidades y Escuelas Politécnicas para la Investigación y Posgrados).

Capítulo de libro sometido al libro: La Falla Porotoyacu: Implicaciones paleosismológicas y sismológicas en la Zona Subandina del Ecuador

CAPÍTULO 2 CARTOGRAFÍA MORFOTECTÓNICA DE LA FALLA POROTOYACU EN LA ZONA SUBANDINA DEL ECUADOR

Henry Conteron[1] https://orcid.org/0009-0004-8681-3594

Samira Lluno[1] https://orcid.org/0009-0002-2899-9007

[1]Universidad Regional Amazónica Ikiam, Tena, Napo, Ecuador.

RESUMEN

La Falla Porotoyacu, ubicada en la ciudad de Tena, Zona Subandina Oriental del Ecuador, ha sido objeto de estudios multidisciplinarios que buscan evaluar su actividad neotectónica. El objetivo de esta investigación es cartografiar detalladamente la traza de la Falla Porotoyacu, usando indicadores morfotectónicos identificados en imágenes satelitales y corroborados en campo. Entre los indicadores identificados se encuentran los escarpes, contraescarpe, terraza colgada, drenaje semi rectilíneos y ortogonales. Todos estos marcadores son coherentes con una traza de falla que se alinea y extiende en dirección Norte-Sur. Finalmente, los resultados obtenidos permitieron delimitar una extensión de la falla con una longitud de 19 km.

Palabras clave: Cartografía, Indicadores morfotectónicos, Falla Porotoyacu

2.0 INTRODUCCIÓN

Ecuador es una región afectada por una intensa actividad sísmica debido a la subducción de la placa oceánica de Nazca bajo la placa continental sudamericana, a un ritmo promedio de 56 mm/año en dirección Norte y 60 mm/año en dirección Sur **(Figura 1A)** (Trenkamp *et al.,* 2002; Kendrick *et al.,* 2003; Nocquet *et al.*, 2014). Este proceso atraviesa el país en dirección NNE-SSO a través de la Cordillera de los Andes (Alvarado, 2012; Tamay *et al.*, 2018). Además, el movimiento hacia el este de un gran bloque en el norte de Sudamérica, conocido como la Astilla Norandina (NAS), y varios complejos de fallas locales constituyen factores geotectónicos que generan una gran actividad sísmica (Nocquet et al., 2014).

La sismicidad en la región ecuatoriana está controlada por aproximadamente 400 segmentos de fallas activas y seis sistemas de fallas mayores, conocidos como fuentes sismogénicas que incluyen el sistema Canandé-San Lorenzo, Chingual-Cosanga-Papallacta-Puna (CCPP), El Ángel-San Gabriel, Papallacta, Quito, Latacunga, Pallatanga-Pisayambo y Cutucú-Napo (Alvarado, 2012; Yepes *et al.,* 2016; Alvarado *et al.,* 2016; Costa *et al.,* 2020).

La Zona Subandina ecuatoriana, piedemonte de la Cordillera Oriental, está caracterizada por una actividad sísmica y volcánica muy intensa, así como por procesos de erosión (Bès de Berc *et al.,* 2004). Este dominio se caracteriza por la inversión tectónica de antiguos sistemas de rift mesozoicos, que han dado lugar a fallas inversas y transpresivas orientadas predominantemente en direcciones N-S y NNE-SSW (Legrand *et al.,* 2005). La sismicidad en la Zona Subandina tiene su origen principalmente en la fuente sismogénica Cutucú-Napo (Alvarado, 2012; Yepes *et al., 2*016). Este sistema está ubicado en el cinturón de deformación más oriental de Ecuador, se caracteriza por cabalgamientos y plegamientos Subandino con una orientación norte-sur (Bès de Berc, 2003; Alvarado, 2012; Yepes *et al.,* 2016; Alvarado *et al.,* 2016; Costa *et al.,* 2020). Dentro de este sistema se encuentra la Falla Porotoyacu, de aproximadamente 15 km de longitud, representa una estructura superficial activa con una cinemática transcurrente-inversa **(Figura 1B)**

(Costa *et al.,* 2020). Sin embargo, estudios paleosismológicos actuales desarrollados al sur del Tena, provincia de Napo, como el de Cornejo *et al.,* (2024); Conteron *et al.,* (2024) y Lluno *et al.,* (2024) , proponen una extensión de la traza de la falla hacia el sur.

La morfotectónica se define como el estudio de la interacción entre la morfología del paisaje y los procesos tectónicos, proporcionando un marco analítico que permite identificar y caracterizar estructuras tectónicas activas en áreas de interés (Scheidegger, 2004). Este enfoque es especialmente relevante para el reconocimiento de anomalías geomorfológicas y cambios recientes en el paisaje, que son indicativos de actividad tectónica reciente (Ollarves *et al.,* 2004). Diversos estudios han enfatizado la importancia de los indicadores morfotectónicos, como escarpes de falla, terrazas colgadas y patrones de drenaje anómalos, en la caracterización de estructuras activas (e.g. Noriega & Caballero, 2015; Alcacer & Perucca, 2017; Rothis *et al.,* 2018; Taesiri *et al.,* 2020). Estos indicadores constituyen expresiones superficiales de la actividad tectónica reciente, que pueden ser detectadas y analizadas con técnicas avanzadas como la teledetección y el procesamiento de modelos digitales de elevación (DEM) (Keller & Pinter, 2002; Papanikolaou *et al.,* 2015; Ren *et al.,* 2023).

La integración de herramientas digitales con observaciones de campo ha demostrado ser una metodología robusta para la delimitación precisa de trazas de fallas activas, así como para evaluar su impacto en la configuración y evolución del paisaje (Keller & Pinter, 2002). Además, esta caracterización morfotectónica es fundamental para la selección de sitios aptos para estudios paleosismológicos, que permiten reconstruir eventos sísmicos prehistóricos e históricos provenientes del registro estratigráfico y así, evaluar la actividad sísmica asociada a estas estructuras (McCalpin & Nelson, 2009).

Aunque los estudios se han centrado en otras zonas del Ecuador y han avanzado en la caracterización de fallas activas y su impacto sísmico (Baize *et al.,* 2015; Baize *et al*., 2020; Jomard *et al.,* 2021), las estructuras de la Zona Subandina requiere más análisis para obtener información geológica, geofísica, sísmica, etc. Para entender el comportamiento de las fallas. Los Proyectos de cartografía de falla activas realizadas

mayormente a nivel regional como (SARA-*South America Risk Assessment*) han destacado la necesidad de una cartografía más homogénea de fallas activas en Ecuador, señalando la importancia de estudios detallados para comprender la dinámica tectónica en regiones inexploradas como la Región Subandina (Costa *et al.,* 2020). Por lo que, este trabajo tiene como objetivo principal la identificación y caracterización de la traza de la Falla Porotoyacu **(Figura 1B)** mediante el análisis de indicadores morfotectónicos analizados de imágenes satelitales, perfiles topográficos que permiten la cuantificación del levantamiento del terreno para la localización de fallas y analizar drenaje, cuyas orientaciones son modificadas por la presencia de fallas (Telbisz *et al.,* 2013; Colavitto *et al.,* 2021). Finalmente, observaciones en campo, para realizar una cartografía detallada de la falla.

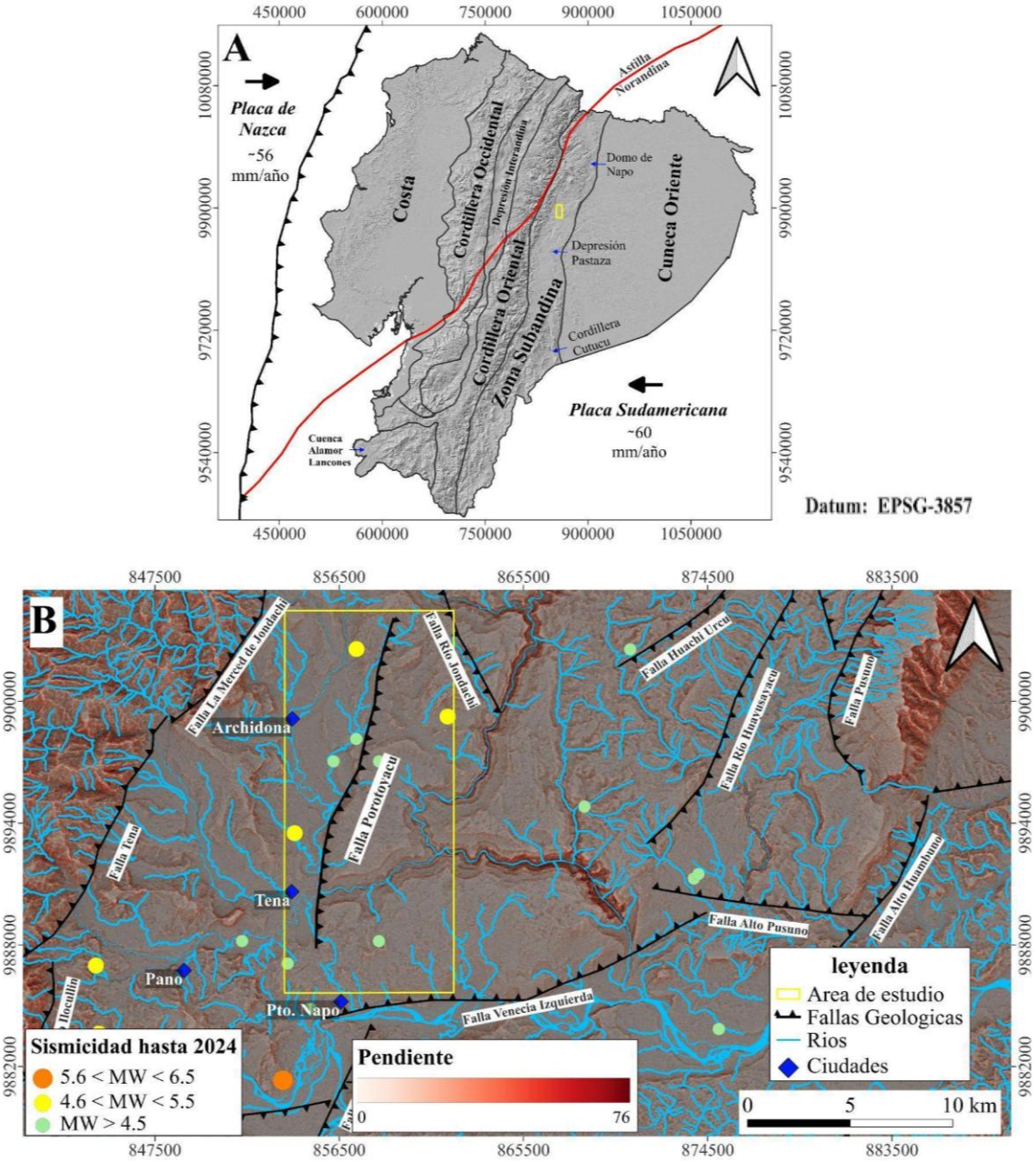

Figura 1. Ubicación del área de estudio y la Falla Porotoyacu. A) Se observa un mapa del Terreno de Ecuador, el cual está dividido en las divisiones morfotectónicas de Ecuador adaptado de Carranco et al., 2023, el cuadro de color Amarillo indica la ubicación de la zona de estudio dentro del país. B) Mapa del área de estudio, donde la pendiente del terreno se representa con una escala que va de tonos blancos para menor pendiente (0) y rojizos para mayor pendiente (76). El mapa se obtuvo a partir de un Modelo Digital de Elevación (DEM) de 30 metros de resolución, correspondiente al producto ALOS PALSAR, descargado desde el Alaska Satellite Facility (ASF). El cuadro de color amarillo delimita el área de estudio. La línea negra indica la traza de la Falla Porotoyacu y su cinemática según Costa et al. (2020). Además, se muestra la sismicidad registrada hasta el año 2024, con puntos de colores que representan la magnitud de los eventos (MW): naranja para 5.6 < MW < 6.5, amarillo para 4.6 < MW < 5.5 y verde para MW < 4.5 (IGEPN).

2.1 METODOLOGÍA

Este estudio emplea fotointerpretación de imágenes satelitales y Modelos Digitales de Elevación (DEM) para identificar indicadores morfotectónicos y definir la traza de la Falla Porotoyacu. Los rasgos identificados fueron verificados en campo para su validación y caracterización. El capítulo se organiza en dos secciones: primero, la metodología de fotointerpretación; luego, la validación en campo

2.1.1 Fotointerpretación de indicadores morfotectónicos

La identificación inicial de rasgos morfotectónicos se realizó mediante la visualización de imágenes satelitales de alta resolución disponibles en Google Earth, complementada con el análisis de un Modelo Digital de Elevación (DEM) de 30 metros de resolución, correspondiente al producto ALOS PALSAR, obtenido desde el Alaska Satellite Facility (ASF). El DEM fue procesado utilizando la técnica Red Relief Image Map (RRIM), desarrollada por Chiba y Hasi (2016). Esta metodología permite resaltar características topográficas sutiles mediante la combinación de información de pendiente (inclinación del terreno) y relieve (variación de altura), generando una representación visual que mejora la detección de rasgos morfológicos y estructuras geológicas de interés.

Para la selección de zonas de interés, se utilizó como referencia la traza de la Falla Porotoyacu, propuesta por Costa *et al*., (2020). Se priorizaron sectores con accesibilidad adecuada y características geomorfológicas que sugieren actividad tectónica reciente, como la presencia de escarpes, terrazas fluviales y patrones de drenaje anómalos. La selección de indicadores morfotectónicos se basó en criterios establecidos en la literatura científica (Audemard, 1999; Keller & Pinter, 2002; Perucca *et al.,* 2015; Onorato *et al.,* 2020), incluyendo:

- **Terrazas fluviales:** Indicadoras de levantamiento tectónico o cambios en el nivel de base.
- **Marcadores lineales:** Como escarpes de falla, alineaciones de crestas y valles.
- **Patrones de drenaje:** Cauces rectilíneos, cambios abruptos en la dirección de los ríos y drenajes semi-rectilíneos, que pueden estar controlados por estructuras tectónicas subyacentes.

2.1.2 Identificación y validación en campo de indicadores morfotectónicos

Los indicadores morfotectónicos previamente identificados mediante fotointerpretación fueron validados en campañas de campo, donde se realizó una descripción detallada de cada uno. Para ello, se registraron su ubicación precisa, altura, distancia, orientación y longitud. Esta información fue documentada a través de fotografías y recopilada en un formulario **(Tabla 1)**. Una vez verificados, los indicadores fueron cartografiados sobre el DEM procesado utilizando un Sistema de Información Geográfica (SIG). Esta herramienta permitió integrar y analizar espacialmente los datos, facilitando la representación cartográfica de los indicadores y contribuyendo a una delimitación más precisa de la traza.

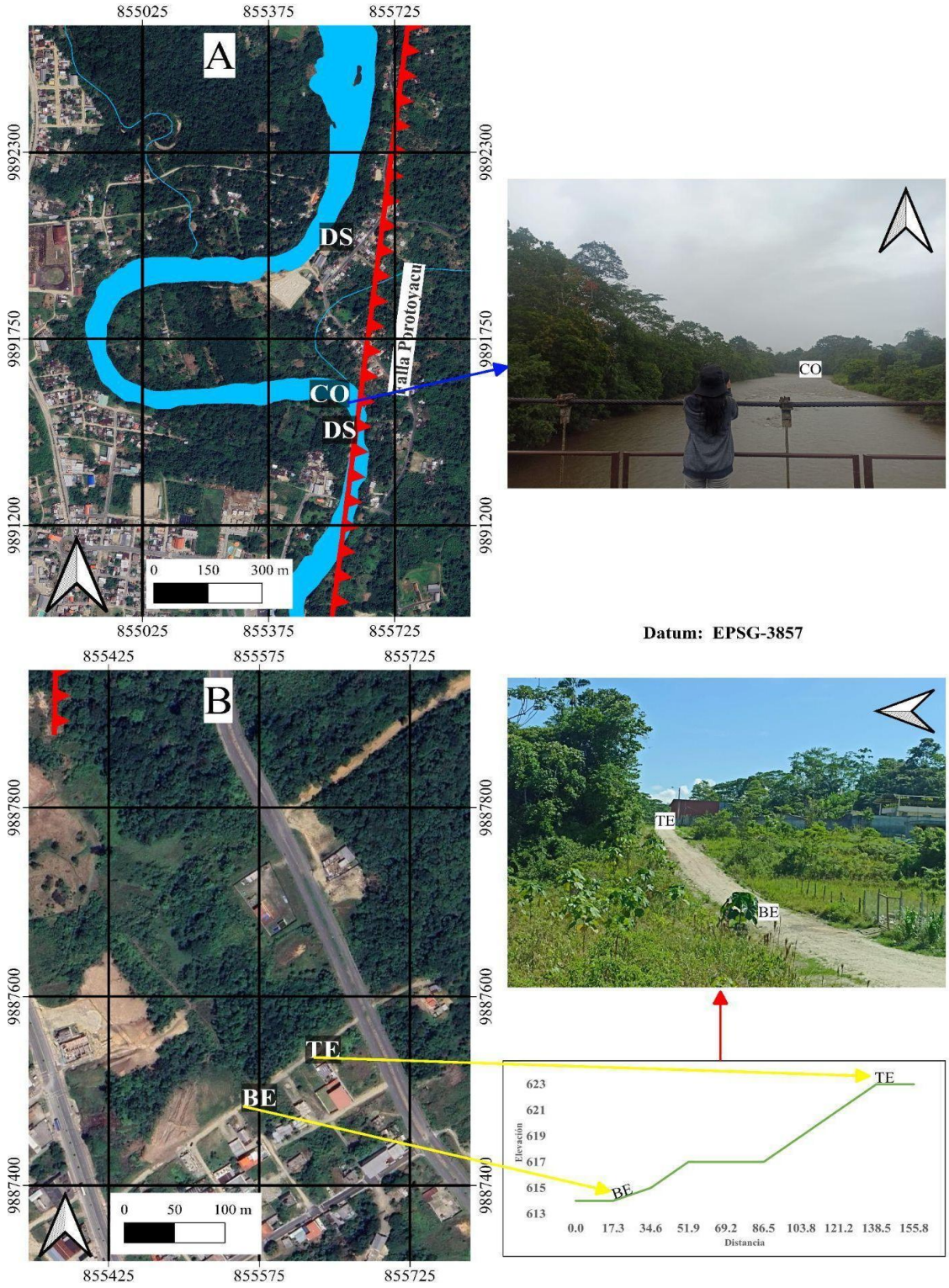

Figura 2. Identificación de indicadores morfotectónicos asociados a la Falla Porotoyacu. La figura A y B muestran imágenes satelitales de Google Earth con la ubicación y detalle de indicadores morfotectónicos relevantes asociados a la Falla Porotoyacu. Estos indicadores están acompañados de sus respectivos perfiles topográficos y fotografías tomadas en campo. (A) Patrones de drenaje. Se observa un patrón Cauce Ortogonal (CO) y dos de drenaje semi rectilíneo (DS). La flecha azul indica la ubicación donde se tomó la fotografía de campo, la cual muestra una vista del río en el sitio de análisis con vista hacia el norte. (B) Escarpe de falla. Se

identifica un escarpe de falla evidenciado por un cambio abrupto en la pendiente del terreno. La base del escarpe está representada con las letras BE, mientras que TE indica su tope. En campo, la fotografía tiene una vista hacia el este. El perfil topográfico correspondiente destaca esta variación altimétrica. La fotografía de campo ilustra la morfología del escarpe.

Tabla 1. Parámetros para caracterizar indicadores morfotectónicos en campo.

Información del Sitio	
ID del Sitio:	
Fecha de Muestreo:	
Investigador Principal:	
Tecnico:	
Coordenadas y Elevación	- **Latitud**: _____ - **Longitud**: _____ - **Altura (msnm)**: _____
Indicadores Geomorfológicos de Fallamiento Activo	
indicador	**Características**
Escarpe	- Pendiente Promedio: _____ - Máxima Pendiente: _____ - Altura de la Cima: _____ - Altura de la Base: _____ - Desnivel Total: _____ - Forma del Perfil: [ ] Convexo [ ] Cóncavo [ ] Recto
Drenaje Rectilíneo	- Geometría: [ ] Recto [ ] Curvo [ ] Sinuoso - Azimuth del Drenaje: _____
Río Ortogonal	- Azimuth del Cauce del Río: Tramo 1: _____ Tramo 2: _____ Tramo 3: _____
Lineamiento Rectilíneo	- Orientación del Lineamiento: _____ - Pendiente de la Cuesta: _____ - Pendiente de la Contracuesta: _____ - Altura de la Cuesta: _____ - Altura de la Contracuesta: _____
Terraza Colgada	- Longitud de la Zona Plana: _____ - Pendiente de la Zona Plana: _____ - Desnivel de Altura: _____
Depresión Lineal	- Profundidad Máxima: _____ - Longitud: _____
Desplazamiento de Infraestructura	- Tipo de Infraestructura: _____ - Magnitud del Desplazamiento: _____ - Dirección del Desplazamiento: _____

2.2 RESULTADOS

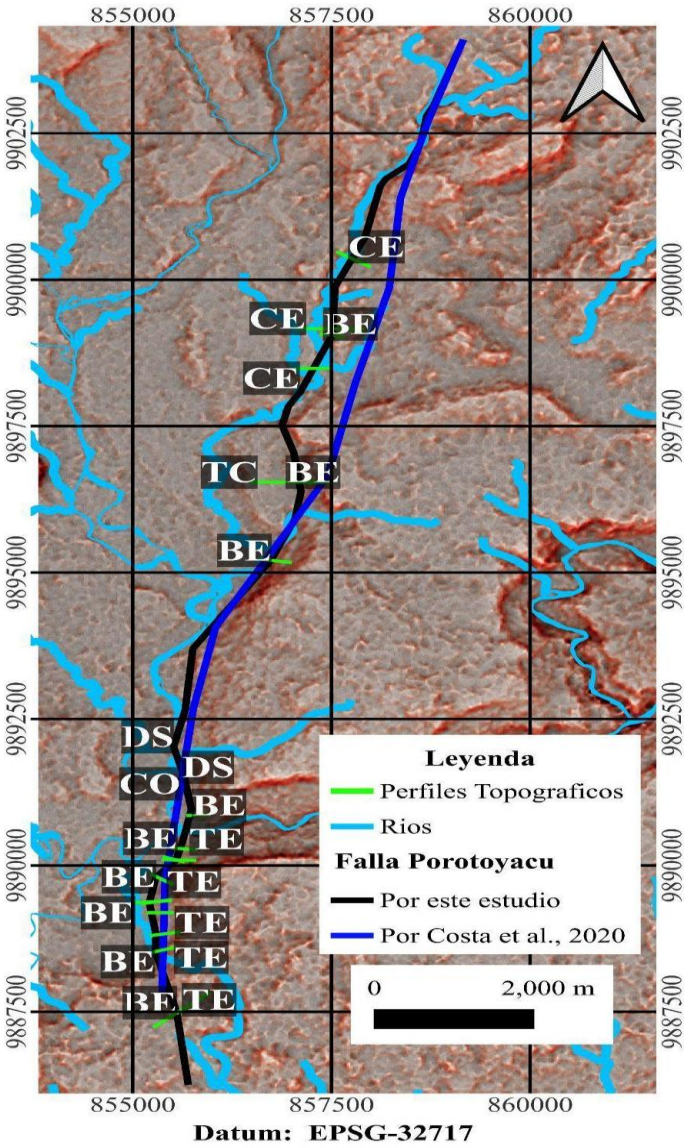

Figura 3. Traza propuesta de la Falla Porotoyacu basada en el análisis de indicadores morfotectónicos. El mapa muestra la traza de la falla representada con una línea negra, mientras que la propuesta por costa et al., 2020 está representada con una línea azul. El mapa de fondo corresponde a un modelo de elevación sombreado en tonos rojos (RRIM), donde la pendiente del terreno se representa con una escala que va de tonos blancos para menor pendiente (0) y rojizos para mayor pendiente (76). Los elementos morfotectónicos identificados se describen como **BE**: Base escarpe; **TE**: Tope escarpe; **TC**: Terraza colgada; **DS**: Drenaje semi rectilíneo; **CE**: Contraescarpe; **CO**: Cauce ortogonal.

2.2.1 Escarpes

Durante la fotointerpretación se identificaron varias zonas con cambios abruptos de pendiente, teóricamente esta morfología es producida por el desplazamiento de terreno debido a la presencia de la falla (Costa *et al.,* 2009) por lo que son considerados como escarpes. Se identificaron un total de 14 escarpes a lo largo del sitio de estudio. Estos escarpes presentan una amplia variabilidad en sus pendientes, orientaciones y formas de perfil descritos en la **Tabla 2**. Para describirlos apropiadamente, se han tomado un ID de cada sitio con datos del tope y base de cada escarpe denominados con números, por ejemplo: 2 (Tope)-3 (Base).

En el sector Sur, predominan los escarpes con orientaciones SO-NE, como los Sitios 2-3 (perfil 1), 4-5 (perfil 2) y 6-7 (perfil 3), que exhiben pendientes promedio de entre 5.1% y 16.6%. Sitios 2-3 (perfil 1) muestra una pendiente irregular, con un ascenso inicial moderado, seguido de un tramo casi horizontal y luego un aumento más pronunciado en la elevación. Sitios 4-5 (perfil 2) presenta una pendiente convexa, con una inclinación fuerte al inicio que se reduce progresivamente. Sitios 6-7 (perfil 3) exhibe una pendiente uniforme, caracterizada por un ascenso continuo con una inclinación constante. Estos escarpes poseen desniveles topográficos que varían entre 6 m y 59m, reflejando posibles variaciones en la actividad tectónica y la evolución geomorfológica del área **(Figura 4)**.

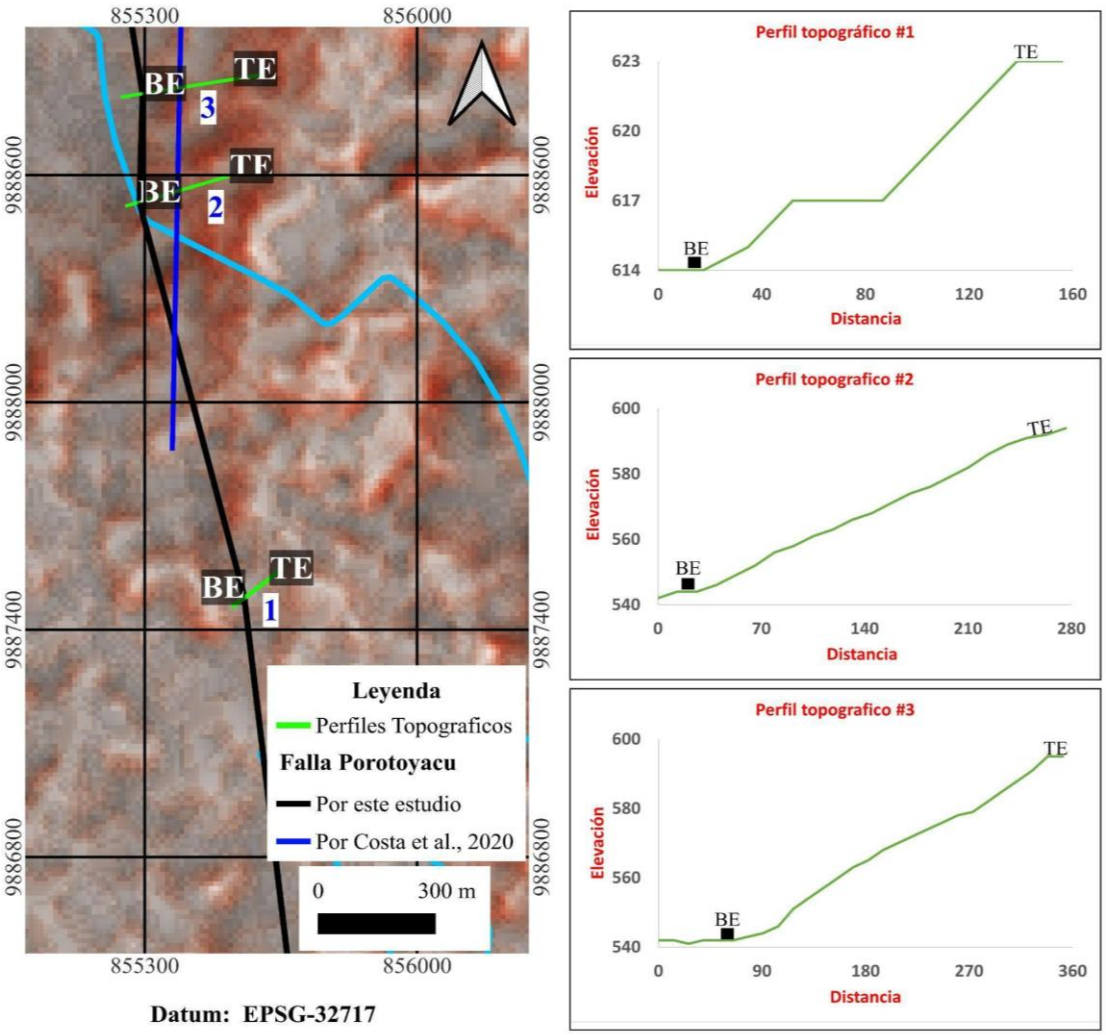

Figura 4. Escarpes de falla en la zona sur. Los sitios 2-3 (perfil superior), 4-5 (perfil medio) y 6-7 (perfil inferior) muestran las variaciones de pendiente asociadas a actividad tectónica. El mapa de fondo corresponde a un modelo de elevación sombreado en tonos rojos (RRIM), que resalta las variaciones topográficas en un rango de 505 (tonos blancos) a 894 metros (tonos rojizos). La traza de la falla identificada en este estudio se representa con una línea negra continua, mientras que la propuesta por Costa et al. (2020) se indica con una línea azul continua. Los elementos morfotectónicos se marcan como "BE" para la base del escarpe y "TE" para el tope del escarpe.

En el sector sur transicionando al sector norte, se observa cambios en las orientaciones de los escarpes, con direcciones NE-SE en los Sitios 14-15 (perfil 7) y NO-SE en los Sitios 16-17 (perfil 8). Las pendientes promedio oscilan entre 2% y 12.9%, mientras que los desniveles topográficos totales varían entre 21 y 25 m. Los Sitios 14-15 presentan una pendiente irregular, con un ascenso inicial moderado, seguido de un tramo de menor inclinación y luego un aumento más pronunciado en la elevación. En contraste, los Sitios 16-17 exhiben una pendiente convexa, caracterizada por una inclinación fuerte al inicio que luego se reduce progresivamente.

Por otro lado, los Sitios 18-19 (perfil 9) presentan una orientación ONO-ESE, con pendientes moderadas de 8% y 9.5%, y desniveles topográficos de 11 a 13 m. Exhiben una pendiente irregular, con pequeños tramos horizontales intercalados con aumentos abruptos en la elevación. Finalmente, el Sitio 20-21 (perfil 10), con la misma orientación ONO-ESE, una pendiente del 8% y un desnivel de 11 m, presenta una pendiente cóncava, donde el ascenso es más abrupto en la parte inicial y se incrementa progresivamente en la parte superior **(Figura 5)**.

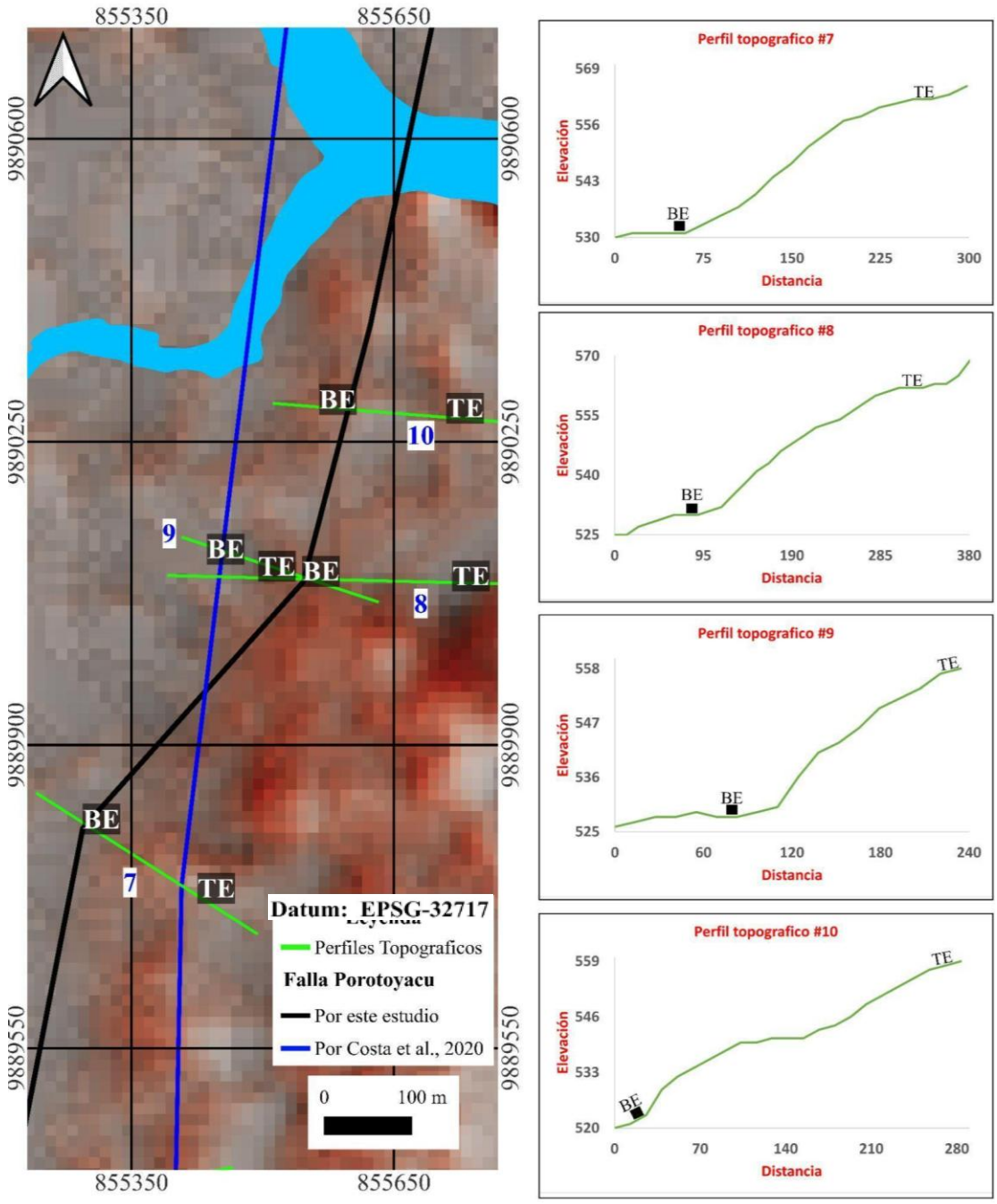

Figura 5. Escarpes de falla en la zona sur transicionando al norte. Los sitios 14-15 (perfil 7), 16-17 (segundo 8), 18-19 (perfil 9) y 20-21 (perfil 10) muestran las variaciones de pendiente asociadas a actividad tectónica. El mapa de fondo corresponde a un modelo de elevación sombreado en tonos rojos (RRIM), que resalta las variaciones topográficas en un rango de 505 (tonos blancos) a 894 metros (tonos rojizos). La traza de la falla identificada en este estudio se representa con una línea negra continua, mientras que la propuesta por Costa et al. (2020) se indica con una línea azul continua. Los elementos morfotectónicos se marcan como "BE" para la base del escarpe y "TE" para el tope del escarpe.

En el sector Norte, los Sitios 22 y 26 (perfil 12), donde la nomenclatura solo es presentada con un valor debido a la inaccesibilidad de las zonas y la limitación a conocer únicamente el valor de su base en campo, se caracterizan por perfiles cóncavos con pendientes de 5.19% y 0.51%, respectivamente. Estos perfiles muestran un inicio suave que asciende de forma más pronunciada hacia el final, destacando una transición hacia una pendiente convexa en tramos limitados.

El Sitio 27-28 (perfil 13), con orientación O-E, presenta un perfil convexo con un desnivel topográfico de 20 m y una pendiente promedio de 5.65%. Este perfil muestra una pendiente inicial uniforme que se torna irregular hacia los tramos finales, combinando ligeras ondulaciones y cambios abruptos en la inclinación. Este rasgo contrasta notablemente con los demás escarpes debido a su forma distinta. Finalmente, el Sitio 31-32 (perfil 15), orientado NO-SE, muestra una combinación de una forma cóncava en su tramo inicial, donde la pendiente desciende suavemente, seguida de un ascenso constante que define una pendiente uniforme hacia el final. Este perfil cierra el análisis al presentar una pendiente estable y progresiva en su último tramo **(Figura 6)**.

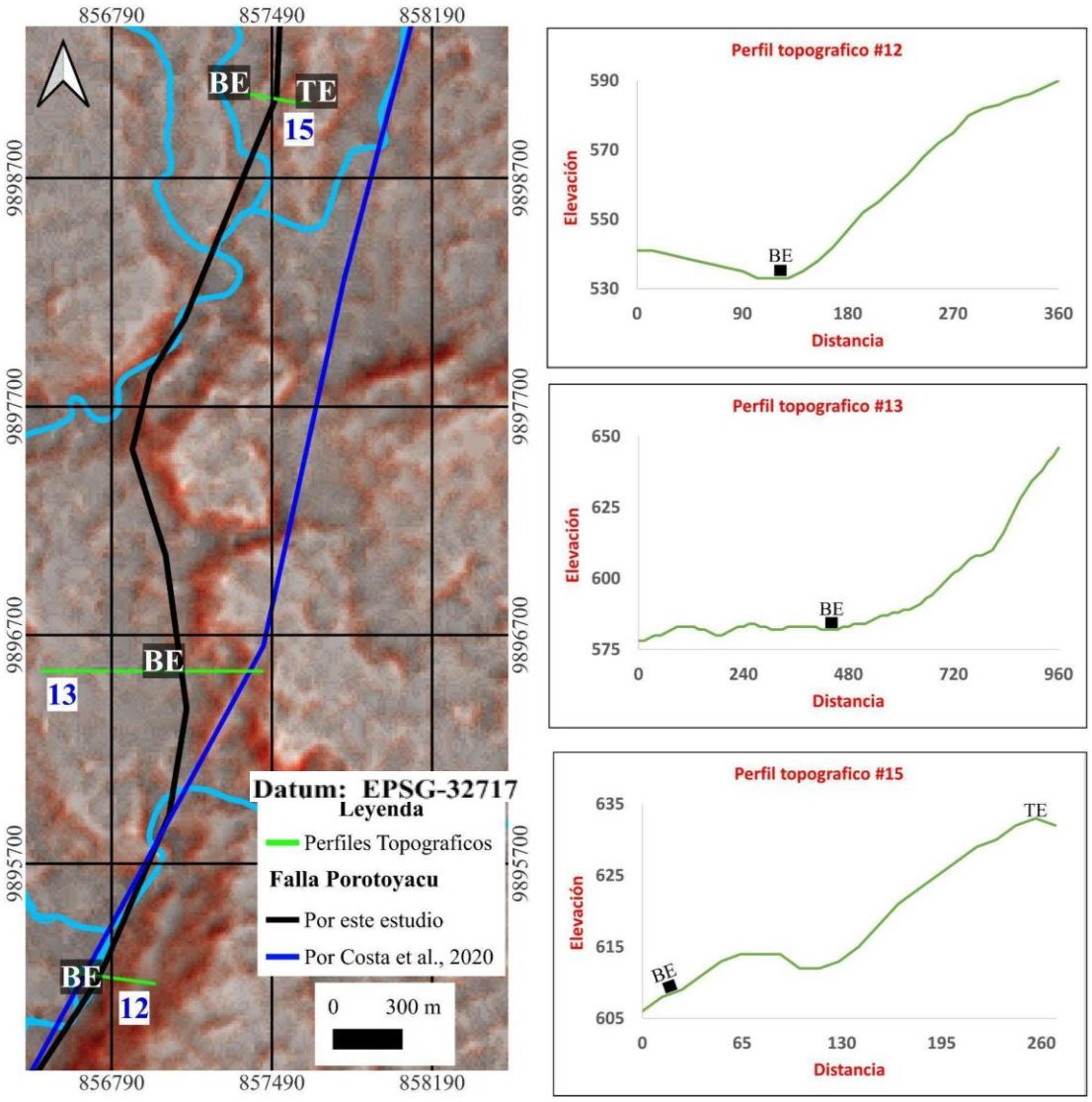

Figura 6. Escarpes de falla en la zona norte. Los sitios 26 (perfil 12), 27-28 (perfil 13) y 31-32 (perfil 15) muestran las variaciones de pendiente asociadas a la traza de la falla. El mapa de fondo corresponde a un modelo de elevación sombreado en tonos rojos (RRIM), que resalta las variaciones topográficas en un rango de 505 (tonos grises) a 894 metros (tonos rojizos). La traza de la falla identificada en este estudio se representa con una línea negra continua, mientras que la propuesta por Costa et al. (2020) se indica con una línea azul continua. Los elementos morfotectónicos se marcan como "BE" para la base del escarpe y "TE" para el tope del escarpe.

Tabla 2. Características de los escarpes identificados a lo largo de la Falla Porotoyacu. Esta tabla presenta información detallada sobre cada escarpe, incluyendo el promedio y la pendiente máxima, las alturas de la cima y la base, el desnivel total y la forma del perfil.

ID del sitio (#Perfil topográfico)	Pendiente Promedio (%)	Dirección	Altura del tope (m)	Altura de la Base (m)	Desnivel Total (m)	Forma del Perfil
2-3 (1)	5.1	SO-NE	604	595	6	Irregular
4-5 (2)	16.6	SO-NE	583	524	59	Convexa
6-7 (3)	16.2	SO-NE	564	521	40	Uniforme
8-9 (4)	12.3	SO-NE	551	522	29	Irregular
10-11 (5)	10	SO-NE	544	518	25	Uniforme
12-13 (6)	3	SO-NE	518	511	7	Convexa
14-15 (7)	12.9	NE-SE	538	512	25	Irregular
16-17 (8)	2	NO-SE	542	521	21	Convexa
18-19 (9)	9.5	ONO-ESE	520	507	13	Irregular
20-21 (10)	8	ONO-ESE	520	509	11	Cóncavo
22 (11)	5.19	SO-NE	530	516	15	Cóncavo
26 (12)	0.51	NO-SE	660	537	25	Cóncavo
27 - 28 (13)	5.65	O-E	607	587	20	Convexo
31 - 32 (15)	20	NO-SE	630	598	21	Cóncavo

2.2.2 Contraescarpes

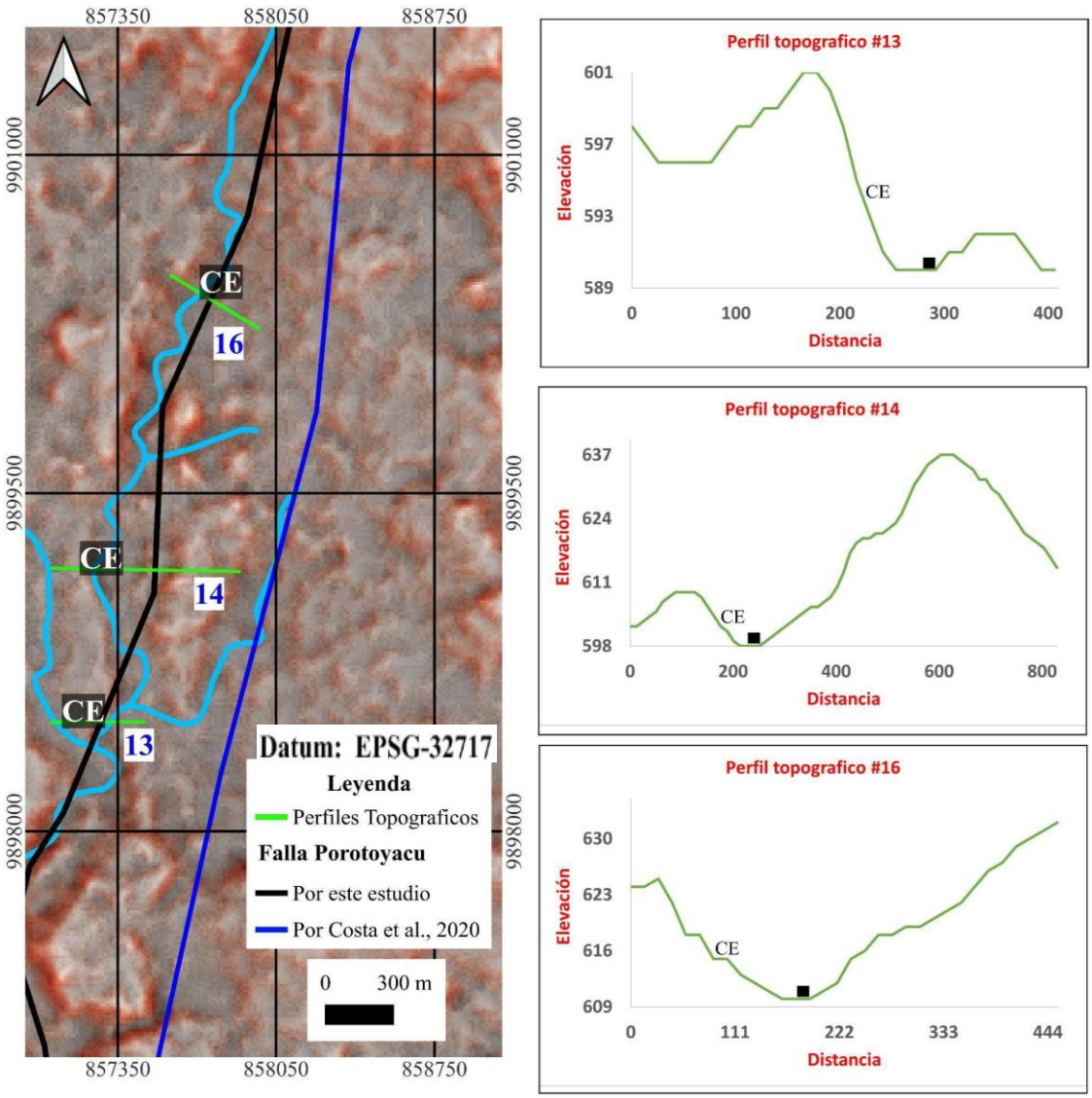

Figura 7. Contraescarpes de falla en la zona norte. Los sitios 28 (Perfil superior), 29 (Perfil intermedio) y 30 (perfil inferior) muestran las variaciones de pendiente asociadas a actividad tectónica. El mapa de fondo corresponde a un modelo de elevación sombreado en tonos rojos (RRIM), que resalta las variaciones topográficas en un rango de 505 (tonos blancos) a 894 metros (tonos rojizos). La traza de la falla identificada en este estudio se representa con una línea negra continua, mientras que la propuesta por Costa et al. (2020) se indica con una línea azul continua. Los contraescarpes se marcan como "CE".

Este indicador está compuesto de un escarpe en una vertiente donde la cara expuesta está a contrapendiente (Proyecto Multinacional Andino, 2009). En el área de estudio se identificaron 3 lineamientos a contrapuesta o contraescarpes, como se presenta en la **Tabla 3 y Figura 7.** Estos elementos destacan por su orientación y variación en la pendiente de las cuestas y contracuestas. Se identificaron 3 contraescarpes a lo largo del área de estudio. Un contraescarpe presenta una orientación diferente a la de los otros dos contraescarpes. Todos los contraescarpes se localizan al norte del área de estudio.

Tabla 3. Características de los contraescarpes identificadas al norte de la traza de la Falla Porotoyacu. Esta tabla muestra los detalles de cada contraescarpe, incluyendo la orientación, la pendiente del escarpe y la contraescarpe, y las alturas respectivas.

ID del Sitio	Orientación	Pendiente Cuesta	Pendiente Contraescarpe	Altura escarpe (m)	Altura Contraescarpe (m)
28	N-S	3.26	0.68	576	580
29	NW-SE	5.90	5.81	587	574
32	NW-SE	7.01	0.57	640	621

2.2.3 Drenaje Semi Rectilíneo

En cuanto a los cambios producidos en los drenajes, tenemos dos indicadores identificados, los rectilíneos se forman un cambio en la geometría adoptando un patrón rectilíneo y los ortogonales que muestran un cambio abrupto de orientación por la presencia de una falla geológica (Holbrook & Schumm,1999; Proyecto Multinacional Andino, 2009). En nuestro estudio, se identificaron dos tramos de drenaje semi rectilíneo, que se resumen en la **Tabla 4**. Ambos se encuentran en la zona norte del área de estudio donde el río tiene un comportamiento meándrico y presentan una orientación predominantemente Norte-Sur. El primer drenaje semi rectilíneo (23) tiene una longitud de 300 m, el segundo drenaje tiene una longitud de 330 m, ambos marcadores vuelven a adoptar un comportamiento meándrico, después de la geometría semi rectilínea **(Figura 8)**.

2.2.4 Drenaje Ortogonal

Un cauce ortogonal es un fenómeno nombrado así porque es una sección de un río que cambia de dirección a ángulos ortogonales debido a fallas (Burbank, D. W., & Anderson, R. S., 2011). En el norte de la zona de estudio, se identificó un drenaje ortogonal (Sitio 3), caracterizado por un cambio brusco en su orientación. El río tiene un comportamiento meandriforme antes del cambio de orientación del Tramo 1 de Oeste-Este con una longitud de 480 m y cambia en el Tramo 2 Norte-Sur donde la sección mide 330 m **(Tabla 4)**. Después de este marcador adopta una geometría de meandro abierto **(Figura 8)**.

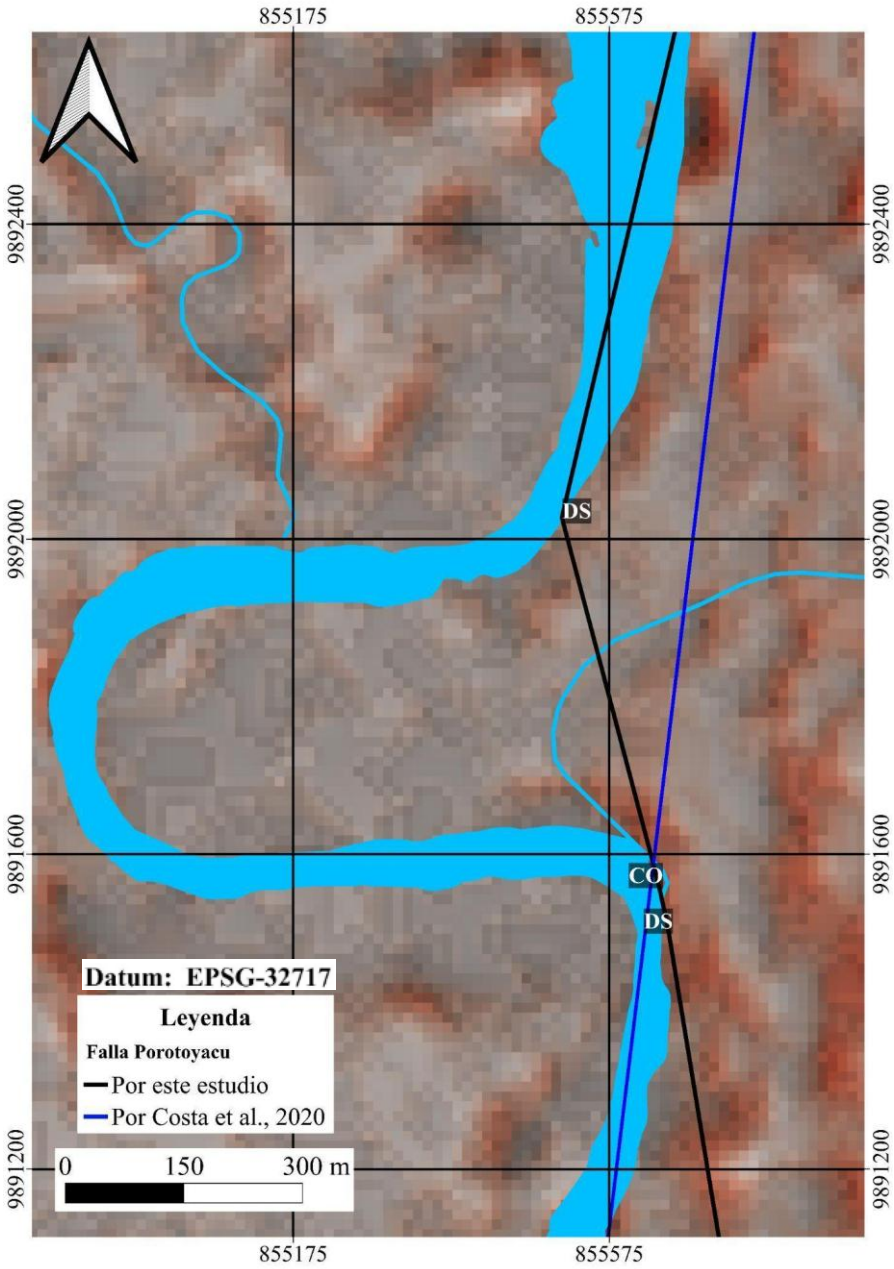

Figura 8. Mapa de los drenajes semi rectilíneos y ortogonales. Los elementos morfotectónicos se marcan como "CO" para el cauce ortogonal y "DS" para el drenaje semi rectilíneo. El mapa de fondo corresponde a un modelo de elevación sombreado en tonos rojos (RRIM), que resalta las variaciones topográficas en un rango de 505 (tonos grises) a 894 metros (tonos rojizos). La traza de la falla identificada en este estudio se representa con una línea negra continua, mientras que la propuesta por Costa et al. (2020) se indica con una línea azul continua.

Tabla 4. Características de los drenajes semi rectilíneos y ortogonales identificados en el sector sur de la Falla Porotoyacu. Esta tabla contiene los detalles de los drenajes semi rectilíneos, como su geometría y el azimut de cada uno.

ID del Sitio	Geometría	Azimuth del Drenaje
23	semirrecto	Norte-Sur
25	semirrecto	Norte-Sur
3	ortogonal	Tramo 1: Oeste-Este / Tramo 2: Norte-Sur

2.2.5 Terrazas Colgadas

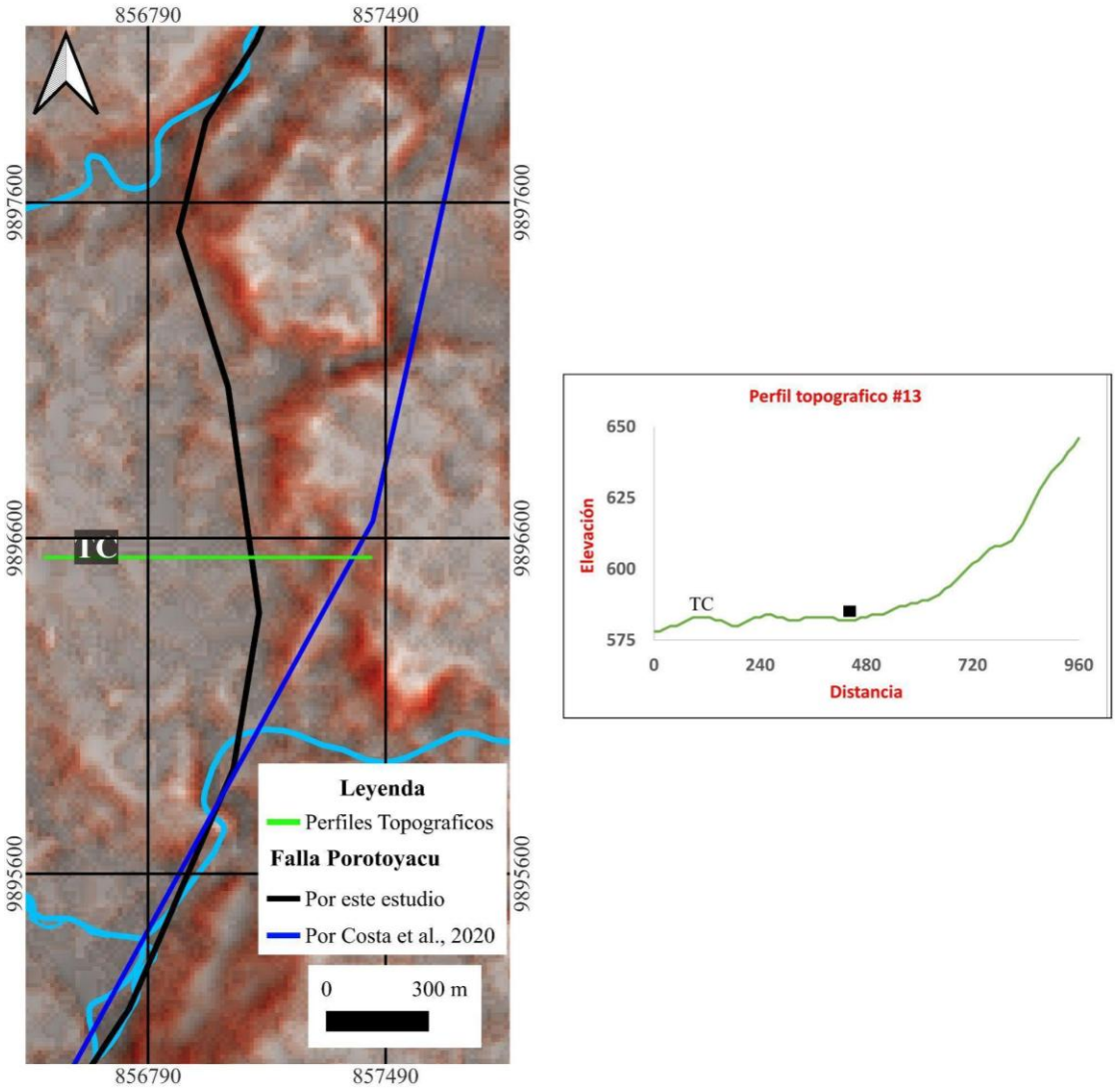

Figura 9. Mapa de la terraza colgada. Los elementos morfotectónicos se marcan como "TC" para la terraza colgada. El mapa de fondo corresponde a un modelo de elevación sombreado en tonos rojos (RRIM), que resalta las variaciones topográficas en un rango de 505 (tonos grises) a 894 metros (tonos rojizos). La traza de la falla identificada en este estudio se representa con una línea negra continua, mientras que la propuesta por Costa et al. (2020) se indica con una línea azul continua.

Las terrazas colgadas son superficies planas o suavemente inclinadas que representan antiguos niveles de depósito fluvial o erosión, pero que se encuentran elevadas respecto al cauce actual del río debido a procesos tectónicos. Estas terrazas se forman cuando un río, que originalmente deposita sedimentos en un valle, es sometido a un levantamiento tectónico (por ejemplo, por fallas, plegamientos o movimientos corticales). Este levantamiento provoca que el río se incise y deje las terrazas antiguas "colgadas" en las laderas del valle, desconectadas del nivel de base actual (Burbank, D. W., & Anderson, R. S., 2011).

Se identificó una terraza colgada en el Sitio 6, ubicada en el sector norte, con una zona plana de 135 metros de longitud y una pendiente de 0° **(Tabla 5)**. La diferencia de altura entre esta terraza y el fondo del valle es de 31 metros.

Tabla 5. Características de la terraza colgada en el Sitio 6, ubicada en el sector norte de la Falla Porotoyacu. La tabla muestra la longitud y pendiente de la zona plana, así como el desnivel de altura.

ID del Sitio	Longitud Zona Plana (m)	ID del Sitio	Longi	ID del Sitio	Longitud Zona Plana (m)
6	135	**6**		**6**	135

2.3 DISCUSIÓN

2.3.1 Análisis de indicadores morfotectónicos

Los indicadores morfotectónicos identificados en el área de estudio, como escarpes de falla, cauces ortogonales, drenajes semi-rectilíneos, terrazas colgadas y contraescarpes, sugieren una actividad tectónica significativa asociada a la Falla Porotoyacu. Estas estructuras son el resultado de procesos tectónicos que han generado deformaciones en el relieve, evidenciando la influencia del régimen tectónico regional en la configuración del paisaje (Yeats *et al.*, 1997). Aunque la accesibilidad limitada en algunas zonas restringe un análisis más detallado, la distribución y características de estos indicadores permiten inferir la continuidad estructural de la falla y su impacto en la evolución geomorfológica del área.

Los escarpes de falla son uno de los indicadores más evidentes de actividad tectónica reciente. Estos se caracterizan por presentar vertientes empinadas o acantilados, resultado directo del movimiento de la falla (Stewart & Hancock, 1990). En el área de estudio, se identificaron 14 escarpes con orientaciones y pendientes variables. La presencia de escarpes con formas convexas, cóncavas e irregulares refleja diferencias en la intensidad y dirección de los esfuerzos tectónicos, así como en la erosión y meteorización posteriores (Bates & Jackson, 1980).

Por otro lado, los drenajes semi-rectilíneos y ortogonales son indicadores sensibles a la actividad tectónica, ya que los ríos tienden a ajustar su curso en respuesta a cambios en el relieve generados por fallas (Keller & Rockwell, 1984). En este estudio, se identificaron dos drenajes semi-rectilíneos y un cauce ortogonal en la zona norte cerca de la ciudad de Tena. El cambio abrupto en la orientación del cauce ortogonal (de Oeste-Este a Norte-Sur) sugiere un control estructural en la dirección del flujo a causa de una falla (Gutiérrez, 2008).

Las terrazas colgadas identificadas en el sector norte también son evidencia de actividad tectónica. Estas estructuras representan antiguos niveles de depósito fluvial que han quedado elevados respecto al cauce actual debido a movimientos verticales asociados a la falla (Proyecto Multinacional Andino, 2009). La presencia de un asentamiento humano en una de estas terrazas colgadas refuerza la idea de que estos rasgos son el resultado de procesos tectónicos que han modificado el nivel de base del río. Finalmente, los contraescarpes identificados en la zona norte muestran orientaciones variables, lo que podría reflejar diferencias en las tensiones tectónicas locales. Estos lineamientos, visibles en imágenes satelitales y modelos de elevación, se alinean con la orientación regional de la Falla Porotoyacu (SSO-NE), lo que sugiere una relación directa con la estructura regional.

2.3.2 Relocalización de la Falla Porotoyacu basada en evidencias morfotectónicas

Para la relocalización de la traza, se consideraron los indicadores morfotectónicos que fueron validados en campo y cartografiados. La selección de puntos específicos para la nueva traza se basó en criterios derivados de los índices geomorfológicos. En el caso de los escarpes de falla, se estableció la traza en el límite entre el bloque deprimido y el bloque levantado, asegurando la correspondencia con la morfología del escarpe y la cinemática del desplazamiento (Burbank & Anderson, 2011). Para los contraescarpes, se ubicó la traza en la intersección entre el escarpe y el contraescarpe, reflejando el control tectónico sobre la topografía (Proyecto Multinacional Andino, 2009). En cuanto a los cauces ortogonales, la traza fue delimitada de manera rectilínea en las proximidades de los cambios abruptos de dirección del drenaje (Keller & Rockwell, 1984).

En el sector sur, cercano a la ciudad de Tena, la traza se encuentra vinculada a una zona con evidencias claras de actividad tectónica. Los escarpes principales delimitan superficies elevadas, donde los perfiles topográficos (Perfiles 1, 2 y 3. **Figura 4**) muestran pendientes pronunciadas.

En el sector sur transicionando al norte, la traza adopta una alineación más rectilínea, en concordancia con patrones de drenaje semi-rectilíneo y cauces ortogonales (**Figura 8**), los cuales indican la influencia de estructuras tectónicas en la configuración del paisaje. Aunque las terrazas colgadas son menos frecuentes en esta zona (**Figura 9**), los escarpes continúan siendo evidentes en los perfiles topográficos analizados (Perfiles 7, 8, 9 y 10 en la **Figura 5**), reflejando la continuidad estructural de la falla en este sector.

En la parte norte, en dirección a Archidona, la traza muestra una ligera desviación hacia el noreste, donde las evidencias geomorfológicas comienzan a dispersarse. Los escarpes presentan menor continuidad. Sin embargo, se identifican contraescarpes (**Figura 7**), los cuales muestran cambios graduales en la elevación con algunas transiciones abruptas en puntos específicos. Estos rasgos sugieren la posible influencia de estructuras secundarias que podrían estar afectando la continuidad de la falla en este sector.

La integración de los indicadores morfotectónicos identificados permitió proponer una nueva traza para la Falla Porotoyacu, con una longitud total de 19.08 km, superior a los 15 km reportados por Costa *et al., (*2020). La traza relocalizada de la falla se caracteriza por una orientación predominante norte-sur, atravesando la ciudad de Tena y Archidona con ligeros cambios en su dirección, adaptándose a las condiciones geomorfológicas locales.

2.4 CONCLUSIONES

En este estudio se reconocieron 5 marcadores morfotectónicos asociados a la Falla Porotoyacu, incluyendo escarpes de falla, drenajes semi-rectilíneos, cauces ortogonales, terrazas colgadas y contraescarpes. Estos indicadores se distribuyen a lo largo de la traza de la falla, con una mayor concentración en los sectores sur y norte del área de estudio. Los escarpes, que presentan pendientes variables entre 5.1 % y 16.6 %, se encuentran principalmente en el sector sur, mientras que los drenajes semi-rectilíneos y ortogonales, así como las terrazas colgadas, se localizan predominantemente en el sector centro. Los contraescarpes, por su parte, muestran orientaciones variables.

La asociación de estos marcadores con la Falla Porotoyacu se estableció mediante el análisis de su distribución espacial, orientación y características morfológicas. Los escarpes, con sus pendientes pronunciadas y desniveles topográficos significativos (hasta 59 m), son evidencia directa de movimientos verticales asociados a la falla. Los drenajes semi-rectilíneos y ortogonales, que muestran cambios abruptos en su orientación, reflejan un control estructural en la dirección del flujo, típico de zonas con actividad tectónica. Las terrazas colgadas, elevadas respecto al cauce actual del río, y los contraescarpes, con sus pendientes contrastantes, confirman la influencia de la falla en la evolución geomorfológica del área.

La nueva traza propuesta para la Falla Porotoyacu tiene una longitud de 19.08 km, en comparación con estudios previos, como el de Costa et al. (2020), que cartografiaron una longitud de 15 km. La traza sigue una orientación predominante norte-sur, esta

propuesta no solo amplía la extensión de la falla, sino que también refina su ubicación, alineándola con las evidencias morfotectónicas y topográficas observadas. Además, se sugiere que la falla podría extenderse hacia el sur, lo que deberá ser confirmado en futuras investigaciones.

Agradecimientos

Esta investigación se llevó a cabo con apoyo del Grupo de investigación de Ciencias de la Tierra y Clima de la Universidad Regional Amazónica Ikiam y en el marco de los proyectos CTC-006-2020, CTC-010-2024 y IGCP-669-Ollin. Especialmente por su valioso respaldo y por el conocimiento de los expertos paleo-sismólogos que ayudaron a la realización de este trabajo. De la misma forma, agradecemos a la comunidad del barrio Las Verónicas por su bienvenida y por el permiso para realizar el trabajo en el sitio. SLL recibió 3 becas de excelencia académica durante 2023-2024 y HC 1 beca en 2022 de la Universidad Ikiam, también recibieron las siguientes becas conjuntamente: beca del proyecto IGCP-669-Ollin-UNESCO para asistir a un curso de amenaza sísmica en Bogotá, beca para ser ponente en el Congreso científico internacional REDU desarrollado en Ikiam, beca de movilidad internacional por trabajo de excelencia por parte de la Universidad Ikiam para el congreso internacional PATAdays 2024.

REFERENCIAS

Alcacer, S, J. M., & Perucca, L. P. A. (2017). Análisis neotectónico en el piedemonte oriental de cordillera frontal, Andes centrales. San Juan, Argentina [Neotectonic analysis in the eastern piedmont of frontal Cordillera, Central Andes. San Juan, Argentina]. Geociencias, 36(4), 691-702. ISSN 0101-9082.

Alvarado, A. (2012). Néotectonique et cinématique de la déformation continentale en Equateur. [Thèse de Doctorat, Université de Grenoble]. https://theses.hal. science/tel-00870332

Alvarado, A., Audin, L., Nocquet, J. M., Jaillard, E., Mothes, P., Jarrín, P., Segovia, M., Rolandone, F., & Cisneros, D. (2016). Partitioning of oblique convergence in the Northern Andes subduction zone: Migration history and the present-day boundary of the North Andean Sliver in Ecuador. Tectonics, 35(5), 1048–1065. https://doi.org/10.1002/2016TC004117

Audemard, F. (1999). Morpho-Structural Expression of Active Thrust Fault Systems in the Humid Tropical Foothills of Colombia and Venezuela. Zeitschrift für Geomorphologie. 118. 1-18.

Baize, S., Audin, L., Winter, T., Alvarado, A., Pilatasig Moreno, L., Taipe, M., Reyes, P., Kauffmann, P., & Yepes, H. (2015). Paleoseismology and tectonic geomorphology of the Pallatanga fault (Central Ecuador), a major structure of the South American crust. *Geomorphology*, *237*, 14–28. https://doi.org/10.1016/j.geomorph.2014.02.030

Baize, S., Audin, L., Alvarado, A., Jomard, H., Bablon, M., Champenois, J., Espin, P., Samaniego, P., Quidelleur, X. & Le Pennec, J.-L. (2020). Active Tectonics and Earthquake Geology Along the Pallatanga Fault, Central Andes of Ecuador. Frontiers in Earth Science, 8, 1-21. doi: 10.3389/feart.2020.00193

Bates, R. L. y Jackson, J. A. (1980). Glossary of geology. American Geological Institute. https://books.google.com.ec/books?id=GS2nFrNLcVUC

Bemis, S. P., Micklethwaite, S., Turner, D., James, M. R., Akciz, S., Thiele, S. T., & Bangash, H. A. (2014). *Ground-based and UAV-Based photogrammetry: A multi-scale, high-resolution mapping tool for structural geology and paleoseismology.* Journal of Structural Geology, 69, 163–178. https://doi.org/10.1016/j.jsg.2014.10.007

Bès de Berc, S., Baby, P., Soula, J., Rosero, J., Souris, M., Christophoul, F., & Vega, J. (2004). The Mera-Upano Surface: Geomorphological Marker of Fluvial Incision and Tectonic Uplift in the Ecuadorian Sub-Andean Zone. Institut Français d'Études Andines. https://doi.org/10.4000/books.ifea.3009

Burbank, D. W., & Anderson, R. S. (2011). Tectonic geomorphology (2nd ed.). Wiley-Blackwell.

Carranco, F., Romero, C., & Calderón, E. (2023). Catálogo de edades radiométricas de Ecuador.

Colavitto, B., Alcacer, J., Rothis, M., Haro, F., Blanc, P., Onorato, M. R., & Perucca, L. (2021). Análisis paleosismológico de la falla Acequión mediante perfiles topográficos de escarpa (Precordillera

de San Juan, Argentina). Boletín de la Sociedad Geológica Mexicana, 73(2). https://doi.org/10.18268/BSGM2021v73n2a090121

Conteron, H., Lluno, S., Guzmán, O., Araujo, S., Campos, C., Valencia, B., Guamán, A., & Villacrés, J. (2024). Cartography of the Porotoyacu Fault in a southern section of the Ecuadorian Amazon. En G. Easton & G. González (Eds.), Proceedings of the 12th International INQUA Meeting on Paleoseismology, Active Tectonics and Archaeoseismology (pp. 116–122). PATA Chile 2024. https://doi.org/10.34720/fc3d-mp19

Cornejo, C., Guzman, O., Campos, C., & Cargua, J. (2024). Análisis paleosismológico en la Zona Subandina de Ecuador. Implicaciones para la Falla Porotoyacu. En Geociencias en la en la Amazonía ecuatoriana: Aportes a la planificación sostenible (1.a ed.). CEDIA. https://doi.org/10.48661/w6dc-q685

Costa, C., Alvarado, A., Audemard, F., Audin, L., Benavente, C., Bezerra, F.H., Cembrano, J., González, G., López, M., Minaya, E., Santibañez, I., Garcia, J., Arcila, M., Pagani, M., Pérez, I., Delgado, F., Paolini, M., Garro, H. (2020). Hazardous faults of South America; compilation and overview. Journal of South American Earth Sciences, 104, 102837. doi: 10.1016/j.jsames.2020.102837

Chiba, T., & Hasi, B. (2016). Ground surface visualization using red relief image map for a variety of map scales. ISPRS - International Archives of the Photogrammetry, Remote Sensing and Spatial Information Sciences, XLI-B2, 393-397. https://doi.org/10.5194/isprsarchives-XLI-B2-393-2016

Font, Y., Segovia, M., Vaca, S., Theunissen, T., (2013). Seismicity patterns along the Ecuadorian subduction zone: new constraints from earthquake location in a 3-D a priori velocity model. Geophysical Journal International 193, 263–286.https://doi.org/10.1093/gji/ggs083

Gutiérrez Elorza, M. (2008). Geomorfología. Pearson/Prentice Hall.

Holbrook, J & Schumm, S. A. (1999). Geomorphic and sedimentary response of rivers to tectonic deformation: A brief review and critique of a tool for recognizing subtle epeirogenic deformation in modern and ancient settings. *Tectonophysics*, *305*(1–3), 287–306. https://doi.org/10.1016/S0040-1951(99)00011-6

Jomard, H., Saqui, D., Baize, S., Alvarado, A., Bernard, B., Audin, L., Hidalgo, S., Pacheco, D., Ruiz, M., & Segovia, M. (2021). Interactions between active tectonics and gravitational deformation along the Billecocha fault system (Northern Ecuador): Insights from morphological and paleoseismological investigations. *Journal of South American Earth Sciences*, *111*(May). https://doi.org/10.1016/j.jsames.2021.103406

Keller, E. A., & Pinter, N. (2002). Active tectonics: Earthquakes, uplift, and landscape (2nd ed.). Prentice Hall. ISBN 0130882305

Keller, E. & Rockwell, T. (1984). Tectonic geomorphology, Quaternary chronology, and paleoseismicity. En Developments and applications of geomorphology (pp. 203-239). https://doi.org/10.1007/978-3-642-69759-3_7

Kendrick, E., Bevis, M., Smalley, R., Brooks, B., Vargas, R. B., Lauría, E., & Fortes, L. P. S. (2003). The Nazca–South America Euler vector and its rate of change. Journal of South American Earth Sciences, 16(2), 125-131. https://doi.org/10.1016/S0895-9811(03)00028-2

Legrand, D., Baby, P., Bondoux, F., Dorbath, C., Bès de Berc, S., & Rivadeneira, M. (2005). The 1999–2000 seismic experiment of Macas swarm (Ecuador) in relation with rift inversion in Subandean foothills. Tectonophysics, 395(1-2), 67–80. https://doi.org/10.4000/books.ifea.3013

Lluno, S., Conteron, H., Guzmán, O., Campos, C., & Cornejo, C. (2024). Paleoseismological study of the Porotoyacu Fault in the Amazonian Ecuadorian Piedmont. En G. Easton & G. González (Eds.), Proceedings of the 12th International INQUA Meeting on Paleoseismology, Active Tectonics and Archaeoseismology (pp. 288–293). PATA Chile 2024. https://doi.org/10.34720/fc3d-mp19

McCalpin, James P & Nelson, A. R. (2009). Introduction to paleoseismology. In *International Geophysics* (1st ed., Vol. 95, pp. 1–27). Elsevier Inc. https://doi.org/10.1016/S0074-6142(09)95001-X

Noriega-Londoño, S., & Caballero-Acosta, J. H. (2015). Morfotectónica de la falla Abriaquí y sismicidad histórica asociada con el sismo de 1903 en Frontino, Antioquia. Revista de la Academia Colombiana de Ciencias Exactas, Físicas y Naturales, 39(150), 100–110. https://doi.org/10.18257/raccefyn.81

Nocquet, J., Villegas-Lanza, J., Chlieh, M., Mothes, P., Rolandone, F., Jarrin, P., Cisneros, D., Alvarado, A., Audin, L., Bondoux, F., Martin, X., Font, Y., Régnier, M., Vallée, M., Tran, T., Beauval, C., Maguiña Mendoza, J., Martinez, W., Tavera, H. & Yepes, H. (2014). Movimiento de astillas continentales y subducción rastrera en el norte de los Andes. Nature Geoscience, 7(4), 287-291.

Ollarves, R., & Audemard, F. (2004): *Evidencias morfotectónicas de actividad cuaternaria enla cuenca de Barlovento*, Venezuela norcentral. XII Congreso Venezolano de Geofísica.Caracas. Venezuela. 8 pp.

Onorato, M. R., Perucca, L., Coronato, A., López, R., & Blanc, P. (2020). Evidencias morfotectónicas en el sistema de fallas Magallanes-Fagnano, borde transformante entre las placas Sudamericana y Scotia, isla Grande de Tierra del Fuego. Revista de la Asociación Geológica Argentina, 77, 47–61.

Papanikolaou, I. D., van Balen, R., Silva, P. G., & Reicherter, K. (2015). Geomorphology of active faulting and seismic hazard assessment: New tools and future challenges. Geomorphology, PII: S0169-555X(15)00107-5. https://doi.org/10.1016/j.geomorph.2015.02.024

Perucca, L., Rothis, M., Bezerra, F. H., Vargas, N., & Lima, J. (2015). Late Quaternary evolution of the La Cantera Fault System (Central Precordillera, Argentina): A morphotectonic and paleoseismic analysis. Tectonophysics, 661, 200–209. https://doi.org/10.1016/j.tecto.2015.08.041

Proyecto Multinacional Andino (2009). *Atlas de deformaciones cuaternarias de los Andes*. Servicio Nacional de Geología y Minería.

Quinde, P., & Reinoso, E. (2016, junio). Estudio de peligro sísmico de Ecuador y propuesta de espectros de diseño para la Ciudad de Cuenca. Revista de Ingeniería Sísmica, 1-26. https://doi.org/10.18867/ris.94.274

Ren, Z., Zhang, P., Oguchi, T., & He, Z. (2023). Perspectivas de teledetección sobre geomorfología y procesos tectónicos. Remote Sensing, 15(9), 2327. https://doi.org/10.3390/rs15092327

Rothis, M., Perucca, L., Santi Malnis, P., Alcacer, J., Haro, F., & Vargas, N. (2018, abril). Análisis morfotectónico en el piedemonte suroccidental del antepaís andino, sierras pampeanas occidentales, San Juan, Argentina. Geociencias, 37(1). https://doi.org/10.5016/geociencias.v37i1.12212

Scheidegger, A. E. (2004). Morphotectonics. Springer. https://doi.org/10.1007/978-3-642-18745-2

Stewart, I. S. y Hancock, P. L. (1990). What is a fault scarp? Episodes, 13(4), 256–263. https://api.semanticscholar.org/CorpusID:204215948

Taesiri, V., Pourkermani, M., Sorbi, A., Almasian, M., & Arian, M. (2020). Morphotectonics of Alborz Province (Iran): A case study using GIS method. Geotectonics, 54(5), 691–704. https://doi.org/10.1134/S001685212005009X

Tamay, J., Galindo-Zaldívar, J., Martos, Y. M., & Soto, J. (2018). Gravity and magnetic anomalies of Ecuadorian margin: Implications in the deep structure of the subduction of Nazca Plate and Andes Cordillera. Journal of South American Earth Sciences, 85, 68–80. https://doi.org/10.1016/j.jsames.2018.04.020

Telbisz, T., Kovács, G., Székely, B., & Szabó, J. (2013). Topographic swath profile analysis: A generalization and sensitivity evaluation of a digital terrain analysis tool. Zeitschrift für Geomorphologie, 57(4). https://doi.org/10.1127/0372-8854/2013/0110

Trenkamp, R., Kellogg, J. N., Freymueller, J. T., & Mora, H. P. (2002). Wide plate margin deformation, Southern Central America and Northwestern South America, CASA GPS observations. Journal of South American Earth Sciences, 15(2), 157–171. https://doi.org/10.1016/S0895-9811(02)00018-4

Vasuki, Y., Holden, E., Kovesi, P., & Micklethwaite, S. (2014). Semi-automatic mapping of geological Structures using UAV-based photogrammetric data: An image analysis approach. Computers & Geosciences, 69, 22–32. https://doi.org/10.1016/j.cageo.2014.04.012

Wu, Z., & Hu, M. (2019). Neotectonics, active tectonics and earthquake geology : terminology, applications and advances. Journal of Geodynamics, 127, 1–15. https://doi.org/10.1016/j.jog.2019.01.007

Yeats, R. S., Sieh, K. y Allen, C. R. (1997). The geology of earthquakes. Oxford University Press. https://books.google.com.ec/books?id=_8bNwAEACAAJ

Yepes, H., Audin, L., Alvarado, A., Beauval, C., Aguilar, J., Font, Y., & Cotton, F. (2016). A new view for the geodynamics of Ecuador: Implication in seismogenic source definition and seismic hazard assessment. Tectonics, 35(5), 1249–1279. https://doi.org/10.1002/2015TC003941

Manuscrito a someter a la revista "Applied Geophysics"

CAPÍTULO 3. FAULT ACTIVE MAPPING BASED ON PHOTOGRAMMETRY AND SEISMIC REFRACTION TOMOGRAPHY: A CASE STUDY OF THE SOUTHERN SECTION OF THE POROTOYACU FAULT, ECUADORIAN AMAZON.

Henry Conteron[1], *Samira Lluno*[1]

[1]Universidad Regional Amazónica Ikiam, Tena, Napo, Ecuador

ABSTRACT

This research investigates the extension and geometry of the Porotoyacu Fault in the southern Sub-Andean zone of Ecuador using a combination of photogrammetry and seismic tomography. High-resolution aerial imagery acquired with a DJI Phantom 4 RTK drone was processed to generate a Digital Elevation Model (DEM) with a 22 cm/pixel resolution, enabling detailed geomorphological mapping. Thirty-two transverse topographic profiles revealed a 684-meter fault trace with NE-SE orientation extending to the south. Complementary seismic tomography, conducted along a 69-meter SW-NE line, identified three seismostratigraphic units with P-wave velocities ranging from 0.3 to 2.5 km/s. These geological units show concordant deformation, evidence of a compressional stress regime, which has allowed defining, for the first time, the geometry of the fault. The fault shows a southwest (SW) vergence, which classifies it as a backthrust, since its orientation is opposite to that observed in other surrounding áreas. The integrated approach used in this study has revealed that the Porotoyacu Fault is more extensive. In addition, it has provided details about its geometry in the subsurface, which is fundamental to understand its tectonic behavior. These findings contribute to the characterization of the seismic hazard associated with this fault, providing a more solid basis for assessing potential risks in the region.

Keywords: fault mapping, photogrammetry, Porotoyacu Fault, seismic tomography, Sub-Andean, tectonic

3.0 INTRODUCTION

Identifying and mapping active faults is essential for forecasting destructive seismic events and mitigating their associated risks, particularly in tectonically active regions (Wu & Hu, 2019; Maldonado *et al.,* 2021; Molins-Vigatà *et al.,* 2022). This process integrates surface observations with advanced geophysical techniques to delineate fault traces and characterize their internal structures (McCalpin, 2009; Papanikolaou *et al.,* 2015; Galone *et al.,* 2024).

Recent advancements in remote sensing and photogrammetry have facilitated the generation of high-resolution digital elevation models (DEMs) and orthophotos using unmanned aerial vehicles (UAVs) (eg. Bemis *et al.,* 2014; Vasuki *et al.,* 2014; Bi *et al.,* 2017). These tools enable detailed analysis of surface morphotectonic features, such as scarps, displaced terraces, and drainage offsets, which are critical for identifying and understanding recent tectonic activity (Graveleau *et al.,* 2015; Valkanou *et al.,* 2024).

Complementing surface mapping, seismic refraction tomography offers a robust method to investigate subsurface fault geometry. By analyzing seismic wave propagation, this method generates velocity models that reveal variations in geological structures at depth (White, 1989; Santos & Bassrei, 2007). Challenges in solving inverse problems in tomography have been addressed using regularization techniques such as the L-curve method, which optimizes the balance between data fit and model smoothness (Sheehan *et al.,* 2005; Araujo *et al.,* 2023).

In Ecuador (**Figure 1A**), the cartography of active faults has been addressed at the continental scale through the South America Risk Assessment project (SARA) and at the national level by Egüez *et al.,* (2003). Underscores the heterogeneity in the representation of these structures across South America, stemming from variations in geographic coverage and data reliability (Costa *et al.,* 2020). While detailed studies have focused on the active structures of the Sierra region (Western Cordillera and Interandean Depression) (**Figure 1B**) (Alvarado *et al.,* 2014; Baize *et al.,* 2014, 2020;

Jomard *et al.,* 2021), the sub-Andean zone, located east of the Sierra region, although it has had earthquakes such as the Baeza earthquake (Mw 7.1, 1987) attributed to the Cutucú-Napo fault system (Legrand *et al.,* 2005; Font *et al.,* 2013), remains scarce of detailed studies, so further research is required to better understand its tectonic and seismic implications (Costa *et al.,* 2020).

Within this context, the Porotoyacu Fault (**Figure 1B**), part of the Cutucú-Napo fault system (Alvarado, 2012; Yepes *et al.,* 2016; Beauval *et al.,* 2018), has been studied at a regional scale through photo interpretation. It has been identified as an active surface structure with transcurrent-inverse kinematics and an approximate length of 16.7 km (Costa *et al.,* 2020). At least eight seismic events with magnitudes of up to 5.5 Mw have been recorded in the vicinity of the fault in recent years, which may be associated with this structure (IGEPN, 2024).

A paleoseismological study conducted on a southern section of the Porotoyacu Fault suggests a possible southward extension of its trace, supported by evidence of potential seismic events (Cornejo *et al.,* 2024). This raises the need to further investigate the proposed extension by analyzing surface features near its presumed termination and characterizing the subsurface geometry to gain a clearer understanding of the fault's structure. To address these questions, this study uses aerial photogrammetry for the mapping of the fault's surface trace and seismic tomography to characterize the subsurface fault geometry in the proposed southern área.

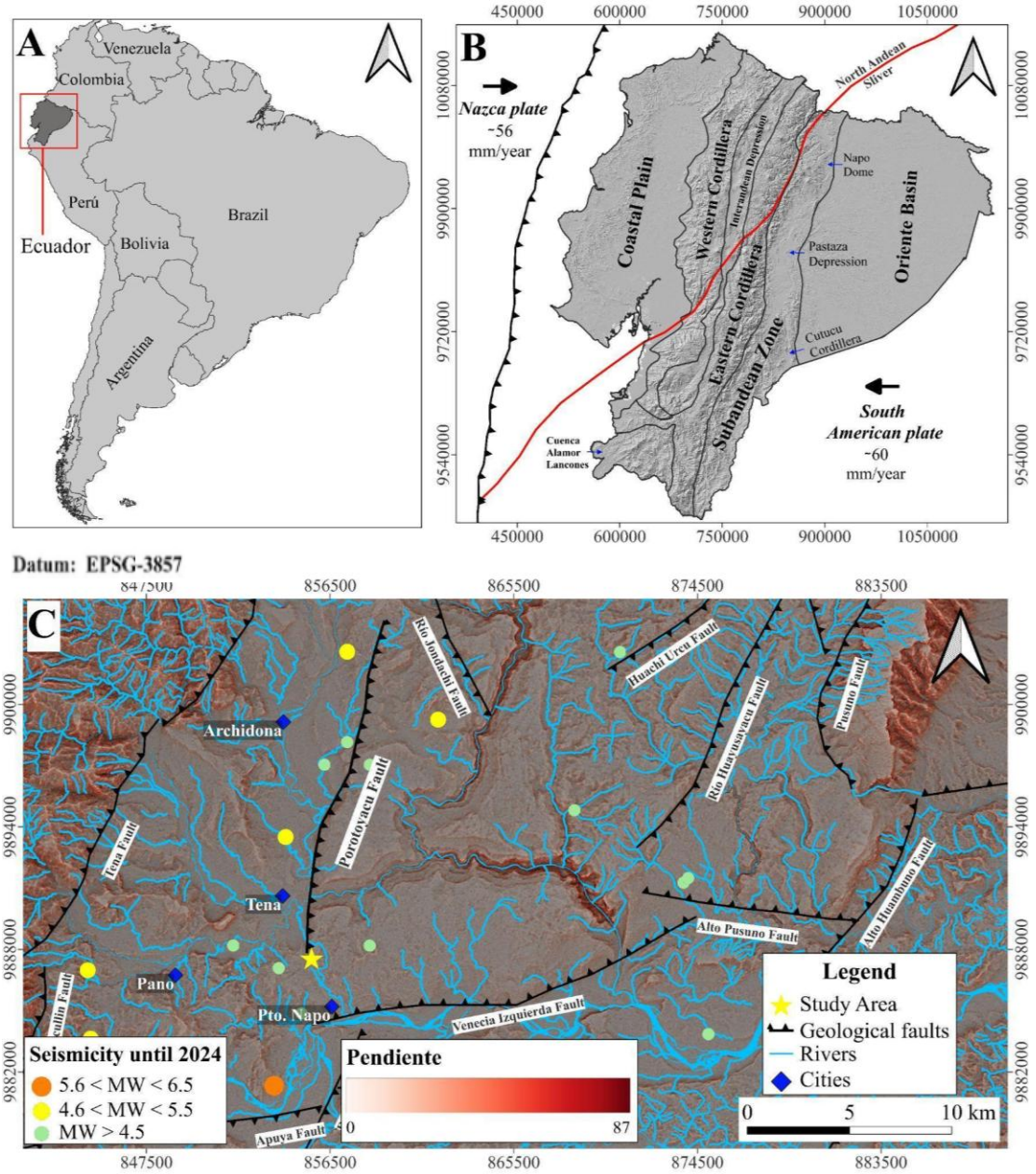

Figure 1. Location of the study area. (A) The gray polygon enclosed in a red box represents Ecuador in the broader context of South America. (B) Nazca Plate controls the geodynamics of Ecuador subducts beneath the South American plate (Trenkamp et al. 2002; Kendrick et al. 2003; Rodríguez et al. 2024), In addition, the Structural zones in the Ecuadorian Andes and Amazonian foreland is divided with black lines adapted from Carranco et al., 2023. (C) The topography of the study área is depicted on a Red Relief Image Map (RRIM) from an ALOS PALSAR Digital Elevation Model (DEM). The trace of the Porotoyacu Fault is visible as a black line (Costa et al., 2020). The red, orange, yellow and green dots indicate the seismic activity until 2024, classified by magnitude (MW) (IGEPN, 2024).

3.0.1. Geodynamics and Seismicity of the Study Área

Ecuador is situated at the hinge between the SSE-NNW-oriented Central Andes and the SSW-NNE Northern Andes (Legrand *et al.,* 2004). This location is dominated by subduction of the Nazca plate and the South American plate (**Figure 1B),** the displacement rate between these plates is 56 mm/year to the North and 60 mm/year to the South (Trenkamp *et al.,* 2002; Kendrick *et al.,* 2003; Nocquet et al., 2014; Rodríguez *et al.,* 2024). With an eastward movement of the Nazca plate concerning the South American plate, considered as fixed, which is oblique to the Ecuador trench (Kellogg & Vega 1995; Trenkamp *et al.,* 2002) and which generates mainly E-W compression (Ego *et al.,* 1996; Gutscher *et al.,* 1999). This phenomenon has led to the formation of a complex system of surface active faults, which represent a significant source of seismic risk, as they can generate shallow earthquakes and increase the seismic vulnerability of the Ecuadorian territory (Chunga *et al.* 2010; Alvarado *et al.,* 2016; Vidal & Granda 2018).

Intraplate seismicity is controlled by approximately 400 active fault segments, grouped into six major fault systems or seismogenic sources, between them there is Cutucú-Napo (Alvarado 2012; Yepes *et al.,* 2016; Beauval *et al.,* 2018). Cutucu-Napo is structured by reverse faults of N-S to NNE-NNW orientation; reflection seismic sections show that these faults are generally high angle, and probably of cortical scale (Bès de Berc *et al.,* 2004). Most of these faults correspond to old inverted normal faults, which controlled Triassic and Jurassic sedimentation (Díaz & Baby 2004). These tectonic structures are responsible for numerous seismic events, ranging from low-magnitude earthquakes to higher-intensity movements that have caused significant damage. Notable examples include the 1987 Baeza earthquake (Mw 7.1) and the 1995 Macas earthquake (Mw 7.0), both linked to the Cutucú-Napo fault system (Baby *et al.,* 2004; Legrand *et al.,* 2005).

According to Alvarado (2012) and Yepes *et al.,* (2016), in the sub-Andean zone seismicity is originate mainly from the Cutucú-Napo seismogenic source, this system, the most eastern deformation belt in Ecuador, is characterized by sub-Andean thrusts and folds

with a north-south orientation, extending from Napo province to Pastaza (Yepes *et al.,* 2016; Costa *et al.,* 2020).

An outstanding case within the Cutucú-Napo system is the Porotoyacu Fault (**Figure 1B**) with an approximate length of 15 km; this fault has transcurrent-inverse kinematics (Costa *et al.,* 2020). A Paleoseismological study suggests a southward extension of its trace (Cornejo *et al.,* 2024). In recent years, at least eight seismic events have been instrumental recorded along the Porotoyacu trace, with magnitudes of down to 6.5 Mw. A notable event occurred on December 28, 2021, with a magnitude of 4.93, located north of the fault and possibly linked to this structure (IGEPN, 2024).

The study área is located in the Ecuadorian sub-Andean zone, in the southern section of the Porotoyacu Fault (**Figure 2**) near a town with a population of approximately 60,880 inhabitants (Censo de Población (INEC), 2010). This location was selected due to morphotectonic scarp characterized by an average slope of 7° between two flat surfaces with SW-NE orientation, located at coordinates 1°0'57.91"S, 77°48'19.89"W. Furthermore, the área contains an anthropogenic shear that exposes sedimentary rocks with evidence of deformation and displacements in the stratigraphic succession.

3.1 METHODOLOGY

We employed a combination of photogrammetric and geophysical techniques to analyze the geomorphological and structural characteristics of the study área. The methodology was divided into two main phases: (1) the generation of a high-resolution Digital Elevation Model (DEM) using aerial photogrammetry, and (2) the application of seismic reflection tomography to investigate subsurface structures.

3.1.1 Photogrammetry

We used 432 original images from a flight conducted with a Drone (DJI Phantom 4 RTK) over the study área to create the Digital Elevation Model (DEM) of approximately 0.36 km² (**Figure 2**) using the photogrammetry software. This software employs the modern Structure from Motion (SfM) photogrammetric technique (Westoby *et al.,* 2012; Yakar *et al.,* 2022), notable for its high degree of automation in recognizing homologous points across images. The original images, 429 were successfully aligned, yielding an average reprojection error of 0.337 pixels, which indicates optimal image overlap and correct photogrammetric adjustment.

In the subsequent phase, the software densified the search for homologous points within the study área until achieving a high-density point cloud model, represented in x, y, z coordinates and intensity. The georeferencing of the model was conducted without ground control points due to equipment constraints. While the absence of ground control points could introduce minor georeferencing inaccuracies, the RTK capabilities of the drone significantly minimized these errors, ensuring a sufficient level of accuracy for the study objectives.

The final product is a Digital Surface Model (DSM), which was filtered to address the presence of buildings and vegetation in the área. Filtering parameters included a maximum angle of 7 degrees, a maximum distance of 0.1 meters, and a cell size of 25 meters to produce the DEM of the terrain. Áreas where data were interpolated by the software due to missing values were identified and smoothed in the DEM.

From the DEM analysis, a morphotectonic scarp was identified and topographic profiles were elaborated with the Qgis program. These profiles were oriented perpendicular to this structure, following the ENE-SWS and SW-NE directions, allowing to observe if there is morphology associated with the Porotoyacu Fault.

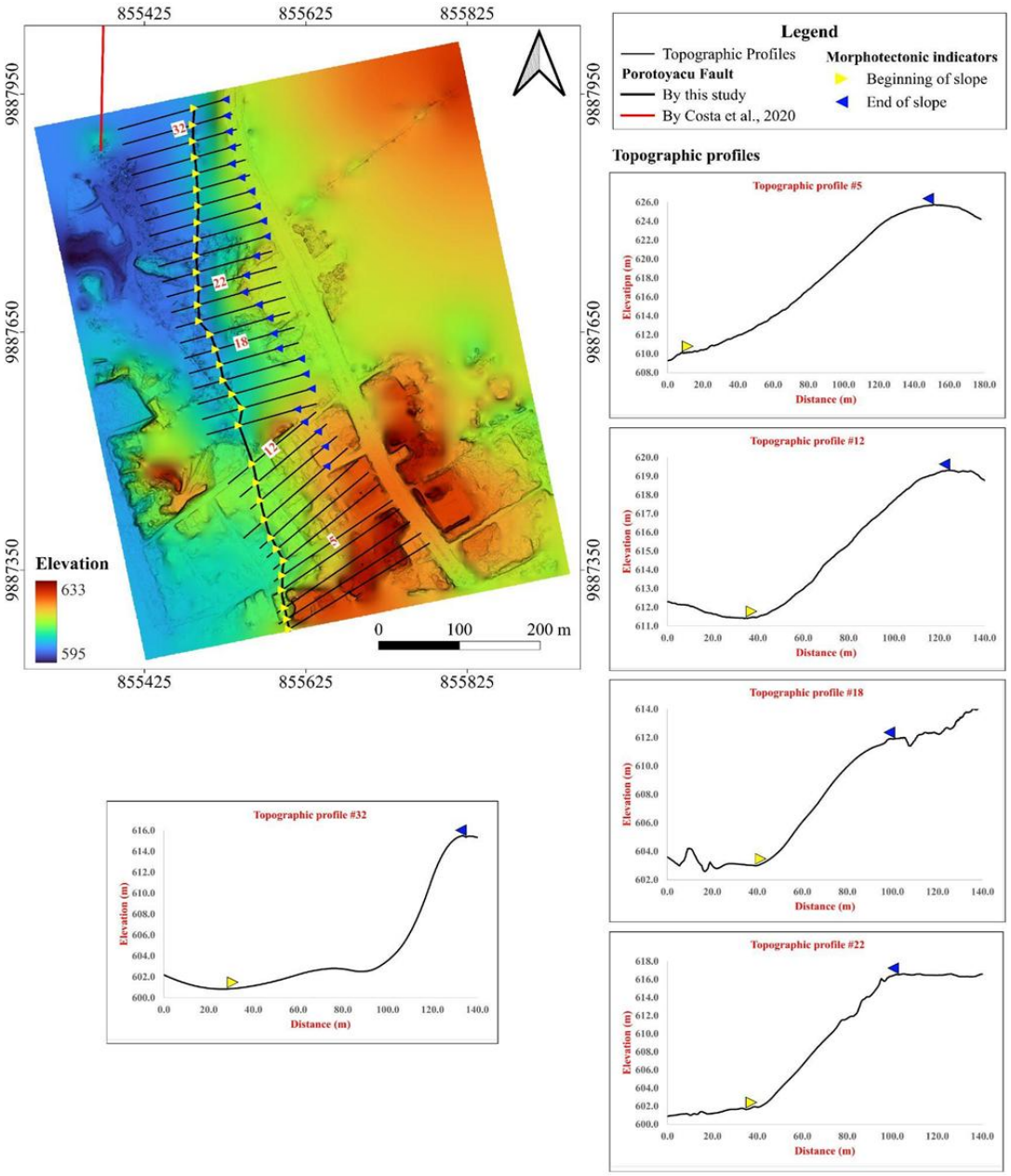

Figure 2. Proposed fault segmentation and associated topographic profiles. This figure shows a DEM derived from photogrammetric data, highlighting the topographic variations within the study área. The color scale in the lower-left corner represents elevations ranging from 595 to 633 meters above sea level, with warm tones (red and orange) indicating higher altitudes and cool tones (blue and green) representing lower elevations. Topographic profiles were generated to capture detailed morphometric features and shown as black lines. Morphotectonic Indicators are represented by specific symbols: yellow triangles indicate the beginning of the slope. Similarly, blue triangles correspond to the end of the slope. The figure includes two fault traces for the Porotoyacu Fault: a previously suggested trace by Costa *et al.,* (2020), shown as a red line and proposed in this study, represented by a black line, which aligns with the beginning of the slope identified along the topographic profiles. On the right, five selected topographic profiles (5, 12, 18, 22, and 32) illustrate variations in elevation along the study área, emphasizing the identified beginning of slope and end of slope associated with the scarp as a morphotectonic indicator.

3.1.2 Seismic Tomography of Refraction

The geophysical survey consists of a seismic line in a section located south, arranged along a sector of morphotectonic scarp identified in the Dem analysis of this study. The geophones have a frequency of 4.5 Hz and are connected to a Geometrics E3000 seismograph. A 6 kg hammer generates the surface percussion on a 2.5 cm thick aluminum metal plate. To solve the inverse tomography problem, we used SeisImager software (Geometrics, 2009).

The seismic line consists of 23 geophones arranged at 3 m intervals, covering a total length of 69 m. The length of the seismic lines was defined taking into account the constraints of the urban environment, avoiding interfering with daily human activities. **Figure 3 A, B, C** presents three examples of shots. The first one located 13.5 m from the start of the line (**Figure 3A**), allows observing the first arrivals. The second, a central shot, located at 31.5 m (Fig. 3B), gives an overview of the arrivals at all geophones. Finally, the third at the 52.5 m position (**Figure 3C**), records the last arrivals in greater detail. Once the first arrivals in the signals were identified, the errors were corrected by reviewing the traveltime curves. Next, the a priori model of the tomography was established. For this, we have made several numerical tests with different minimum and maximum velocity values at various depths. Then, we use race tracing to verify the depth range of the a priori model.

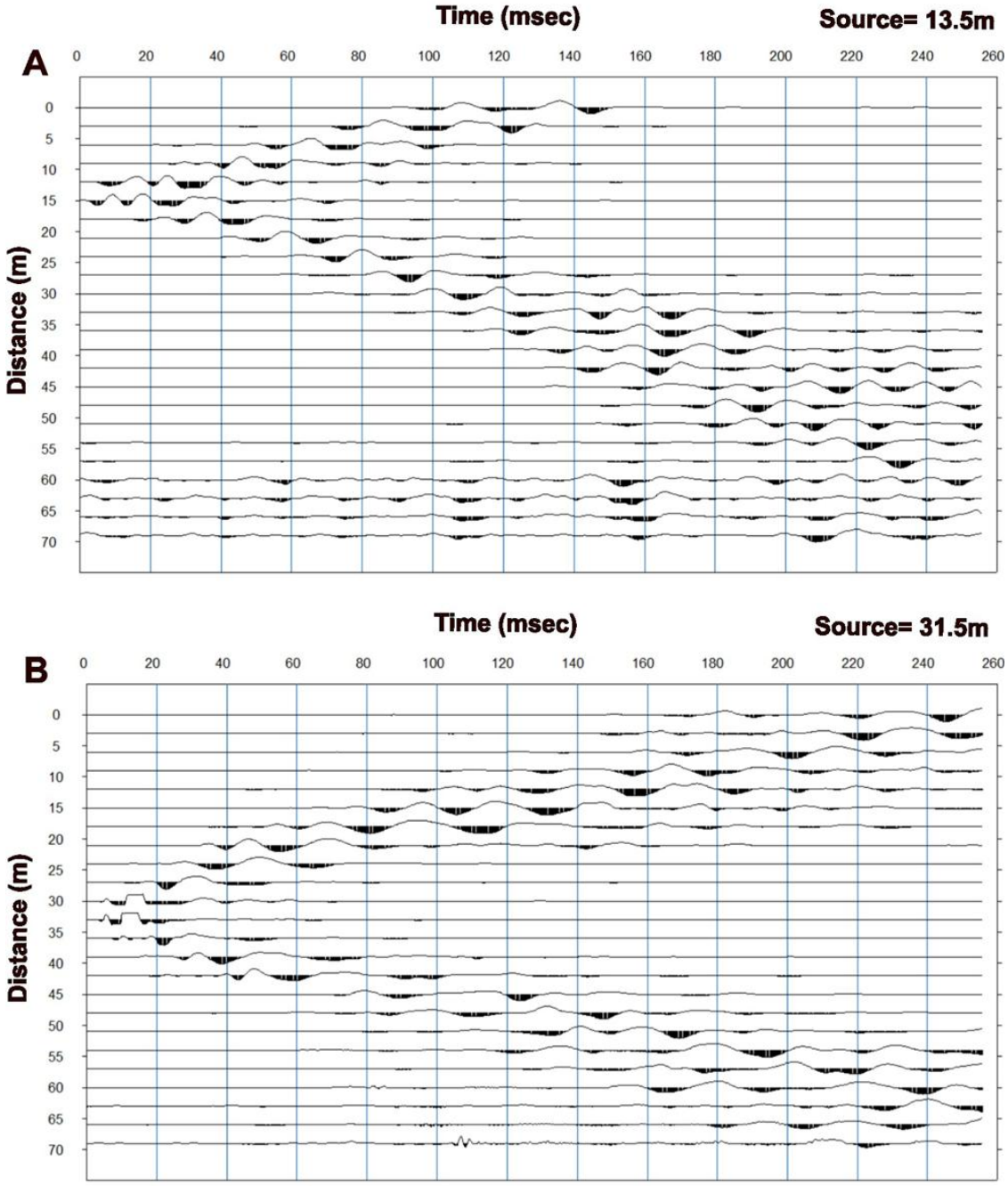
A
Time (msec)
Source= 13.5m
0 20 40 60 80 100 120 140 160 180 200 220 240 260
Distance (m)
0 5 10 15 20 25 30 35 40 45 50 55 60 65 70
B
Time (msec)
Source= 31.5m
0 20 40 60 80 100 120 140 160 180 200 220 240 260
Distance (m)
0 5 10 15 20 25 30 35 40 45 50 55 60 65 70

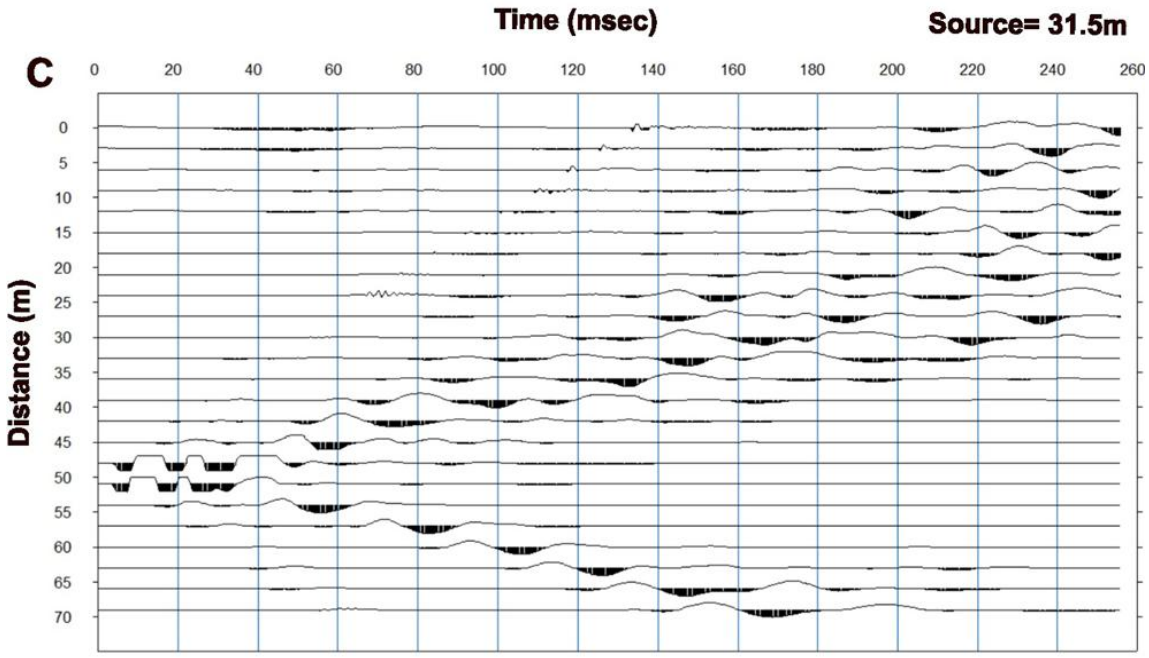

Figure 3. Examples for the seismic line of the experiment: A) First shot, B) Second shot, and C) Third shot. The source gives the position of each shot on the distance scale. The horizontal scale is in milliseconds. Each waveform represents the recorded seismic response at different geophone positions along the seismic line. The x-axis indicates time in milliseconds, while the y-axis corresponds to the distance along the seismic profile. The progressive arrival of waves from top to bottom in each graph illustrates how seismic energy propagates through the subsurface.

3.1.3. Regularization strategy

The tomography problem is based on the equation describing the travel time of a seismic ray through a medium whose velocity, **v(x)**, varies according to the position **x**. For simplicity, the slowness **s(x) = 1/v(x)** is used. In discretized media, the integral is transformed into a sum of the lengths traveled by the ray within each cell, multiplied by its slowness, as described in equations (1) and (2) of Hansen (1992) and Zhdanov (2015).

$$t_i = \int_x s(x)dx(\mathbf{1})$$

$$t_i = \sum_{j=1}^{N} l_{ij}s_j \quad (\mathbf{2})$$

In this study, SeisImager software uses the least squares method to solve the tomography problem and obtain the slowness values using travel times as data (Geometrics, 2009).

Once the a priori model is proposed, it is necessary to solve the seismic tomography inverse problem. Since this problem has no unique solution, we use a Tikhonov regularization (Zhdanov, 2015) to find an optimal solution to this ill-posed problem with d data and m parameters. This regularization consists of finding the regularization parameter α that minimizes the parametric functional P (m,d) defined as:

$$P^{\alpha}(m,d) = \|Am - d\|^2 + \alpha\|m - m_{apr}\|^2 \quad \textbf{(3)}$$

We use the L-curve criterion to practically apply the Tikhonov regularization (Hansen, 1992; Zhdanov, 2015). This curve is a plot between the error norm and a posteriori model norm where the L-corner gives the optimal solution. In our case, we use the root mean square error (RMS) for the error norm. The RMS is given by the summand term in Eq. (3) **RMS=‖Am d‖**. The RMS represents the fit of the data to the tomography result, and is the parameter reported by the SeisImager software as the result of the inversion.

We propose calculating the norm between the resulting and initial models for the model norm after inversion. This choice is because the variations between seismic tomography models are minuscule. It is well known that lateral velocity variations are better highlighted using the relative velocity model than the absolute values. Then, using this distance, we have a better resolution in the plot of the curve L. For the distance between the model and the a priori model, we tested three types of norms: the Euclidean norm **ℓ2**, the taxicab norm **ℓ1** and the infinity norm **ℓ∞ (**Araujo *et al.,* 2023, 2024**)**. We explored these three norms because they can be sensitive to different outliers in the data (Tarantola, 2005). These outliers commonly influence the final result due to different experimental errors. In our a priori model m_i^{apr} has **n** discrete points, and the posterior model is in the vector is mi; Eqs define the three norms. **(4)**.

$$l_2 = \sqrt{\frac{1}{n}\sum_{i=1}^{n}(m_i - m_i^{apr})^2}$$

$$l_1 = \frac{1}{n}\sum_{i=1}^{n}\left|m_i - m_i^{apr}\right| \quad \textbf{(4)}$$

$$l_\infty = max\left\{\left|m_i - m_i^{apr}\right|\right\}$$

We repeat this plot for each smoothing value and represent these values with a color scale. The corner of the L-curve gives the smoothing parameter, which regularizes the problem. In the software Plotrefa, we can modify the vertical and horizontal smoothing. A good strategy is to set the vertical value to the maximum and vary the horizontal value. We choose the values of smoothing by looking at the vertex of the curve L.

We built a synthetic layered model and computed synthetic data with noise to test our regularization scheme. In SeisImager software, we defined a horizontally varying velocity model. The resulting synthetic traveltime curves are shown in **Figure 4**. We can use these traveltime curves with an a priori layered model to solve the tomography problem with the different smoothing values.

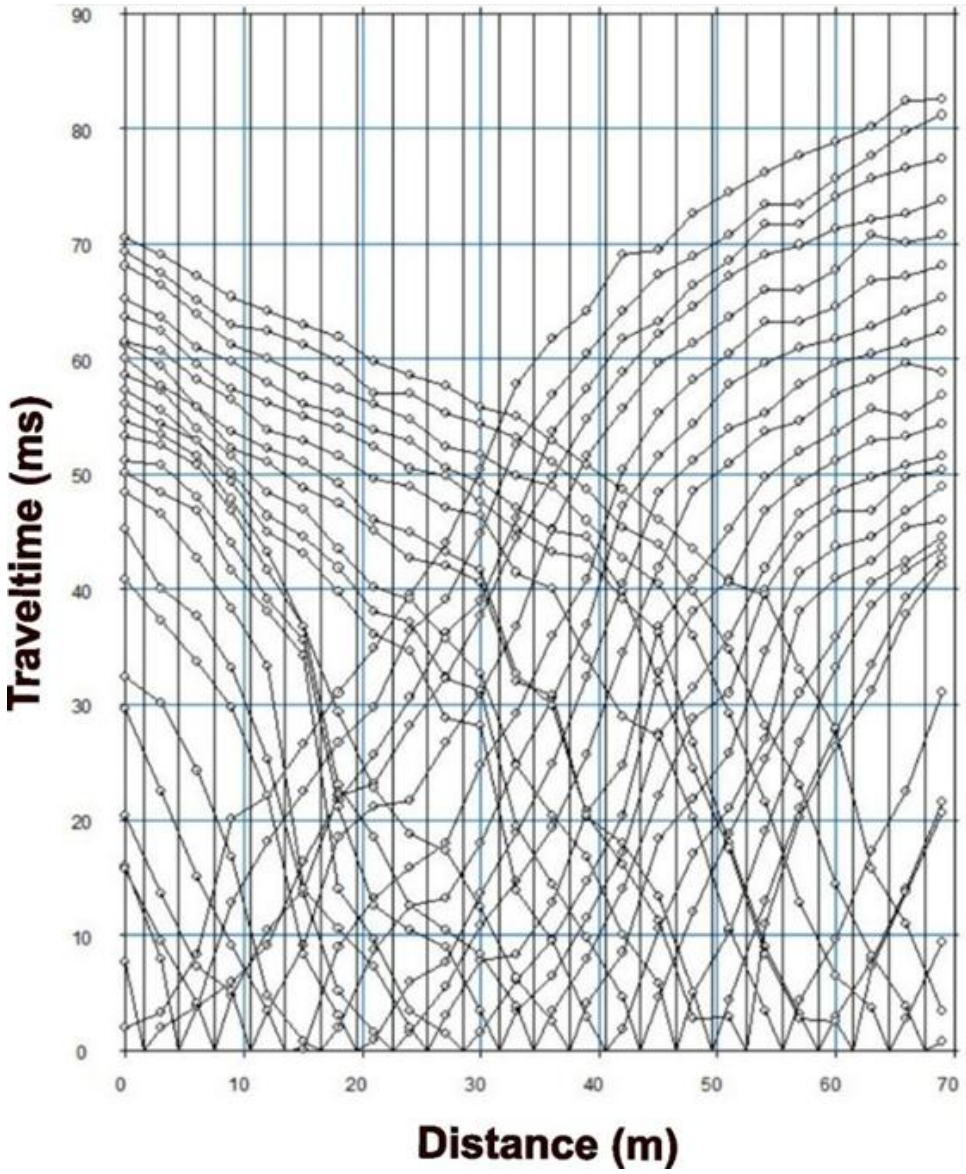

Figure 4. Travel time curves for seismic tomography inversion. This figure represents the recorded first-arrival travel times for different geophone positions along the seismic line. The x-axis denotes the distance along the seismic profile (in meters), while the y-axis shows the travel time (in milliseconds) of seismic waves. Each line corresponds to a seismic ray path, with intersections indicating wave refractions and velocity contrasts in the subsurface. These data serve as input for the tomographic inversion process, where the L-curve method is applied to optimize regularization and improve the velocity model.

3.2 RESULTS

3.2.1. Local Cartography

The photogrammetric point cloud generated a detailed Digital Elevation Model (DEM) with a spatial resolution of 22 cm/pixel and a point density of 20.6 points/m². The DEM revealed elevation variations between 595 and 633 meters above sea level, highlighting distinct topographic differences between the eastern and western sectors of the study área. The western sector predominantly features gentle slopes with elevations ranging from 607 to 620 meters for less than 100 meters. In contrast, the eastern sector exhibits steeper slopes with an average inclination of 7 degrees, characterized by higher elevations forming a southwest-facing slope.

To complement the analysis, 32 cross-sectional topographic profiles were generated perpendicular to the direction of the scarp morphology using QGIS's Cross Profiles tool. The characteristics of the morphotectonic scarp by topographic profiles are in **Table 1**. These profiles enabled a detailed characterization of slope morphology, as demonstrated in previous studies (Telbisz *et al.,* 2013; Colavitto *et al.,* 2021).

Table 1. Characteristics of the morphotectonic scarp. Presents detailed information on each escarpment, Topographic profile, Slope shape, Direction, Length (m), Top height (m) and Base height (m)

#Topographic profile	Slope shape	Direction	Length (m)	Top height (m)	Base height (m)
1	Uniform	SW-NE	110	625	615
2	Irregular	SW-NE	110	624	613
3	Uniform	SW-NE	150	624	612
4	Irregular	SW-NE	160	631	611
5	Uniform	SW-NE	155	625	609
6	Irregular	SW-NE	140	627	609
7	Irregular	SW-NE	155	625	609
8	Irregular	SW-NE	145	625	609
9	Uniform	SW-NE	170	622	609
10	Irregular	SW-NE	110	620	612
11	Concave	SW-NE	80	620	612
12	Concave	SW-NE	70	619	611
13	Concave	ENE-SWS	100	618	607
14	Concave	ENE-SWS	90	616	607
15	Concave	ENE-SWS	90	614	606
16	Concave	ENE-SWS	80	611	605
17	Concave	ENE-SWS	100	612	603
18	Concave	ENE-SWS	70	611	602
19	Convex	ENE-SWS	80	615	602
20	Concave	ENE-SWS	70	615	602
21	Convex	ENE-SWS	70	617	602
22	Uniform	ENE-SWS	60	616	601
23	Uniform	ENE-SWS	100	617	601
24	Uniform	ENE-SWS	105	616	601
25	Uniform	ENE-SWS	85	616	602
26	Uniform	ENE-SWS	80	615	603
27	Uniform	ENE-SWS	75	615	605
28	Uniform	ENE-SWS	65	615	605
29	Uniform	ENE-SWS	55	614	605
30	Irregular	ENE-SWS	55	614	605
31	Convex	ENE-SWS	50	615	603
32	Convex	ENE-SWS	40	615	602

3.2.2. Refraction Seismic Tomography

3.2.2.1 Regularization

The regularization method was applied to the seismic line obtained in the experiment. The tomographic inversion algorithm was run up to the maximum number of iterations allowed by the software, checking convergence in all cases.

To draw the L-curve we start with the vertical smoothing value 1, which is no smoothing. Next, we obtain the tomography solutions with all values of the horizontal smoothing parameter from 0.3 to 0.9. In **Figure. 5A**, we can see the RMS convergence for all values of the horizontal smoothing value from 0.3 to 0.9. We plot the L curve with the ℓ2 model norm (L2 norm) in **Figure. 5B**, with the ℓ1 model norm (L1 norm) in **Figure. 5C**, and with the ℓ ∞ norm (inf norm) in **Figure. 5D**.

We clearly see that with **ℓ2, ℓ1**, and **ℓ∞** norms, the value of the error norm decreases as we increase the horizontal smoothing parameter. From the value 0.8, marked on the graphs with an arrow, the decreasing error rate slows down, and the model norm increases sharply, obtaining the characteristic L-shape. In the ℓ2, ℓ1, and ℓ∞ norms the parameter 0.8 (green dot) gives us less error.

In **Figure. 6**, we can see the a priori model. The result of tomography with the regularization parameters 1.0 vertical and 0.8 horizontal are in **Figure. 7**. The velocity values recover well after inversion. However, the tomographic solution loses the sharpness of the vertical discontinuities in the synthetic model, even if we work with the minimum smoothing values. For this reason, it is essential to find the regularization with the highest values of horizontal and vertical parameters of the SeisImager software, which are the lowest smoothing values. We can see from the experiments that only sometimes is it possible, and sometimes we need to introduce smoothing to obtain an L-curve and therefore a regularization.

However, setting the vertical smoothing parameter and varying the horizontal parameter is the best strategy to obtain a regularization with the lowest smoothing. On the other hand, we need more smoothing to regularize if we set the vertical parameter to 1.0 and vary the horizontal parameter. This result can be attributed to the fact that we need some vertical smoothing in a stratified model because the main variations of the model a priori are vertical. The seismic profile obtained along 69 meters, with a final RMS of 3.50 ms, revealed three distinct seismostratigraphic units as a function of P-wave velocities (**Figure. 7**). These units are described below.

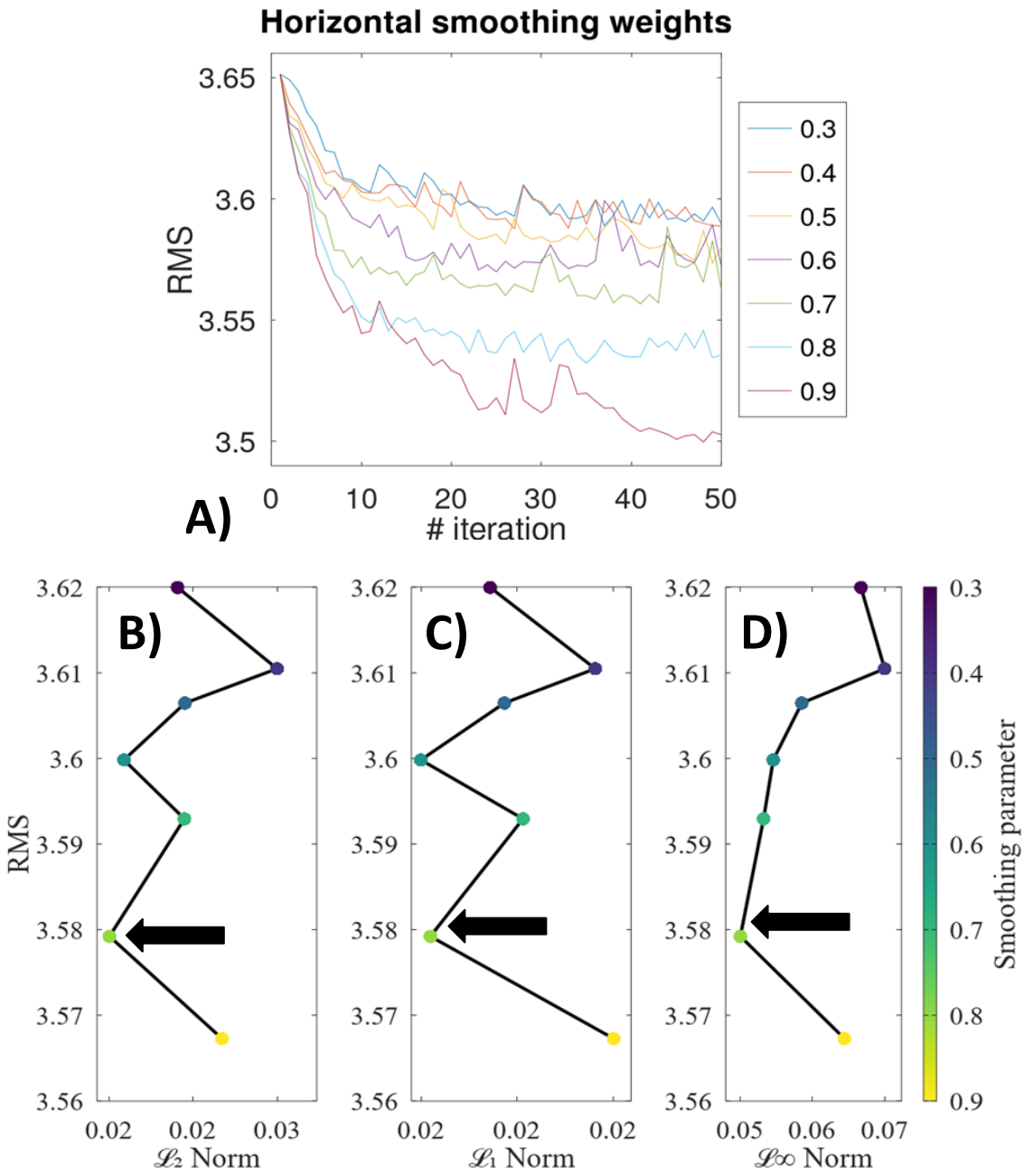

Figure 5. Regularization. A) RMS convergence of the tomography for all horizontal parameter values, with a fixed vertical smoothing parameter of 1. A total of 50 iterations were performed, showing that all initial values converge except the test with a 0.3 smoothing parameter with high oscillations. B) The L curve for norm ℓ2, C) The L curve for norm ℓ1, and D) The L curve norm ℓ∞. The vertical axis represents the RMS, while the horizontal axis corresponds to the norm values. The optimal regularization parameter is identified at the corner point, marked with a black arrow at 0.8 in all three cases.

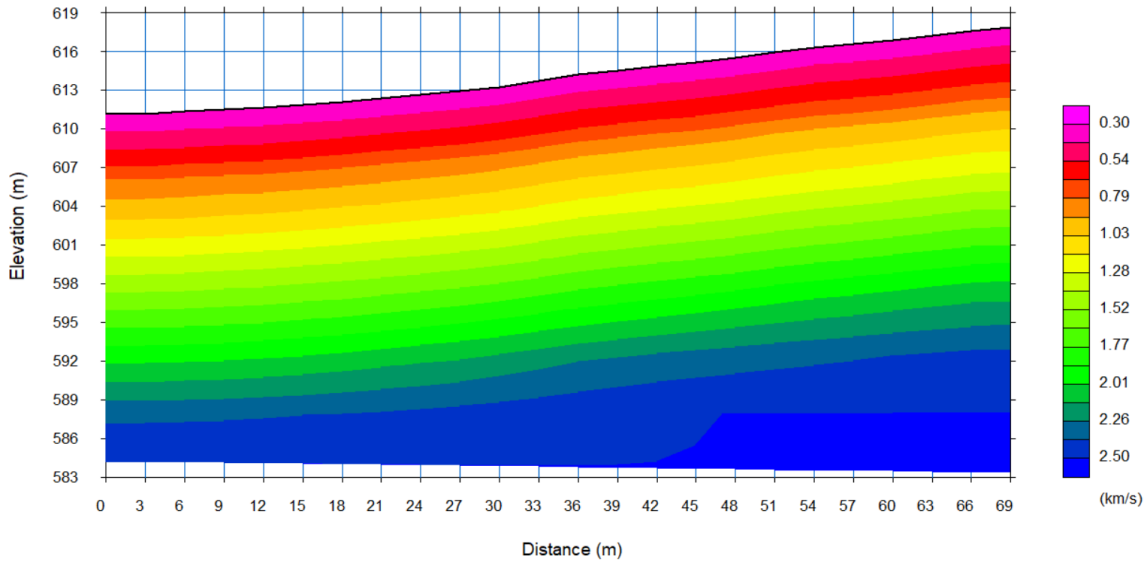

Figure 6. A priori model. The initial model of the seismic tomography reflection is present with gamma of colors revealing velocities between 0.30 (Pink) to 2.50 (Blue). This model has 69 m of distance and its elevation starts at 584 m and finally at 618 m.

3.2.3. Seismostratigraphic description

Based on the observed geometry (thickness and deformation) and the average seismic velocities in the seismic tomography of the line, it is possible to distinguish three seismostratigraphic units (**Figure. 7**). Their characteristics are outlined below.

Unit 1 is the most superficial. It is located between 0 and 8 meters. Its lower boundary is defined by a change in the lateral behavior of seismic velocities, which vary between 0.4 and 0.7 km/s. At the SW end, between 0 and 6 meters, the thickness fluctuates between 5 and 5.5 meters with NE-SW dip. From 6 to 9 meters, the thickness increases from 5.5 to 8 meters with SW-NE dip. Subsequently, from 9 to 22.5 meters, the unit shows a progressive thinning from 8 to 5 meters, indicating significant deformation at the base. In the central part of the profile (between 22.5 and 42.5 meters), the thickness varies between 4 and 5 meters, showing some deformation. From 42.5 meters to the NE end (69 meters), slight deformations are observed, although the thickness remains constant at 5 meters, with NE-SW inclination.

Unit 2 is the intermediate unit. It is located between 8 and 12.5 meters depth. The boundary with the lower unit is proposed from the difference in deformation frequency. It has average seismic velocities between 0.7 and 1.1 km/s (Figure 7). The unit has a wedge-shaped geometry. At the SW end, between 0 and 6 meters, its thickness varies from 6 to 8.5 meters, with a lower NE-SW dip. Between 6 and 9 meters, the thickness decreases from 8.5 to 5.5 meters taking a SW-NE dip. Then, from 9 to 22.5 meters, the thickness stabilizes around 6 meters with a NE-SW dip. From 42 to 63 meters, a deformation that alters the inclination of the unit is observed. However, beyond 63 meters, no major structural changes are identified and the unit maintains an approximate thickness of 6.5 meters up to the NE end (69 meters). Dip changes, along with thickness variations, indicate the presence of folds of greater amplitude and more pronounced deformation than in Unit 1.

Unit 3 is the deepest unit illuminated in the exploration. It is located between 12.5 and 25 meters depth (vertical limit of acquisition). It has average seismic velocities between 1.1 and 2.4 km/s (Fig. 7). Like unit 2, unit 3 has a wedge geometry, where the lowest thickness is at the SW end with 5 m and the highest at the NE end with 13 m. From the SW end, between 0 and 9 meters distance, the thickness remains constant at 5 meters, with a slight SW-NE inclination. Between 9 and 24 meters, the thickness increases progressively from 5 to 9.5 meters, accompanied by a marked NE-SW slope. Finally, from 24 to 54 meters, the thickness varies from 9.5 to 13 meters, with a gentler dip in the same direction (NE-SW).

Towards the SW end, the folds exhibit greater amplitude and wavelength, causing variations in unit dips. This suggests the presence of differential stresses that have affected the geometry and arrangement of the strata.

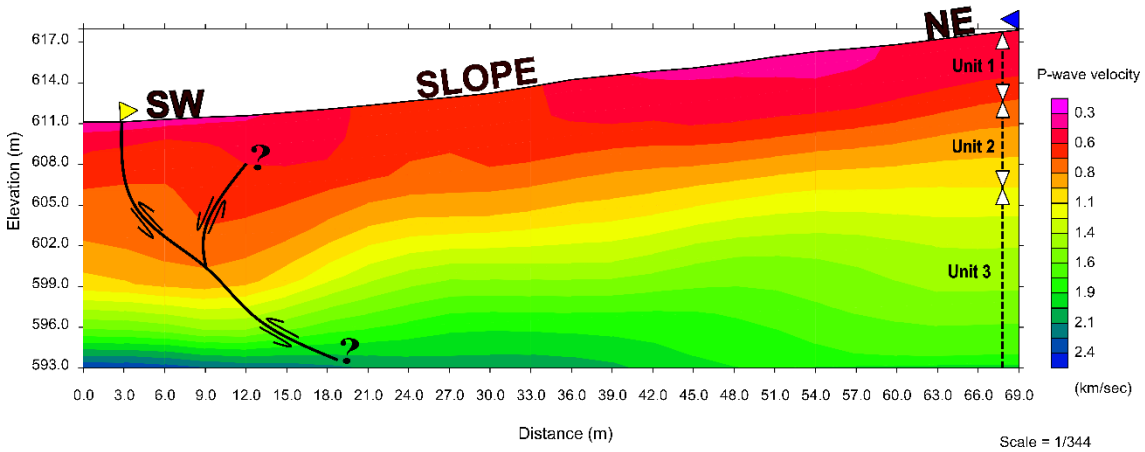

Figure 7. Seismostratigraphic and structural interpretation of the line. The 69-meter-long seismic profile (oriented SW-NE) illustrates elevation on the vertical axis (in meters) and distance on the horizontal axis (in meters). The yellow triangulum marks the beginning of the slope and the approximate location of the surface trace of the fault, while the blue identifies the point where the terrain levels off. The color scale on the right represents P-wave velocities (in km/s), with values ranging from 0.3 km/s (pink) to 2.4 km/s (dark blue). The seismostratigraphic units interpretation is in the NE part of the line (dashed line), with no noticeable deformation and maximum elevation. The Porotoyacu fault and the antithetic fault are indicated in the figure with a black line. The kinetamica of both are indicated by arrows.

3.3 DISCUSSION

3.3.1. Porotoyacu Fault extensión

The primary objective of this study was to assess the southern extension of the Porotoyacu Fault, as understanding implies a greater length, which impacts hazard evaluation.

The analysis of slope values and morphology revealed anomalies that align with the proposed extension of the Porotoyacu Fault. The topographic profiles (**Figure. 2 and see Table. 1**) generated from the DEM consistently show variations in slope morphology, particularly in the transition zones where steep slopes begin. These anomalies are interpreted as evidence of fault-related activity, confirming the fault's extension.

The Porotoyacu Fault, oriented NE-SE, was mapped with a total length of 610 meters. Of this, 430 meters remain unaffected by anthropogenic activities, while 180 meters are impacted by urban infrastructure. In contrast to the work of Costa *et al.,* (2020), which

relied on regional photo interpretation, our study utilized a DEM of 22 cm/pix. While Costa *et al.,* (2020) proposed a more westerly fault trace, our findings indicate an eastward extension of the fault, with a further prolongation to the south.

This refinement underscores the value of integrating high-resolution data with geomorphic analyses to improve fault mapping accuracy, especially in regions with complex tectonic and erosional processes (e.g., Johnson *et al.,* 2014; Ren *et al.,* 2023).

3.3.2. Subsurface Fault Geometry

We obtain the following interpretation from the deformation observed in the three seismostratigraphic units (**Figure 7**). These units show concordant deformation among them (except for the upper zone towards the southwest), indicating that the same structural elements and deformational events affect all three units. In the áreas of greatest deformation, located towards the ends of the profile, the structures exhibit a downward concave geometry.

However, the axial axes of these concavities are not vertically aligned between units, suggesting that the deformation is associated with faulting rather than simple folding, which would be characterized by vertical axial planes. The concavities are found at greater depth compared to neighboring sectors without concavity. This indicates that the stress regime responsible for the deformation is compressional, at least at the scale of the observed structures. The wave amplitudes of the deformations increase towards the shallower units (unit 1), while their lengths decrease. This variation suggests that the vertical shear strength is higher in the lower units than in the upper units.

From these observations, the first time that the geometry of the Porotoyacu Fault has been observed at shallow depths (shallower than 25 meters) characterized by a low angle at depth and a high angle towards the surface is proposed. This fault affects at least the basal part of unit 1 and the middle zone of unit 3. In addition, an antithetical

fault that affects only the upper part of unit 2 and at least the basal part of unit 1. This confirms the presence of the fault to the south and coincides with the surface anomalies.

3.3.3. Fault Classification

The Porotoyacu Fault is part of the Cutucú-Napo Fault System, the easternmost and most active deformation belt in the Ecuadorian sub-Andean region. This system, characterized by thin-skinned tectonics affecting Mesozoic and Cenozoic deposits, is responsible for the eastward propagation of a continental accretionary wedge (Bès de Berc, 2003; Legrand et al., 2005). Generally, the faults of this system show eastward vergences, in agreement with the compressional regime generated by the subduction of the Nazca plate under the South American plate (Kellogg & Vega, 1995; Trenkamp et al., 2002).

The analysis of the seismic profile of the Porotoyacu Fault reveals a southwestward (SW) vergence, evidenced by the movement of the hanging block in that direction. This observation aligns with the geological characteristics of the surface units, where the Napo Formation is exposed to the east at higher elevations compared to the Tena Formation to the west. Such a relief difference cannot be explained solely by folding, supporting the interpretation of the Porotoyacu Fault as a backthrust. This fault's geometry, with a steeper dip at the surface and a gentler dip at depth, further corroborates its classification as a backthrust fault. According to Saklani (2008) and Kearey (1993), backthrusts are reverse faults with a vergence opposite to the predominant tectonic transport direction in the region.

3.4 CONCLUSIONS

The high-resolution aerial photogrammetry data enabled the precise identification of the Porotoyacu Fault's surface trace, revealing an extension of approximately 610 meters to the south. This extension was determined through the detection of topographic anomalies in the generated profiles, which consistently showed variations in slope morphology, particularly at the transition zones where steep slopes begin. The

fault aligns with the frontal slope of an anticline, which is more extensive than previously observed in the seismic line. On the other hand, seismic tomography data provided detailed insights into the subsurface seismostratigraphic and structural characteristics. Three seismostratigraphic units were identified, all affected by a compressional structure interpreted as the Porotoyacu Fault and an antithetic fault. The fault exhibits a low-angle geometry at depth, transitioning to a steeper dip towards the surface, consistent with a backthrust mechanism. This subsurface geometry aligns with the surface observations, confirming the fault's continuity and its influence on both surface and subsurface structures

Acknowledgments

This research was carried out with the support of the Earth Sciences and Climate Research Group of the Universidad Regional Amazónica Ikiam and in the framework of projects CTC-006-2020, CTC-010-2024 and IGCP-669-Ollin. Especially for their valuable support and for the knowledge of the expert paleoseismologists who helped in the realization of this work. Likewise, we thank the community of the Las Veronicas neighborhood for their welcome and for permission to conduct work at the site. SL received 3 scholarships for academic excellence during 2023-2024 and HC 1 scholarship in 2022 from Ikiam University, they also received the following scholarships together: scholarship from the IGCP-669-Ollin-UNESCO project to attend a seismic hazard course in Bogotá, scholarship to be a speaker at the REDU international scientific congress developed in Ikiam, international mobility scholarship for work of excellence by Ikiam University for the international congress PATAdays 2024.

REFERENCES

Alvarado, A. (2012). Néotectonique et cinématique de la déformation continentale en Equateur. [Thèse de Doctorat, Université de Grenoble]. https://theses.hal. science/tel-00870332

Alvarado, A., Audin, L., Nocquet, J. M., Lagreulet, S., Segovia, M., Font, Y., Lamarque, G., Yepes, H., Mothes, P., Rolandone, F., Jarrín, P., & Quidelleur, X. (2014). Active tectonics in Quito, Ecuador, assessed by geomorphological studies, GPS data, and crustal seismicity. Tectonics, 33(2), 67–83. https://doi.org/10.1002/2012tc003224

Alvarado, A., Audin, L., Nocquet, J. M., Jaillard, E., Mothes, P., Jarrín, P., Segovia, M., Rolandone, F., & Cisneros, D. (2016). Partitioning of oblique convergence in the Northern Andes subduction zone: Migration history and the present-day boundary of the North Andean Sliver in Ecuador. Tectonics, 35(5), 1048–1065. https://doi.org/10.1002/2016TC004117

Araujo, S., Guzmán, O., Guamán, A., Espín, R., García, I., & Chulde, E. (2023). Seismic refraction tomography in San Luis, headward Coca River erosion zone. Journal of Applied Geophysics, 212, 104981. https://doi.org/10.1016/j.jappgeo.2023.104981

Araujo, S., Guzmán, O., Rubio, R., Guerrero, P., Rojas, E., Moposita, W., García, I., Puetate, M. F., & Guamán, A. (2024). Seismic surveys and inverse problems regularization in the Ecuadorian Amazon. In L. M. Quishpe, P. Aramburuzabala, H. M. Ortega-Andrade, C. Ávila, R. Espinosa, & M. Herrera-Robledo (Eds.), Nature Based Living Lab (pp. 74-97). CEDIA.

Baize, S., Audin, L., Alvarado, A., Jomard, H., Bablon, M., Champenois, J., Espin, P., Samaniego, P., Quidelleur, X. & Le Pennec, J.-L. (2020). Active Tectonics and Earthquake Geology Along the Pallatanga Fault, Central Andes of Ecuador. Frontiers in Earth Science, 8, 1-21. doi: 10.3389/feart.2020.00193

Beauval, C., Marinière, J., Yepes, H., Audin, L., Nocquet, J. M., Alvarado, A., Baize, S., Aguilar, J., Singaucho, J. C., & Jomard, H. (2018). A new seismic hazard model for Ecuador. *Bulletin of the Seismological Society of America*, *108*(3), 1443–1464. https://doi.org/10.1785/0120170259

Bemis, S. P., Micklethwaite, S., Turner, D., James, M. R., Akciz, S., Thiele, S. T., & Bangash, H. A. (2014). *Ground-based and UAV-Based photogrammetry: A multi-scale, high-resolution mapping tool for structural geology and paleoseismology.* Journal of Structural Geology, 69, 163–178. https://doi.org/10.1016/j.jsg.2014.10.007

Bi, H., Zheng, W.-J., Ren, Z., Zeng, J., & Yu, J. (2016). Using an unmanned aerial vehicle for topography mapping of the fault zone based on structure from motion photogrammetry. International Journal of Remote Sensing, 38, 1–16. https://doi.org/10.1080/01431161.2016.1249308

Carranco, F., Romero, C., & Calderón, E. (2023). Catálogo de edades radiométricas de Ecuador.

Chunga, K., Michetti, A., Gorshkov, A., Panza, G., Soloviev, A., & Martillo, C. (2010). Identificación de nudos Sismogénicos Capaces de Generar Potenciales Terremotos de M>6 y M>6,5 en la Región Costera

y Cadenas Montañosas de los Andes septentrionales del Ecuador. *Revista Tecnológica ESPOL-RTE*, *23*(December), 61–89.

Cornejo, C., Guzman, O., Campos, C., & Cargua, J. (2024). Análisis paleosismológico en la Zona Subandina de Ecuador. Implicaciones para la Falla Porotoyacu. En Geociencias en la en la Amazonía ecuatoriana: Aportes a la planificación sostenible (1.a ed.). CEDIA. https://doi.org/10.48661/w6dc-q685

Costa, C., Alvarado, A., Audemard, F., Audin, L., Benavente, C., Bezerra, F.H., Cembrano, J., González, G., López, M., Minaya, E., Santibañez, I., Garcia, J., Arcila, M., Pagani, M., Pérez, I., Delgado, F., Paolini, M., Garro, H. (2020). Hazardous faults of South America; compilation and overview. Journal of South American Earth Sciences, 104, 102837. doi: 10.1016/j.jsames.2020.102837

Díaz, M., Baby, P., Rivadeneira, M., & Christophoul, F. (2004). El pre-aptense en la cuenca oriente ecuatoriana. In P. Baby, M. Rivadeneira, & R. Barragán (éds.), La Cuenca Oriente: Geología y petróleo (1-). Institut français d'études andines. https://doi.org/10.4000/books.ifea.2989

Ego, F., Sébrier, M., Lavenu, A., Yepes, H., & Egues, A. (1996). Quaternary state of stress in the Northern Andes and the restraining bend model for the Ecuadorian Andes. *Tectonophysics*, *259*, 101–116. https://doi.org/10.1016/0040-1951(95)00075-5

Egüez, A., Alvarado, A., Yepes, H., Machette, M.N., Costa, C., Dart, R.L. & Bradley, L. (2003). Database and map of Quaternary faults and folds of Ecuador and its offshore regions. US Geological Survey Open-File Report 03-289 3, 289. https://pubs.usgs.gov/of/2003/ofr-03-289/

Eltner, A., & Sofia, G. (2020). Structure from motion photogrammetric technique. En P. Tarolli & S. M. Mudd (Eds.), Remote Sensing of Geomorphology (Vol. 23, pp. 1–24). Elsevier. https://doi.org/10.1016/B978-0-444-64177-9.00001-1

Font, Y., Segovia, M., Vaca, S., Theunissen, T., (2013). Seismicity patterns along the Ecuadorian subduction zone: new constraints from earthquake location in a 3-D a priori velocity model. Geophysical Journal International 193, 263–286.https://doi.org/10.1093/gji/ggs083

Galone, L., Villani, F., Colica, E., Pistillo, D., Baccheschi, P., Panzera, F., Galindo-Zaldívar, J., & D'Amico, S. (2024). Integrating near-surface geophysical methods and remote sensing techniques for reconstructing fault-bounded valleys (Mellieha valley, Malta). Tectonophysics, 875, 230263. https://doi.org/10.1016/j.tecto.2024.230263

Geometrics Inc., 2009. SeisImager/2DTM Manual (Version 3.3). Available at:https://ge ometrics.com/wp-content/uploads/2019/05/SeisImager2D_Manual_v3.3.pdf

Graveleau, F., Strak, V., Dominguez, S., Malavieille, J., Chatton, M., Manighetti, I., & Petit, C. (2015). Experimental modelling of tectonics–erosion–sedimentation interactions in compressional, extensional, and strike–slip settings. Geomorphology, 244, 146–168. https://doi.org/10.1016/j.geomorph.2015.02.011

Gutscher, M. A., Malavieille, J., Lallemand, S., & Collot, J. Y. (1999). Tectonic segmentation of the North Andean margin: Impact of the Carnegie Ridge collision. *Earth and Planetary Science Letters*, *168*(3–4), 255–270. https://doi.org/10.1016/S0012-821X(99)00060-6

Hansen, P. C. (1992). Analysis of discrete ill-posed problems by means of the L-curve. SIAM Review, 34(4), 561–580. https://doi.org/10.1137/1034115

Instituto Geofísico de la Escuela Politécnica Nacional (IGEPN) (2024). Seismic Catalog 2012-Present. Geophysical Institute - EPN. Retrieved from http://www.igepn.edu.ec

Jomard, H., Saqui, D., Baize, S., Alvarado, A., Bernard, B., Audin, L., Hidalgo, S., Pacheco, D., Ruiz, M., & Segovia, M. (2021). Interactions between active tectonics and gravitational deformation along the Billecocha fault system (Northern Ecuador): Insights from morphological and paleoseismological investigations. *Journal of South American Earth Sciences*, *111*(May). https://doi.org/10.1016/j.jsames.2021.103406

Kellogg, J. N. & Vega V. (1995). Tectonic development of Panama, Costa Rica, and the Colombian Andes: Constraints from Global Positioning System geodetic studies and gravity. Geological Society of America Special Paper 295, 75-90.

Kendrick, E., Bevis, M., Smalley, R., Brooks, B., Vargas, R. B., Lauría, E., & Fortes, L. P. S. (2003). The Nazca–South America Euler vector and its rate of change. Journal of South American Earth Sciences, 16(2), 125-131. https://doi.org/10.1016/S0895-9811(03)00028-2

Legrand, D., Baby, P., Bondoux, F., Dorbath, C., Bès de Berc, S., & Rivadeneira, M. (2005). The 1999–2000 seismic experiment of Macas swarm (Ecuador) in relation with rift inversion in Subandean foothills. Tectonophysics, 395(1-2), 67–80. https://doi.org/10.4000/books.ifea.3013

Legrand, D., Baby, P., Bondoux, F., Dorbath, C., Bès de Berc, S., & Rivadeneira, M. (2004). El enjambre sísmico de Macas (cordillera de Cutucú). In P. Baby, M. Rivadeneira, & R. Barragán (eds.), La Cuenca Oriente: Geología y petróleo (1–). Institut français d'études andines. https://doi.org/10.4000/books.ifea.3013

Maldonado, V., Contreras, M. & Melnick, D. A comprehensive database of active and potentially-active continental faults in Chile at 1:25,000 scale. Sci Data 8, 20 (2021). https://doi.org/10.1038/s41597-021-00802-4

McCalpin, James P & Nelson, A. R. (2009). Introduction to paleoseismology. In *International Geophysics* (1st ed., Vol. 95, pp. 1–27). Elsevier Inc. https://doi.org/10.1016/S0074-6142(09)95001-X

Molins-Vigatà, J., García-Mayordomo, J., Ortuño, M., García-Sellés, D., & Gómez-Novell, O. (2022). Caracterización geológica de la falla del Llano del Águila en Campo Dalías (Almería): posible fuente sismogénica del terremoto de 1804. Revista De La Sociedad Geológica De España, 35(1), 71–83. https://doi.org/10.55407/rsge.94908

Nocquet, J., Villegas-Lanza, J., Chlieh, M., Mothes, P., Rolandone, F., Jarrin, P., Cisneros, D., Alvarado, A., Audin, L., Bondoux, F., Martin, X., Font, Y., Régnier, M., Vallée, M., Tran, T., Beauval, C., Maguiña Mendoza, J., Martinez, W., Tavera, H. & Yepes, H. (2014). Movimiento de astillas continentales y subducción rastrera en el norte de los Andes. Nature Geoscience, 7(4), 287-291.

Papanikolaou, I. D., van Balen, R., Silva, P. G., & Reicherter, K. (2015). Geomorphology of active faulting and seismic hazard assessment: New tools and future challenges. Geomorphology, PII: S0169-555X(15)00107-5. https://doi.org/10.1016/j.geomorph.2015.02.024

Rodríguez, E. E., Beck, S. L., Ruiz, M., Meltzer, A., Portner, D. E., Hernández, S., Segovia, M., Agurto-Detzel, H., & Charvis, P. (2024). Seismic imaging of the Northern Andean subduction zone from teleseismic tomography: a torn and fragmented Nazca slab. Geophysical Journal International, 236(1), 593–606. https://doi.org/10.1093/gji/ggad421

Santos, E. T. F., & Bassrei, A. (2007). L- and Θ-curve approaches for the selection of regularization parameter in geophysical diffraction tomography. Computers & Geosciences, 33(5), 618–629. https://doi.org/10.1016/j.cageo.2006.08.013

Sheehan, J., Doll, W., & Mandell, W. (2005). An evaluation of methods and available software for seismic refraction tomography analysis. Journal of Environmental and Engineering Geophysics, 10(1), 21–34. https://doi.org/10.2113/JEEG10.1.21

Trenkamp, R., Kellogg, J. N., Freymueller, J. T., & Mora, H. P. (2002). Wide plate margin deformation, Southern Central America and Northwestern South America, CASA GPS observations. Journal of South American Earth Sciences, 15(2), 157–171. https://doi.org/10.1016/S0895-9811(02)00018-4

Valkanou, K., Karymbalis, E., & Tsanakas, K. (2024). Identification of geomorphic and morphotectonic features using geographic information system techniques. En G. P. Petropoulos & C. Chalkias (Eds.), Geographical Information Science (pp. 3–28). Elsevier. https://doi.org/10.1016/B978-0-443-13605-4.00009-6

Vasuki, Y., Holden, E., Kovesi, P., & Micklethwaite, S. (2014). Semi-automatic mapping of geological Structures using UAV-based photogrammetric data: An image analysis approach. Computers & Geosciences, 69, 22–32. https://doi.org/10.1016/j.cageo.2014.04.012

Westoby, M., Brasington, J., Glasser, N., Hambrey, M., & Reynolds, J. (2012). 'Structure-from-Motion' photogrammetry: A low-cost, effective tool for geoscience applications. Geomorphology, 179, 300–314. https://doi.org/10.1016/j.geomorph.2012.08.021

White, D. J. (1989). Two-dimensional seismic refraction tomography. Geophysical Journal International, 97(2), 223–245. https://doi.org/10.1111/j.1365-246X.1989.tb00498.x

Wu, Z., & Hu, M. (2019). Neotectonics, active tectonics and earthquake geology : terminology, applications and advances. Journal of Geodynamics, 127, 1–15. https://doi.org/10.1016/j.jog.2019.01.007

Yepes, H., Audin, L., Alvarado, A., Beauval, C., Aguilar, J., Font, Y., & Cotton, F. (2016). A new view for the geodynamics of Ecuador: Implication in seismogenic source definition and seismic hazard assessment. Tectonics, 35(5), 1249–1279. https://doi.org/10.1002/2015TC003941

Zhdanov, M.S., 2015. Inverse theory and applications in geophysics, vol. 36. Elsevier.

Manuscrito a someter a la revista "Quaternary International".

CAPÍTULO 4. DETERMINATION OF THE ACTIVE TECTONIC ACTIVITY OF THE POROTOYACU FAULT, SUB-ANDINE OF ECUADOR APPLY MORPHOTECTONIC, MORPHOLOGIC, AND PALEOSEISMOLOGY ANALYSIS

Samira Lluno[1] https://orcid.org/0009-0002-2899-9007

Henry Conteron[1] https://orcid.org/0009-0004-8681-3594

[1]Universidad Regional Amazónica Ikiam, Tena, Napo, Ecuador.

ABSTRACT

Knowledge about the neo-tectonic activity of a region is important to evaluate seismic risk, protect infrastructure, and plan land use safely and sustainably. Despite this, the neo-tectonic activity of the Sub-Andean Zone of Ecuador has not been thoroughly studied in depth. This is the case of the Porotoyacu Fault, which crosses the cities of Tena and Archidona in the province of Napo. This geological structure has an SSW-NE orientation, with seismic event magnitudes that have only been calculated from one trench study, while its active tectonics remain poorly understood. The objective of the investigation is to determine the paleo-seismicity and recent tectonic activity in an anthropogenic outcrop. To achieve this, morphotectonic, morphological, and paleoseismological analyses were conducted using satellite imagery and field observation in an outcrop. The paleoseismological study is based on the observation of ruptures and measured vertical displacements to identify the number of earthquakes. Similarly, the identification of seismites is another way to estimate the magnitude. In the study área were identified two paleo-ruptures (R1 and R2). R1 with normal cinematic has two seismic events with a $6.68 < Mw < 6.70$ and $Ms = 6.9$. R2 with reverse cinematic has only $6.13 < Mw < 6.51$ and $Ms = 6.24$. Between the seismites identified are load cast, flame structures, pseudonodules, and dykes. All evidence found such as surface deformation and seismites in the upper units on the outcrop indicated a recent tectonic activity in this section of the Porotoyacu Fault.

Keywords: Active fault, deformation, Porotoyacu Fault, Morfotectonic, Seismites

4.0 INTRODUCTION

Seismicity in Ecuador is primarily controlled by the subduction zone of the Plates of Nazca and South America **(Figure 1)**. These plates are localized at a depth of 90 to 110 km (Trenkamp *et al*., 2002; Anderson *et al*., 2007; Rodriguez *et al*., 2024). The displacement rate between these plates is 56 mm/year to the North and 60 mm/year to the South (Nocquet *et al.*, 2014). For this reason, Ecuador is characterized by mild to moderate seismicity (Chunga et al., 2010; Font et al., 2013)

Previous investigations identified 92 surface-active faults in Ecuador by photo-interpretation of satellite imagery (Egüez *et al*., 2003). However, current research has recognized at least 400 segments of active faults (Alvarado, 2012; Costa *et al*., 2020) capable of producing earthquakes with a magnitude ranging from Mw 4.5 to 7.8 (Chunga *et al*., 2010; Font *et al*., 2013). These seismogenic sources significantly contribute to seismic hazard in the region.

The Sub-Andean Zone experiences earthquakes with magnitudes Mw 4.5 or less (IGEPN, 2024). However, there are records of atypical events $M_w 6.1 \; and \; 6.9$, in the northwestern Oriental Andes, whose epicenter is located in Napo province (Kawakatsu & Cadena, 1991). An additional example is the studies by Alvarado et al., (1996, 2016) and Yepes et al., (1996), which link two seismic events a Baeza in 1987 with a M_w =7.1 related to a fault system called CCPP and another earthquake $M_w = 7.0$ in 1995 to the fault systems known as Cutucú-Napo. These events demonstrate a high seismicity in the Ecuadorian Amazon.

In this context, the Cutucú-Napo fault system is located in the Sub-Andean Zone and represents a significant seismic hazard due to its activity in the northern Amazon region (Bès de Berc, 2003; Alvarado *et al*., 2016). Its component faults result from tectonic inversions of normal faults, therefore, the faults are currently reversed (Baby *et al*., 2004; Legrand *et al*., 2005). In 2020 the South America Risk Assessment Project (SARA)

established a new geological structure belonging to this system: the Porotoyacu Fault (Costa *et al.*, 2020).

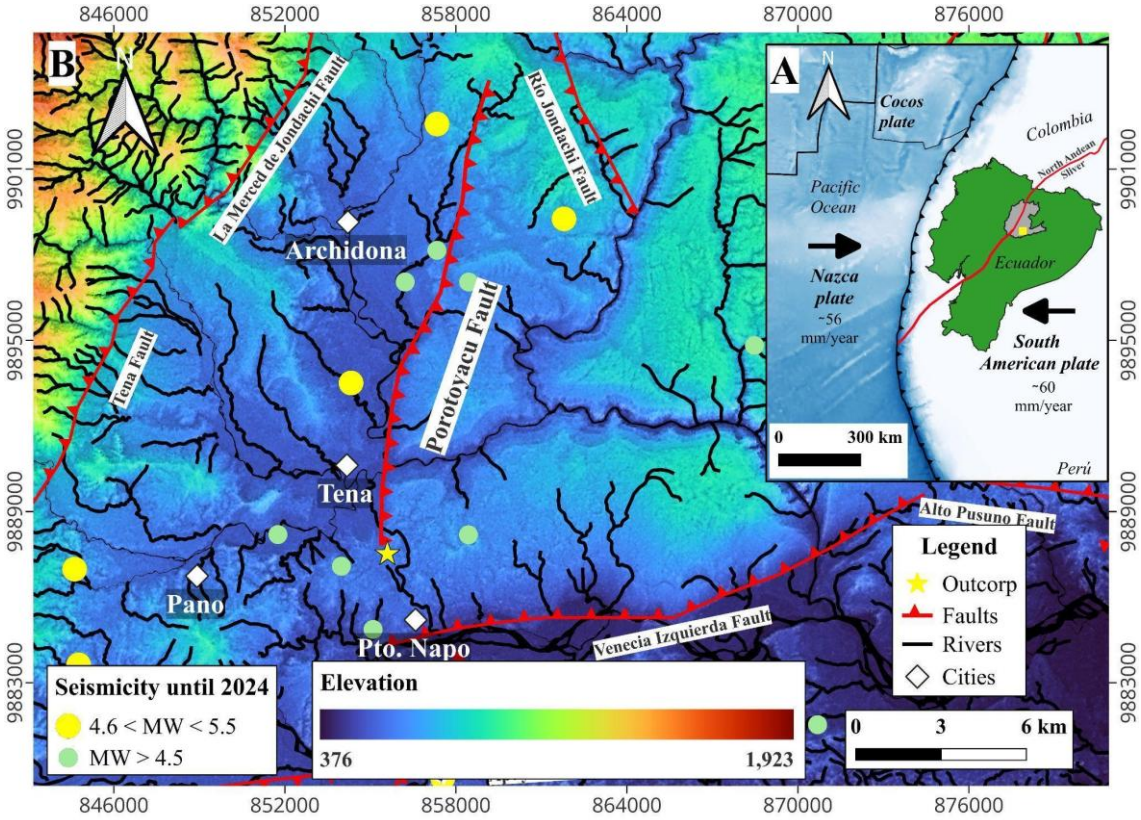

Figure 1: Ubication of the study area: A) Regional location of the study área: In the Ecuadorian territory base map from ESRI. The black line in the limit represents the contact and direction movement of the Nazca and South American plates. The presence of the North-Andean Splinter is a red line that divides two blocks of Ecuador. The yellow square delimits the study área. B) Ubication of the Porotoyacu Fault and study área in Napo (DEM corresponding to the ALOS PALSAR product, obtained from the Alaska Satellite Facility (ASF)): The numerous red lines represent geologic faults that cross the country. The yellow star represents the outcrop where the paleo-seismological study is performed. The big red line in the center represents the Porotoyacu Fault with its kinematics of Project SARA (Costa et al., 2020), and the red rectangles represent the cities. The yellow and green circles are seismic events close to the Porotoyacu Fault. The map contains the topographic base, instrumental earthquakes as points until 2024, rivers, and the population centers of Tena and Archidona.

Porotoyacu Fault has transcurrent-reverse kinematics with SSW-NE orientation, this structure crosses the towns of Tena and Archidona in the Napo Province **(Figure 1).** This structure, classified as quaternary, has a length of 15 kilometers, with its last activity dated to 1.8 Ma (Costa *et al*., 2020). However, this data is based on photo interpretation by satellite images and not directly with fieldwork. For this reason, the precise trace, length, recent seismic events, and magnitudes remain uncertain. The limited

understanding of the recent tectonics of the Porotoyacu Fault created the need to apply an analysis of morphotectonic, morphological, and paleoseismology to obtain more information about its behavior.

First, according to McCalpin & Nelson (2009), it's possible to study paleo-seismic events recorded in stratigraphy through vertical displacements, which allows us to deduce the number of events and calculate their magnitude. On the other hand, soft-sediment deformation structures can be identified and characterized as being caused by various phenomena. However, when they are caused by earthquakes, they are nominated as seismites (Seilacher, 1969).

The seismites are products of liquefaction/fluidization process and their analysis allows the estimation of magnitudes (Audemard & de Santis, 1991; Bhattacharya & Bandyopadhyay, 1998; Rodríguez-Pascua *et al*., 2000; Montenat *et al*., 2007; Masana *et al*., 2011; Lafuente *et al.,* 2008; Benhamouche *et al*., 2014). The elements mentioned are of great interest in paleo-seismological studies since they provide information about tectonic history.

In Ecuador, paleo-seismological studies have primarily focused on the highlands, where population density is higher. For instance, significant research efforts have been conducted on the Pallatanga Fault and the Billecocha Fault System, located north of Quito (Baize *et al*., 2015, 2020; Jomard *et al*., 2021). In contrast, only one paleo-seismological study has been developed in the Ecuadorian Amazon. This study was performed by Cornejo *et al*., (2024) located 1.67 km South of the trace, conducted in an outcrop that revealed seismic evidence such as ruptures and seismites associated with the Porotoyacu Fault.

The research work aims to evaluate the Porotoyacu Fault as an active seismogenic source in a section located South of the trace of this fault, applying morphotectonics, morphological, and paleo seismological analysis in an outcrop to contribute information about seismic risk.

4.0.1 Tectonic and seismic setting of study área

The geodynamic context to which Ecuador is subjected, converter the Ecuadorian Andes in a region with high seismicity, with a displacement rate of $56\,mm/year\ to\ North\ and\ 60\,mm/year\ to\ South$ (Trenkamp *et al*., 2002, Kendrick *et al*., 2003, Rodríguez *et al.,* 2024). The compression of plates of Nazca and South America has an E-W orientation (Ego *et al*., 1996; Gutscher *et a*l., 1999), generating bigger systems of superficial active faults and causing slight to moderate seismicity (Baby *et al.*, 2004; Alvarado, 2012; Cajamarca-Zuniga & Kabantsev, 2023).

This tectonic activity has resulted in the presence of several seismogenic sources and fault systems including the Quito, Latacunga, Chingual-Cosanga-Pallatanga-Puna (CCPP), Pallatanga-Puna, and Cutucú-Napo systems, among others (Alvarado, 2012, 2016; Yepes *et al*., 2016), which are distributed in various regions of Ecuador. In this research, we focus on the Cutucú-Napo system, located in the Sub-Andean zone, extending northward through Napo Province to Puyo and Pastaza (Bès de Berc, 2003). The Sub-Andean zone is formed by the Napo uplift from NO and the Cutucú mountain range from SO (Baby et al., 2004) where formations Triassic-Jurassic are deformed by the fault system Cutucú-Napo (Legrand et al., 2004, Pratt et al., 2005, Beauval et al., 2018).

The system Cutucu-Napo is controlled for deformations compressive-transgressive (Baby *et al*., 1999; Pratt *et al*., 2005) and is configured by reverse faults with high angles with N-S and NNE-NNW orientations (Baby *et al*., 2004). Seismic events in the region are generally of lower magnitude. However, recorded instrumentally earthquakes with atypical magnitude have occurred. For instance, on 5 March 1987 two earthquakes of magnitude 6.1 to 6.8 were recorded in the Sub-Andean Amazon (Hall, 2011). Additionally, other investigations have linked two earthquakes occurring in Macas (Mw 7.0, 1995) and Baeza (Mw 7.1, 1987) to the Cutucú-Napo fault system (Legrand *et al*., 2005; Font *et al*., 2013).

Between 1927-2024, approximately 24 seismic events of Mw 2.5~6.3 have been instrumental records close to this fault system, as visualized in **Figure 1** (IGEPN, 2024). Characterizing the region with slight and moderate seismicity (Beauval *et al*., 2018; Tamay *et al*., 2021). Furthermore, at least 8 earthquakes can be associated with the Porotoyacu Fault. Notable, one of the most recent seismic events instrumentally recorded occurred on 28 December 2021 by IGEPN, at a distance of 0.98 km from the town of Archidona with a magnitude of Mw 4.54, but in the research of Araujo. S., (2023) was able to locate in detail -77.748393 -0.907595, a depth of: 23.7316 with a vertical error of 2.5 Km and horizontal error of 2.1 km.

The área of investigation is located in a section South of the Porotoyacu Fault in Tena City, Napo Province. It is located in an anthropogenic outcrop in the coordinates 1° 0 '57.91 "S, 77°48' 19.89" O at a distance of 0.43 km from the established trace by the SARA project (Costa *et al.*, 2020) with SW-NE orientations being perpendicular to the course of Porotoyacu Fault that show seismic characteristics appropriate to paleoseismological analysis.

4.0.2 Geological context

The Tena Formation is a fluvial continental deposit part of the Upper Cretaceous. Additionally, according to the research of (Jaillard *et al.*, 1997; Canfield *et al*., 1982; Gramal-Aguilar *et al*., 2021), this formation is characterized by the composition of mudstone, siltstone, and sandstone with granulometry from coarse to fine, and also has a sandy siltstone or mudstone. The stratigraphic units have sedimentary structures such as parallel lamination, cross lamination in sandstone, or massive layers of mudstone. The lithology presents a usually reddish or brown color and gray or green occasionally. In our study, the sedimentology analysis coincides with the lithology of the research by Cornejo *et al*., (2024) by the characteristics of colorimetric and lithological findings that belong to the Tena Formation.

4.1 METHODOLOGY

4.1.1 Selection of Study Área

The methodology for this study was performed on an anthropogenic outcrop (road cut) located in Tena, south of the trace of the Porotoyacu Fault. The study área was selected based on criteria such as the presence of morphotectonic indicators, outcrops exhibiting deformation structures caused by liquefaction/fluidization, ruptures or discontinuities in strata, and disordered or mixed sediment deposits. Additionally, its proximity to the fault trace was a determining factor. The regional characteristics as indicators were identified from the analysis of satellite images and subsequent field verification.

The morphological regional analysis was performed by the methodology proposed by Baize *et al.*, (2015); Choi *et al*., (2015); Jomard *et al*., (2021); and Gómez-Hurtado *et al*., (2022), An ALOS PALSAR Digital Elevation Model (DEM) from the Alaska Satellite Facility (ASF) was used to obtain interesting relief information. With QGIS tools, subtle topographic features were identified, facilitating the discrimination of morphotectonic structures. The morphotectonic analysis seeks to understand the relationship between the evolution of landscape morphology and the tectonic processes that have acted there. To study topographic features in even greater detail, topographic profiles were created using the Qgis tools. Topographic profiles allow the quantification of tectonic uplift and the location of geological faults. With all information gathered it performs a field control to the observatory and corroborates the indicators morphotectonics identify. *Fieldwork:* Describe the location of each zone with indicators and add information such as height, length, distance, and photographs. The morphometric information was cartography on a DEM processed through the use of SIG (System Information Geographic).

The paleoseismological analysis was applied on a rocky outcrop which measures 20 meters in longitude and 6.5 m in height. The site displayed several deformation characteristics, including displacement between units, fault plane with striations,

deformed units, and seismites in an anthropogenic outcrop, we applied 1m x 1m grid cells covering the entire length of the outcrop. Subsequently, each stratigraphic unit was identified and described based on textural and colorimetric characteristics (Munsell Table-Rock Color Chart of Munsell) and geometrics features such as inclination, height, and thickness. All major features of the observed outcrop were used for the digital representation. This representation allowed the identification of the major ruptures that facilitated the measurement of vertical displacement between stratigraphic units to estimate the number of seismic events. Additionally, deformation structures were identified and their causes were analyzed.

To estimate magnitudes, the empirical equations proposed by Wells & Coppersmith, (1994), Wesnousky, (2008) and Bonilla *et al*., (1984) were applied, using the vertical displacements measured obtained from the outcrop and the mapped length of the Porotoyacu Fault. For this last, the magnitude was calculated with several scenarios, varying the length. The first scenario is affected ¼ of the fault, ½ the half, and all length. These equations considered several parameters such as the type of cinematic (normal, reverse, or transverse faults), rupture length, and displacement value.

The identification and classification of seismites were conducted. To classify these structures, we adopted the categorization proposed by Rodríguez-Pascua *et al*., (2000), and Montenat *et al.*, (2007) which is based on stratigraphic observation to examine characteristics such as morphology, lithological description, diameters, and length. Correlations were established between the seismites and the earthquakes of magnitude that caused their formation.

4.2 RESULTS

In the south zone of the Porotoyacu Fault, we perform a morphotectonics and paleoseismological analysis. The results are presented below:

4.2.1 Morphotectonic in the south of the Porotoyacu Fault

By observing satellite images, we identified 4 main morphotectonic indicators. The first indicator is the relief difference, where is proposed the pass of the trace of the Porotoyacu Fault because is located between a higher relief to the east with maximum elevations above sea level reaching of 692m and a flat surface to the west with low elevations between 500-550m **(Figura 2)**.

The morphotectonic analysis provides cartographic detail located south of the Porotoyacu Fault by the number of forms of relief and indicators morphotectonic identified in the área, such as abrupt changes in slope interpreted as scarps, which are analyzed by topographic profiles ***(Profiles 1, 2, 3)***, a orthogonal pattern, and two semi-rectilinear drainage systems.

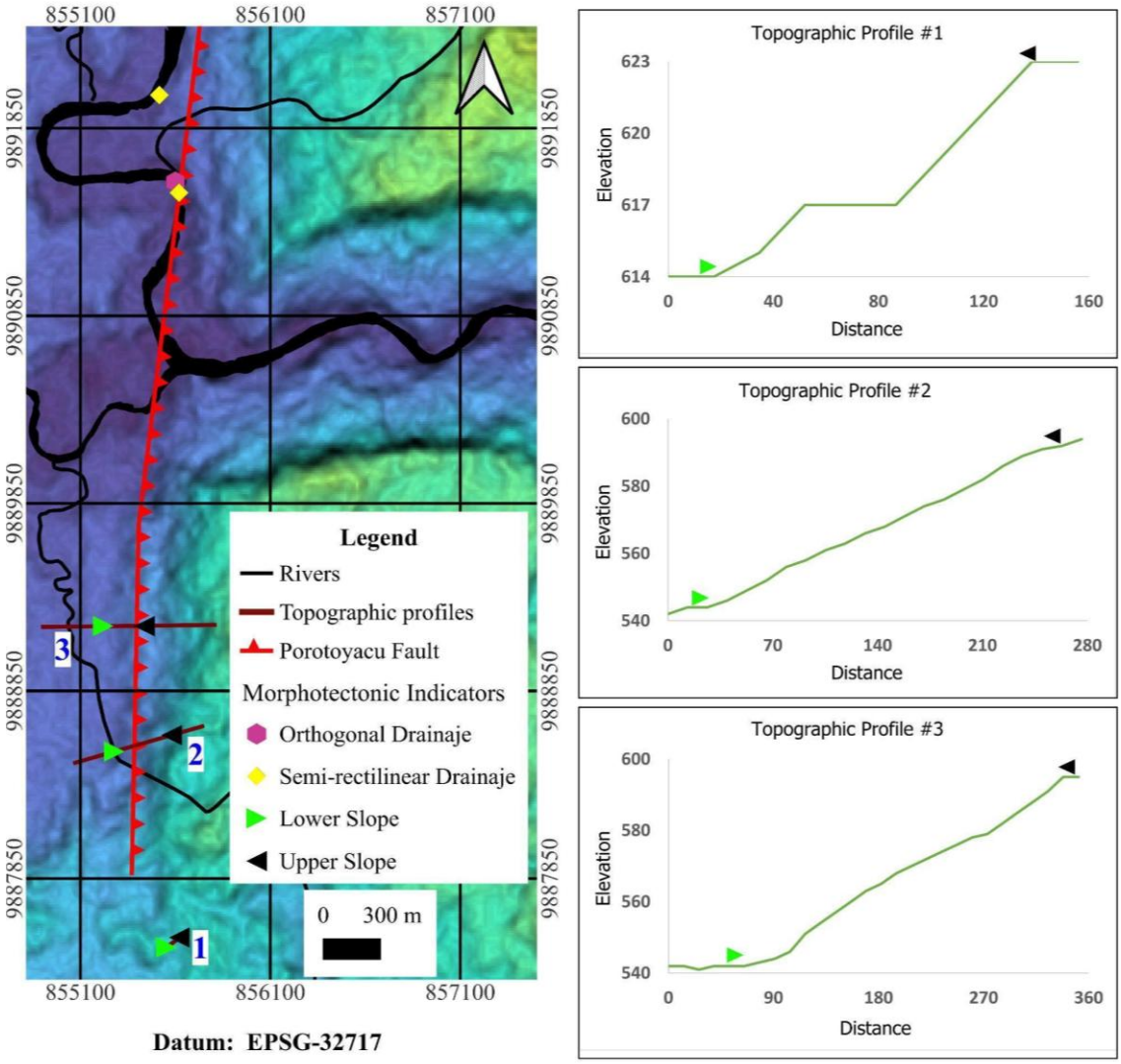

Figure 2. Morphotectonic Indicators in the South of Porotoyacu Fault: The map base was obtained from the Alaska Satellite Facility. The trace of the Porotoyacu Fault proposed by Costa et al., (2020) is shown In red color through the Tena and Archidona cities. Also, along with three types of morphotectonic indicators: orthogonal drainage (pink square), semi-rectilinear drainage (yellow diamond), and scarps (green and black triangles) to identify the slope and base used to detail the course of the Porotoyacu Fault. The profiles of scarps are indicated by green and red triangles indicating the superior and inferior parts of scrap. Close to the green square at the South indicates the outcrop

The scarps are configured by a flat base interrupted by a slope and flat top; this indicator is a product of terrain displacement by the presence of a fault (Proyecto Multinacional Andino, 2009). The indicators indicated in **Figure 2** as scarp with an SW-NE orientation, where the topographic profile shows a height of the top is from 540 m to 640 m, the relief varies from 3˚ to 9.42˚. The topographic profiles of scarp have morphologies irregular **(Profile 1)** and uniform **(Profile 2, 3)**. The profile 1 is located in our site to paleoseismological analysis.

Likewise, the identified orthogonal drainage results from abrupt changes in the rivers caused by variations in material stress due to the influence of interposed active structures, such as the Porotoyacu Fault. Finally, the semi-rectilinear drainages reflect changes in geometry by the presence of a Fault, adopting a more rectilinear pattern (Holbrook & Schumm,1999; Proyecto Multinacional Andino, 2009). The same zone of the Porotoyacu Fault is determined by the presence of an orthogonal drainage, which has an abrupt change of orientation from O-E to N-S. The section west-east has a length of 480 m and the section north-south has a length of 330 m. This orthogonal shift is aligned with the relief of the terrain.

Finally, we observed two semi-rectilinear drainage next to orthogonal in the south zone, the river has the same orientation N-S. The river has a meandering behavior which adopts a semi rectilinear pattern in the zones where the Porotoyacu Fault is crossing **(Figure 2)**. The first semi rectilinear drainage has a length of 300 m and continues with an open meander pattern interrupted by the orthogonal drainage. The second semi rectilinear section has a length of 330 m and again has an open meandering.

The morphology local of the study site is located approximately 400 meters above sea level. Currently, the área is populated and features one of the scarps previously identified, with a length exceeding 70 meters **(Figure 2-Profile 1)**. In the field, the terrain configuration consists of a flat zone at 615 meters of elevation (indicated by the green triangle), interrupted by a slope with a gradient of 7° at 620 meters. The morphology then resumes a flat profile at 623 meters of elevation (indicated by the black triangle). The scarp has a SW-NE orientation, which may indicate vertical displacement associated with the Porotoyacu Fault.

4.2.2 Stratigraphic and paleoseismic analysis

Based on morphological, sedimentary, and textures studies, we constructed a stratigraphic profile of the outcrop, which is composed of siliciclastic cretaceous rocks. This analysis revealed that the outcrop comprises nine units predominantly composed of claystone, siltstone, and breccia. The basal units have been identified as cretaceous and covered by higher units undergoing pedogenetic processes and are considered as quaternary units, which is deduced by their lithological properties and color. The sedimentary column and general description of units are as follows.

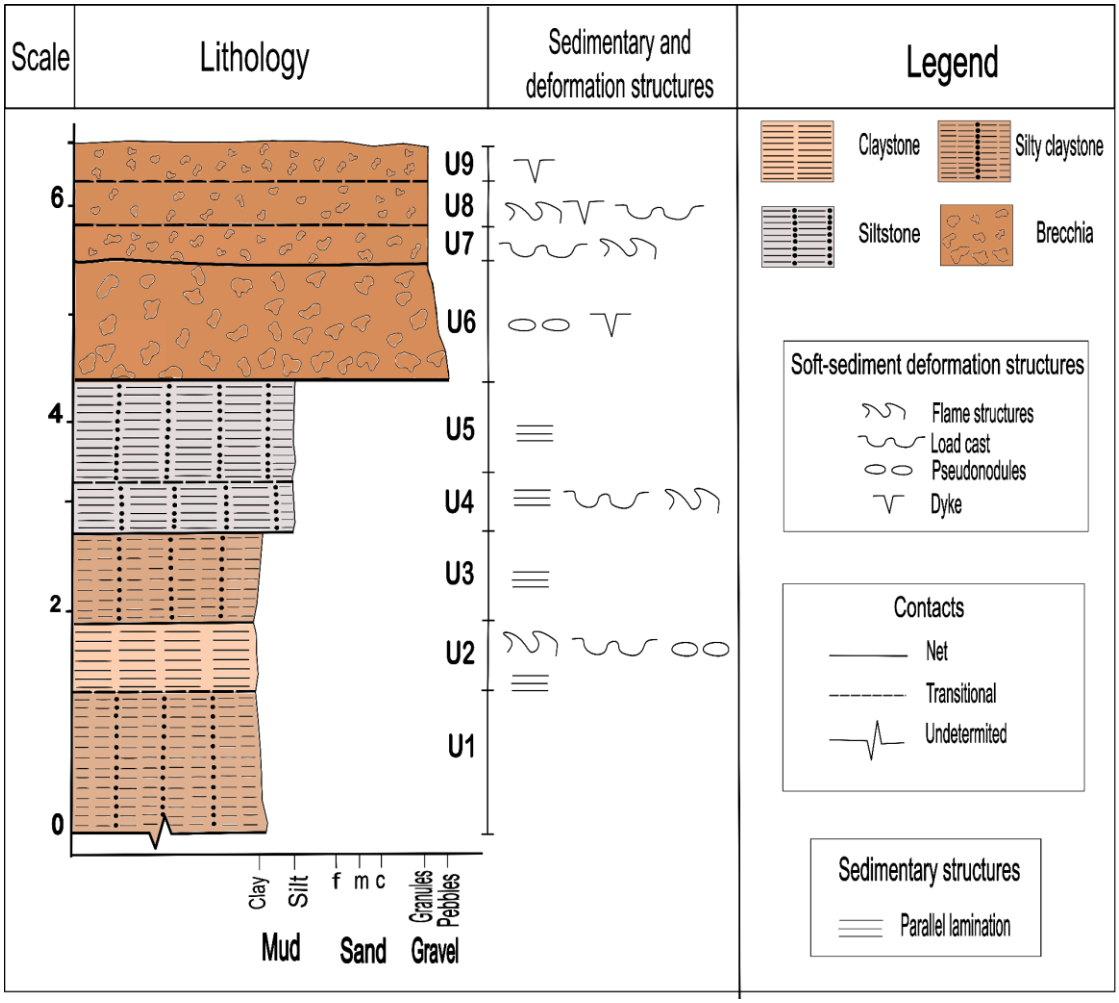

Figure 3. Sedimentary Column of the outcrop. The figure illustrates the stratigraphic units in code U1-U9, along with their lithology, thickness, and color. For the upper units, it also includes the quantity and size of clasts. Additionally, the figure specifies the type of contact between units, the location of the outcrop, and the types of sedimentary and deformation structures present.

Unit 1 (U1): Claystone with silt grains of grayish orange (10 YR 7/4) and a slightly mottled light brown appearance. The unit has a varying thickness of 31 cm to 1.83 cm. U1 presents micas of approximately 2 mm and magnesium levels. The fault mirror in SW displacement U1. This unit has a massive appearance and their basal contact is not visible.

Unit 2 (U2): Claystone with few silt grains with a light brown color (5 YR 5/6). The unit has a thickness of 3 to 45 cm. The unit has micas and incipient lamination that follows the direction of deformation. This unit is affected by R1 displacing the unit. U2 has seismites as load cast, flame structures at the base of the unit with a size >10cm, and pseudonodules of 38 cm in length inside the U1. U2 has parallel lamination and a transitional contact with U1.

Unit 3(U3): Claystone with grains of silts predominantly massive of a grayish orange color (10YR 7/4). The unit has a varying thickness of 54 to 1.23 cm. U3 has parallel lamination of white (N9) and light brown (5YR 5/6) distributed at the base and middle of the unit composed of siltstone. This unit is affected by R1 and does not have seismites but presents parallel lamination in the base of the unit with a net contact with the U2, and U4.

Unit 4 (U4): Siltstone of moderate pinkish-orange color (10R 7/4) and has a slightly red mottled appearance. The unit has a thickness of 28 to 39 cm. It presents micas and magnesium in smaller quantities and parallel lamination of white color (N9) located from the base to the middle of the unit. U4 has a slightly mottled brown moderate appearance (5YR 4/4). This unit has seismites as load cast and flame structures with a size of >10cm in the base of the unit and presents parallel lamination. Finally, U4 has a transitional contact with U5.

Unit 5 (U5): Siltstone with Grayish orange-pink (5 YR 7/2) with micas, traces of magnesium, and some black parallel lamination (N1) composed siltstone. This unit has a slightly mottled brown moderate appearance (5YR 4/4) similar to U4 The unit has a varying thickness of 44 to 1.47 cm. U5 has been penetrated by a dyke belonging to U6 and presents parallel lamination. This unit has a net contact with U6.

Unit 6 (U6): Breccia with a predominantly silty matrix. The unit is moderately brown (5YR 4/4). The thickness of this unit is 1.50 to 2.56 cm. The basal part is highly concentrated with clasts >3cm in diameter as opposed to the upper part. This unit has

seismites as dyke >15 cm in length and pseudonodules 1.2 cm in diameter, both penetrating the underlying unit (U5). This unit is massive and has a net contact with the U7.

Unit 7 (U7): Breccia with a silty matrix with clasts larger than 1cm. The unit has a dark yellowish-orange color (10 YR 6/6). The varying thickness of this unit is 25 to 67 cm. This unit presents clasts of quartz and fragments of rock <1 cm. In this unit there is a dike penetrated that belongs to U9. The U7 is massive and has a transitional contact with the U8.

Unit 8 (U8): Breccia with silty matrix with <1 mm clasts. The unit has a moderate yellowish-brown color (10 YR 5/4) with a content of organic material. The thickness of this unit is 13 cm to 1,10 cm. Also, this unit is affected by R2, load cast, flame structures of a size >3cm, the dyke belonging to U9, and another dyke belonging to this unit located SO in the cut-affected U6. It should be noted that this unit could be a recent soil and has a transitional contact with U9.

Unit 9 (U9): Breccia with silty matrix and smaller clasts <5mm in size. The unit is a dark yellowish-brown color and high content of organic material (10YR 4/2). The unit is considered a soil layer. The varying thickness is 38 to 50 cm. This unit presents a dyke with a 1m in length that intrudes underlying units until U6. Next to the dyke is deformed the surface of the outcrop Las Veronicas.

4.2.3 Characteristics and paleo magnitude obtained from the outcrop

The general construction of the outcrop was documented through detailed drawings in millimetric sheets **(Figure 4a)**, which illustrate deformation and displacement between units, due to seismic activity. The rock units are numbered from U1 to U9, which are being displaced by two rupture planes, denoted R1 and R2, **(Figure 4b)**.

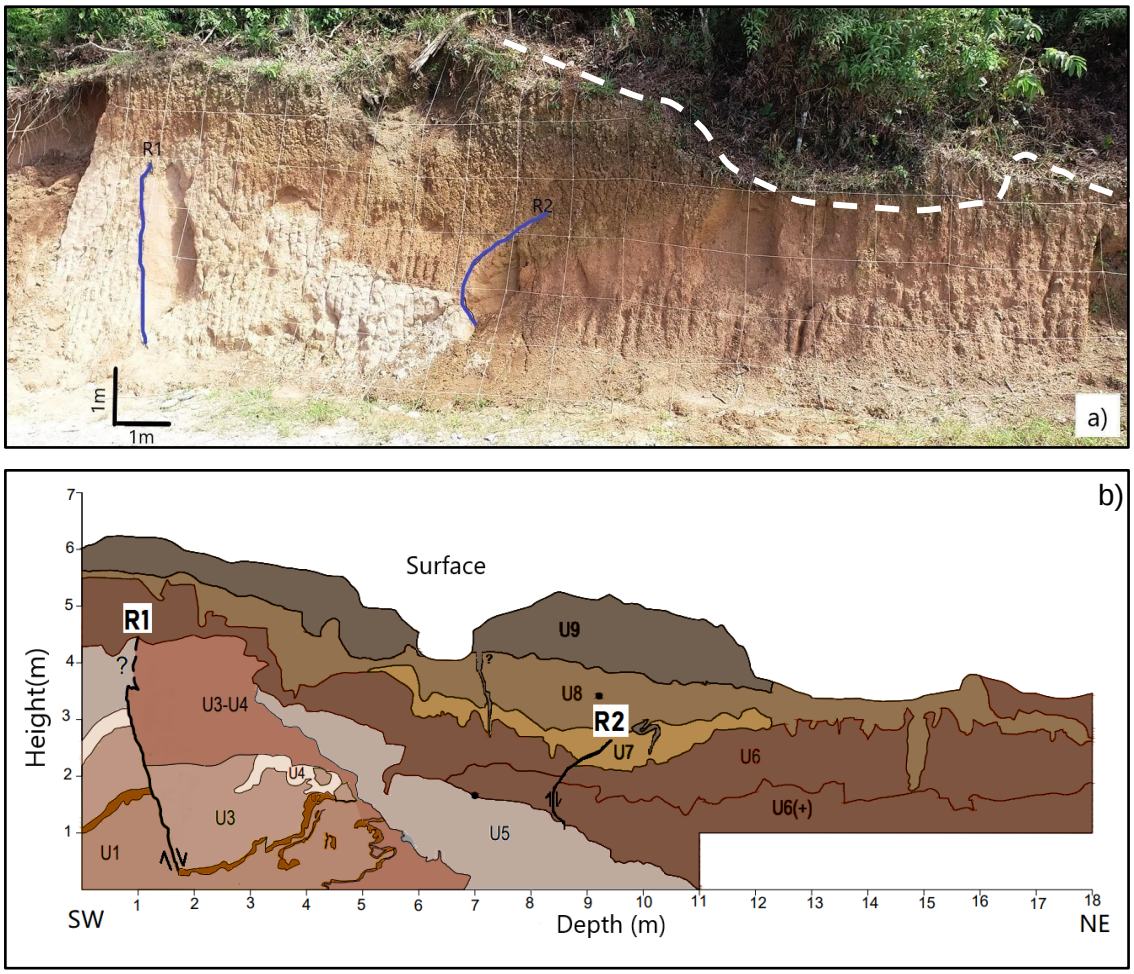

Figure 4. The outcrop profile. a) Photomosaic of outcrop with nine stratigraphic units identified, rupture planes, and deformation structures. The broken white line superficially defines the deformation of the outcrop. b) Digitating the outcrop with the nine stratigraphic units, paleo-ruptures denominated R1 and R2 with cinematics and seismites.

The level of detail in the drawing permits an interpretation of tectonic history, helping to rebuild past seismic events and understand the impact on the geological and tectonic configuration. The rupture plane R1 exhibits normal kinematics, and two seismic events were recorded. This rupture affects units U1, U2, and U3. Otherwise, R2 shows reverse kinematics with a single event that displaces units U6 and U7 **(see Table 1)**.

Table 1. Summary of ruptures and vertical displacements caused by paleo-seismic events in the affected units of the outcrop

Rupture (R)	Events (Ev)	Stratigraphic unit affect	Vertical displacement
R1	Ev.1	U1-U2	0.76
	Ev.2	U1-U3	0.70
R2	Ev.1	U6-U7	0.11

We identified three seismic events in total whose magnitudes were determined based on vertical displacements obtained from the stratigraphic units defined in the study área (**Figure 4b**). The moment magnitude (Mw) was calculated using the equations proposed by Wells & Coppersmith (1994), a method for two events associated with R1 characterized by normal kinematics. While R2 exhibits reverse kinematics both the magnitude of a single event and the surface wave magnitude (Ms) were estimated using the method proposed by Bonilla *et al*., (1984).

Additionally, the magnitude based on rupture length was estimated using the equation of Wesnousky, (2008). The mapped fault length, up to the trench described by Cornejo *et al*., (2024) measures 16.77 kilometers. The following magnitudes were calculated for three scenarios: ¼ of the rupture length (4.75 km), ½ of the length (9.5 km), and the entire fault length (19 km) **(see Table 2)**.

Table 2. The summary of magnitudes calculated for each rupture used the empirical equations (Bonilla et al., 1984; Wells & Coppersmith, 1994; Wesnousky, 2008; Turcotte, D. L., & Schubert, G. (2014) identified in the outcrop. Where N: Normal faults; R: Reverse faults and All: All types of faults

Rupture (R)	Events (Ev)	Stratigraphic unit affect	Mw (Wells and CopperSmith	Ms(Bonilla)	Mw(Wesnousky)	Strike-slip model (10 km in depth) Turcotte, D. L., & Schubert, G. (2014)	Strike-slip model (5 km in depth) Turcotte, D. L., & Schubert, G. (2014)
R1	Ev.1	U1-U2	6.70 **N** 6.83 **All**	6.91			
	Ev.2	U1-U3	6.68 **N** 6.80 **All**	6.88			
R2	Ev.1	U6-U7	6.13 **R** 6.5**All**	6.24			
Length of rupture of Fault(Km)							
L=4.7					5.38	5.72	5.52
L=9.5					5.95	6.32	6.12
L=19					6.51	6.92	6.72

The ruptures do not extend to the superficial units. However, the superficial morphology of the outcrop is characterized by zones of ductile deformation **(Figures 3a, 3b)**, which are delineated by making the soft flexures formed on the surface.

4.2.4 Soft sediment deformation (SSDS) in the outcrop

The paleo seismological analysis of the outcrop allows for the identification and classification of the following deformation structures distributed across U1 to U9. The outcrop presents recent and old seismites such as load cast, flame structures, pseudonodules, and dykes **(Figure 4)**. However, this study focused on characterizing the current activity of the Porotoyacu Fault, we will only discuss the description of the dykes identified on the quaternary deposits of the outcrop. Most of the seismites observed are appropriately described in Lluno *et al*., (2024).

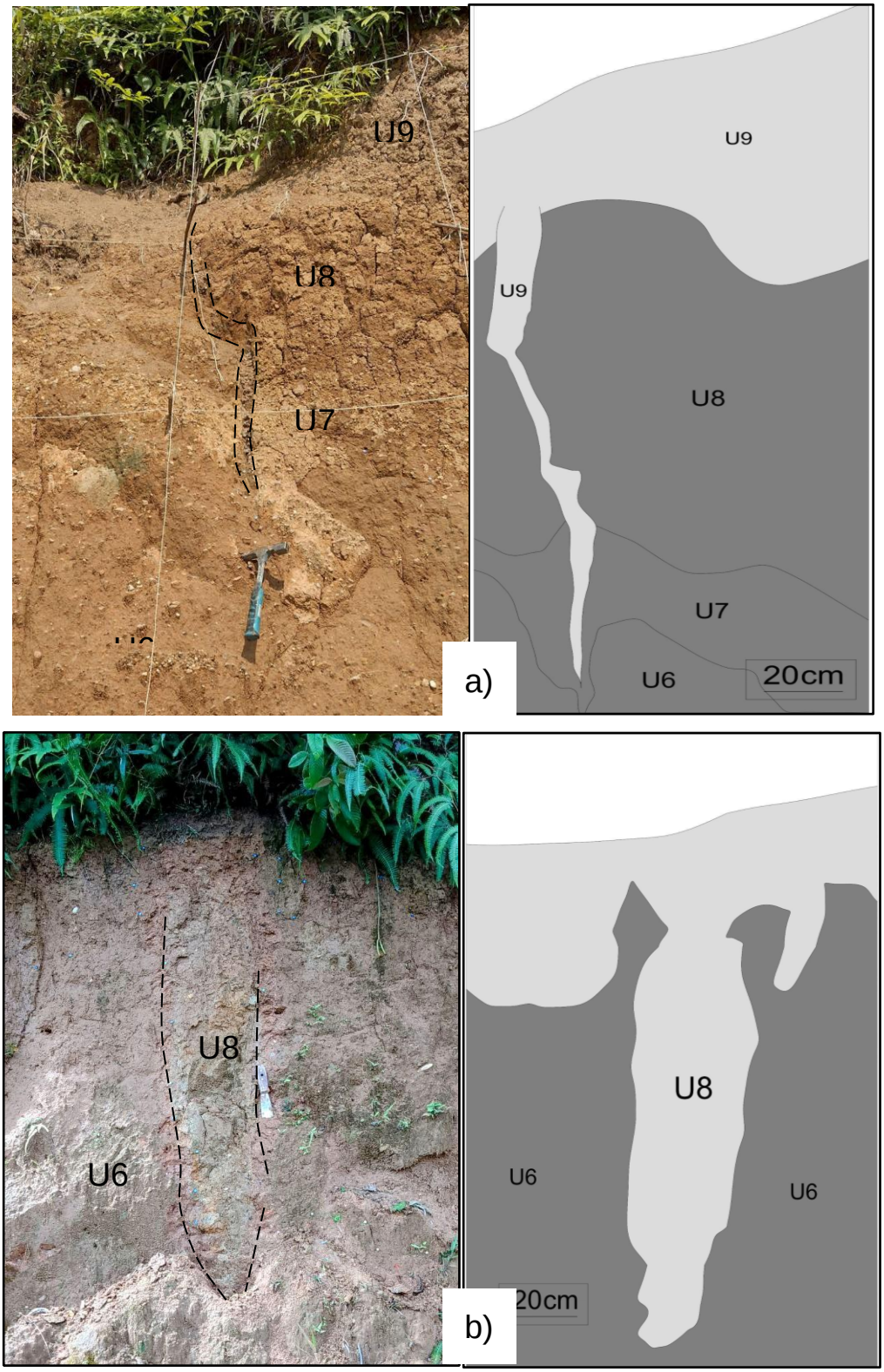

Figure 5. Dykes observed at the top of the outcrop: a) The first dyke is located in the northeastern part of the outcrop and is composed of U8. Similarly, this dyke intrudes upward to U6. b) The second dyke is located in the central part of the outcrop, originating from U9 and extending to U6.

The first dyke is situated in the southwest and central part, 7 m long and 3-4 in high of the outcrop, this deformation structure exhibits a morphology of columns measuring a 1m in length and 6 cm in diameter and intrudes underlying units, This dyke is composed of material from U9, which is liquefied breccia that intruded the U8, U7, and U6 **(Figure 5a)**. The second dyke is located in the northeast, specifically 15 m long and 2-3 m high in the profile of the outcrop. Its primary dimensions are 2 m long and 30 cm in diameter. This deformation structure has a similar morphology to the first dyke and it's composed of U8 and intrudes only up to U6 **(Figure 5b).**

4.3 DISCUSSION

4.3.1 Morphotectonic indicators and fault length

This work studied morphotectonics elements in the southern segment of the Porotoyacu Fault, through photo interpretation and field verification to determine the extension of the fault. These analyses based on indicators are classified as planar and linear as terraces, scarps, semi-rectilinear, and orthogonal drainages (Audemard, 1999; Perucca *et al*., 2015; Onorato *et al*., 2020). In this research, we identified most indicators as scarps, orthogonal drainage, and semi rectilinear drainage. These indicators provide evidence of the tectonic activity associated with the Porotoyacu Fault (Figure 2).

4.3.2 Superficial deformation of the outcrop-Pedogenesis process

The pedogenesis process explains that soil forms and transforms from its parental material under the influence of climatic and vegetative factors. During pedogenesis, the superficial soil typically begins as a thin layer that gradually increases in thickness over time. Additionally, the underlying and horizontal layers become differentiated by their colorimetric, textural, and structural characteristics (Duchaufour, R. 1982).

Several studies used pedogenesis as a tool to identify current soils, often through their color. For instance, the yellowish-brown color and dark-brown caused by the deposition

of iron oxide minerals are characteristics of Subtropical and Tropical regions (Torrent *et al*., 1983; Schwertmann & Taylor, 1989), such as the Ecuadorian Amazon.

This colorimetric property of soil can indicate the degree of meteorization or pedogenesis (González *et al*., 2008). Based on field observations and literature, the superficial units of the outcrop exhibit these characteristics, including the color observed in U8 and U9. Additionally, the thickness increases in these units in some áreas. Therefore, these units are associated with recent soils.

The superficial deformation observed in the relief of the Las Veronicas outcrop can be attributed to the tectonic activity associated with the Porotoyacu Fault. The first flexure is located in the center of the outcrop, 11-12 m and a height of 4-5 m in the general profile. This flexure shows a slope of approximately 1 meter. The second flexure is located at 16 m at the northeastern part of the outcrop, with a height of 3.5 m and a slope of 0.5 m in the outcrop **(Figure 3b).**

It is agreed that the pedogenesis observed in the surface part of the outcrop corresponds to recent deposits, where the ductile deformation may have been caused by a seismic event after the paleo ruptures R1 and R2 **(Figure 5a)**. Similarly, studies by Sagripanti & Villalba (2009) and Tejada *et al*., (2021) have identified surface flexures composed of unconsolidated sediments considered recent soil, providing evidence of a Quaternary activity of the Porotoyacu Fault in this study.

4.3.3 Dykes, mechanisms, and tectonic feature

The identification of seismites has primarily been used to estimate magnitude as emphasized by the authors Audemard & de Santis, (1991) and Marco & Agnon, (1995) who noted that seismic events with magnitude greater than M>5 can generate processes such as liquefaction or fluidization (Moretti *et al*., 1999) resulting in deformation structure. However, it is important to consider that the formation of seismites can also be influenced by the type of material undergoing liquefaction or by

the triggering mechanisms that produce different types of seismites. These structures may form through seismic processes or other depositional effects (Allen & Banks, 1986; Van Loon, A. J. & Brodzikowski, 1987; Obermeier, 1996; Rodríguez-Pascua *et al*., 2000).

4.3.3.1 Trigger mechanisms of seismites

Seismites can form due to various phenomena, such as glacial activity, bioturbation, tsunamis, and more. In our study área, the first is unlikely, as the Amazon Basin during the Upper Cretaceous experienced arid to semi-arid climatic conditions (Batezelli *et al*., 2019). The second phenomenon, bioturbation, is also disposable because, as previously mentioned, the Tena Formation primarily consists of continental deposits. Additionally, in the study área has been identified no evidence of trace fossils indicating this process (Tschopp, 1953; Jaillard *et al*., 1997; Romero *et al*., 2019). In our outcrop observatory, fine-grained deposits such as claystone and siltstone in the basal units suggest a low-energy sedimentary environment. Thus, events such as tsunamis or wave influence are unsuitable as triggering mechanisms. The seismites identified in these units are interpreted as products of seismic waves. On the other hand, the upper unit consists of fine-grained breccias, which rule out the possibility of high slopes and indicate a high-energy process, capable of transporting larger particles.

4.3.3.2 Triggering Mechanisms of dykes

In this study, we identified various dykes. Now, it is crucial to highlight the process involved in the formation of dykes. Usually, the size of dykes varies from 30 cm to 1 m (Topal & Özkul, 2014). In this research, the dykes have a maximum length of 1-1.5m. The dykes can be generated by earthquakes or depositional processes, according to Jolly and Lonergan (2002) are the most common triggering mechanism of clastic injections, where classified the dikes. Among the trigger are: sedimentary slumping (Truswell, 1972); Glacial loading (Le Heron y Etiene, 2005); Tectonic stress and liquefaction induced by earthquakes (Peterson, 1966; Obermeier, 1989, 1998b); Igneous intrusion (Andersen et al., 1998). Now, we discard some processes and the morphology of dykes and trigger

mechanics observed in this study are consistent with those associated with earthquake activity.

The formation mechanism is related to the process of gravitational collapse (Lowe., 1975, Rodríguez-Pascua, 2005), which follows liquefaction-fluidization processes induced by seismic shocks. This occurs when the overlying units U8 and U9, collapse and penetrate the underlying units such as U6 (Alfaro *et al*., 1995, 1997; Moretti & Sabato., 2007) **(Figura 6a, 6b)**. Additionally, the dykes of U8 and U9 are located in units that are subsequently followed by deformed layers. This does not align with one of the conditions outlined by Obermeier, (1996), and Marco & Agnon, (1995), who mentioned that structures must be present between non-deformed layers. Despite of the dyke do not meet these conditions, we rule out the influence of depositional processes

After having defined the triggering process to dykes. The second purpose of its classification in this research is to establish their relationship with the activity tectonics of the Porotoyacu Fault as mentioned above, the last units U8 and U9 of the outcrop that present a pedogenesis process, forming a quaternary soil. Therefore, the dykes of the upper units indicated a recent tectonic activity of the Porotoyacu Fault. This suggests a seismic event with a high magnitude because Rodríguez-Pascua., (2005) mentioned that the liquefaction in gravel is associated with a magnitude $Mw \geq 7.5$. In this case, the lithology of superficial units like U8 and U9 can be gravel as unconsolidated sediments, which is not unusual according to (Obermeier, 1998). These structures are typically associated with earthquakes with Mw 5~8 (Audemard & de Santis, 1991), these values serve as potential magnitude of current events.

4.4 CONCLUSIONS

The present work examines elements to the south of the fault, as morphotectonic indicators, the surface morphology of the study área, and an outcrop with seismic events and deformation structures recorded in the stratigraphic units. To reveal the influence of the Porotoyacu Fault and provide evidence about an active tectonics, concluding that: The analysis of morphotectonics, morphological, and paleo- paleoseismological of Las Veronicas demonstrated a quaternary activity of the Porotoyacu Fault. It is supported by: 1-The morphotectonic indicators served as evidence of recent tectonics and indicated an extension to the Fault of 1.67 km **(Figure 1)**. 2- The superficial morphology of the study área with abrupt changes of slope is considered a scarp **(Figure 2)**. The outcrop analyzed content 3 three seismic events in their stratigraphic, whose magnitude in R1 6.68 < Mw < 6.70 and 6.88 < Ms < 6.91. In R2 $6.13 < Mw < 6.51$ **(Table 1, 2)**. On the other side, the magnitudes obtained by the rupture length are $5.38 < Mw < 6.92$ **(Table 2)** associated with ancient events of the Cretaceous. 3-The pedogenesis process in superficial units such as U8 and U9 is based on colorimetric and thickness characteristics**.** 4-The surface, instead of being lateral continuous, is deformed with soft flexures **(Figure 4a, 4b)**. 5-The presence of Dykes in the superficial units close to deformation zones in the outcrop **(Figure 5a, 5b)**. All of the evidence mentioned is more concrete than active tectonics in this section of the Porotoyacu Fault.

The principal recommendations are realized studies to relocate the Porotoyacu Fault and paleoseismology in another trench to determine the seismic activity to the North of the Fault.

Acknowledgments

This research was carried out with the support of the Earth Sciences and Climate Research Group of the Universidad Regional Amazónica Ikiam and in the framework of projects CTC-006-2020, CTC-010-2024 and IGCP-669-Ollin. Especially for their valuable support and for the knowledge of the expert paleoseismologists who helped in the realization of this work. Likewise, we thank the community of the Las Veronicas neighborhood for their welcome and for permission to conduct work at the site. SL received 3 scholarships for academic excellence during 2023-2024 and HC 1 scholarship in 2022 from Ikiam University, they also received the following scholarships together: scholarship from the IGCP-669-Ollin-UNESCO project to attend a seismic hazard course in Bogotá, scholarship to be a speaker at the REDU international scientific congress developed in Ikiam, international mobility scholarship for work of excellence by Ikiam University for the international congress PATAdays 2024.

REFERENCES

Alfaro, P., Doménech, C., Estévez, A., & Soria, J. M. (1995). Estructuras de deformación en sedimentos del Cuaternario reciente de la cuenca del Bajo Segura (Alicante). Discusión sobre su posible origen sísmico. *Geogaceta*, *17*, 91–94.

Alfaro, P., Moretti, M., & Soria, J. M. (1997). Soft-sediment deformation structures induced by earthquakes (seismites) in pliocene lacustrine deposits (Guadix-Baza Basin, Central Betic Cordillera). Eclogae Geologicae Helvetiae, 90(3), 531–540.

Allen, J., & Banks, N. (1986). An interpretation and analysis of recumbent-folded deformed cross-bedding. *Sedimentology*, *19*, 257-283. https://doi.org/10.1111/j.1365-3091.1972.tb00024.x

Alvarado A., Segovia M., Yepes H., Guillier Bertrand, Chatelain Jean-Luc, Egred J., Villagomez D., Ruiz M., Samaniego P., Santacruz R. (1996). The Mw 6.8 Macas earthquake in the subandean zone of Ecuador, october 3, 1995. In : Géodynamique andine : résumés étendus = Andean geodynamics : extended abstracts. Paris : ORSTOM, p. 129-132. (Colloques et Séminaires). ISAG 96 : Symposium International sur la Géodynamique Andine, 3., Saint-Malo (FRA), 1996/09/17-19. ISBN 2-7099-1332-1. ISSN 0767-2896.

Alvarado, A. (2012). Néotectonique et cinématique de la déformation continentale en Equateur. [Thèse de Doctorat, Université de Grenoble]. https://theses.hal. science/tel-00870332

Alvarado, A., Audin, L., Nocquet, J. M., Jaillard, E., Mothes, P., Jarrín, P., Segovia, M., Rolandone, F., & Cisneros, D. (2016). Partitioning of oblique convergence in the Northern Andes subduction zone: Migration history and the present-day boundary of the North Andean Sliver in Ecuador. Tectonics, 35(5), 1048–1065. https://doi.org/10.1002/2016TC004117

Araujo, S. (2023, diciembre). Earthquake relocation with stochastic inverse problem resolution in the Northern Ecuadorian Amazon. CIREDDU, Tena, Napo, Ecuador.

Anderson, M., Alvarado, P., Zandt, G., & Beck, S. (2007). Geometry and brittle deformation of the subducting Nazca Plate, Central Chile and Argentina. *Geophysical Journal International*, *171*(1), 419–434. https://doi.org/10.1111/j.1365-246X.2007.03483.x

Andersen, J.C.Ø., Rasmussen, H., Nielsen, T.F.D., Rønsbo, J.G., 1998. The Triple Group and the Platinova gold and palladium reefs in the Skaergaard intrusion: stratigraphic and petrographic relations. Economic Geology and the Bulletin of the Society of Economic Geologists, 93, 488e509. https://doi.org/10.2113/gsecongeo.93.4.488

Audemard, F. (1999). Morpho-Structural Expression of Active Thrust Fault Systems in the Humid Tropical Foothills of Colombia and Venezuela. Zeitschrift für Geomorphologie. 118. 1-18.

Audemard, F. A., & de Santis, D. (1991). Survey of liquefaction structures induced by recent moderate earthquakes. *Bulletin of the International Association of Engineering Geology*, *44*, 5–16. https://doi.org/10.1007/bf02602705

Baby, P., Rivadeneira, M. & Barragán, R. (Eds.) (2004). La cuenca Oriente: geología y petróleo. Institut français d'études andines, Institut de Recherche pour le Développement (IRD), Petroecuador. https:// doi.org/10.4000/books.ifea.2971

Baby, P., Rivadeneira, M., Christophoul, F., & Barragán, R. (1999). Style and timing of deformation in the Oriente Basin of Ecuador. *Fourth International Symposium on Andean Geodynamics (Germany)*, *2*, 68–72.

Baize, S., Audin, L., Winter, T., Alvarado, A., Pilatasig Moreno, L., Taipe, M., Reyes, P., Kauffmann, P., & Yepes, H. (2015). Paleoseismology and tectonic geomorphology of the Pallatanga fault (Central Ecuador), a major structure of the South American crust. *Geomorphology*, *237*, 14–28. https://doi.org/10.1016/j.geomorph.2014.02.030

Baize, S., Audin, L., Alvarado, A., Jomard, H., Bablon, M., Champenois, J., Espin, P., Samaniego, P., Quidelleur, X. & Le Pennec, J.-L. (2020). Active Tectonics and Earthquake Geology Along the Pallatanga Fault, Central Andes of Ecuador. Frontiers in Earth Science, 8, 1-21. doi: 10.3389/feart.2020.00193

Batezelli, A., Ladeira, F.S.B., Nascimento, D.L.D., Da Silva, M.L., (2019). Facies and palaeosol analysis in a progradational distributive fluvial system from the Campanian-Maastrichtian Bauru Group, Brazil. Sedimentology 66 (2), 699–735. https://doi.org/10.1111/sed.12507

Beauval, C., Marinière, J., Yepes, H., Audin, L., Nocquet, J. M., Alvarado, A., Baize, S., Aguilar, J., Singaucho, J. C., & Jomard, H. (2018). A new seismic hazard model for Ecuador. *Bulletin of the Seismological Society of America*, *108*(3), 1443–1464. https://doi.org/10.1785/0120170259

Benhamouche, A., Nedjari, A., Bouhadad, Y., Machane, D., Oubaiche, E., & Sidi Said, N. (2014). *Field evidence of seismites in Quaternary deposits of the Jijel (Eastern Algeria) coastal region.* Journal of Seismology*, 18*(2), 289–299. https://doi.org/10.1007/s10950-013-9384-1

Bès de Berc, S. (2003). *Tectonique de chevauchement, surrection et incision fluviatile : exemple de la zone subandine équatorienne, haut bassin amazonien*.

Bhattacharya, H. N., & Bandyopadhyay, S. (1998). Seismites in a Proterozoic tidal succession, Singhbhum, Bihar, India. *Sedimentary Geology*, *119*(3–4), 239–252. https://doi.org/10.1016/S0037-0738(98)00051-7

Bonilla, M. G., & Mark, R. K., & Lienkaemper, J. J. (1984). Statistical Relations Among Earthquake Magnitude, Surface Rupture Length, and Surface Fault Displacement. *Bulletin of the Seismological Society of America*, *74(6)*(9), 2379-2411.

Cajamarca-Zuniga, D., & Kabantsev, O. (2023). Influence of the Carnegie Ridge on the Development of Seismogenic Sources and Seismicity of Ecuador. In Proceedings of FORM 2022: Construction The Formation of Living Environment (pp. 299-310). Cham: Springer International Publishing. https://doi.org/10.1007/978-3-031-10853-2_28

Canfield, R. W., Bonilla, G., & Robbins, R. K. (1982). Sacha Oil Field of Ecuadorian Oriente. *AAPG Bulletin*, *66*(8), 1076–1090. https://doi.org/10.1306/03b5a642-16d1-11d7-8645000102c1865d

Choi, J. H., Kim, Y. S., & Choi, S. J. (2015). Identification of a Suspected Quaternary fault in eastern Korea: Proposal for a paleoseismic research procedure for the mapping of active faults in Korea. *Journal of Asian Earth Sciences*, *113*, 897–908. https://doi.org/10.1016/j.jseaes.2015.09.014

Chunga, K., Michetti, A., Gorshkov, A., Panza, G., Soloviev, A., & Martillo, C. (2010). Identificación de nudos Sismogénicos Capaces de Generar Potenciales Terremotos de M>6 y M>6,5 en la Región Costera y Cadenas Montañosas de los Andes septentrionales del Ecuador. *Revista Tecnológica ESPOL-RTE*, *23*(December), 61–89.

Cornejo, C., Guzman, O., Campos, C., & Cargua, J. (2024). Análisis paleosismológico en la Zona Subandina de Ecuador. Implicaciones para la Falla Porotoyacu. En Geociencias en la en la Amazonía ecuatoriana: Aportes a la planificación sostenible (1.a ed.). CEDIA. https://doi.org/10.48661/w6dc-q685

Costa, C., Alvarado, A., Audemard, F., Audin, L., Benavente, C., Bezerra, F.H., Cembrano, J., González, G., López, M., Minaya, E., Santibañez, I., Garcia, J., Arcila, M., Pagani, M., Pérez, I., Delgado, F., Paolini, M., Garro, H. (2020). Hazardous faults of South America; compilation and overview. Journal of South American Earth Sciences, 104, 102837. doi: 10.1016/j.jsames.2020.102837

Díaz, M., Baby, P., Rivadeneira, M., & Christophoul, F. (2004). El pre-aptense en la cuenca oriente ecuatoriana. In P. Baby, M. Rivadeneira, & R. Barragán (éds.), La Cuenca Oriente: Geología y petróleo (1-). Institut français d'études andines. https://doi.org/10.4000/books.ifea.2989

Duchaufour, P. (1982). Pedology: pedogenesis and classification. In *Springer*. (pp. 3–4).

Ego, F., Sébrier, M., Lavenu, A., Yepes, H., & Egues, A. (1996). Quaternary state of stress in the Northern Andes and the restraining bend model for the Ecuadorian Andes. *Tectonophysics*, *259*, 101–116. https://doi.org/10.1016/0040-1951(95)00075-5

Egüez, A., Alvarado, A., Yepes, H., Machette, M.N., Costa, C., Dart, R.L. & Bradley, L. (2003). Database and map of Quaternary faults and folds of Ecuador and its offshore regions. US Geological Survey Open-File Report 03-289 3, 289. https://pubs.usgs.gov/of/2003/ofr-03-289/

Font, Y., Segovia, M., Vaca, S., Theunissen, T., (2013). Seismicity patterns along the Ecuadorian subduction zone: new constraints from earthquake location in a 3-D a priori velocity model. Geophysical Journal International 193, 263–286.https://doi.org/10.1093/gji/ggs083

Gómez-Hurtado, E., Aguirre-Hoyos, L. M., Diederix, H., Audemard M, F. A., Mora-Páez, H., Bohórquez-Orozco, O. P., Muñoz, O. F., González, D. A., López-Isaza, J. A., Escobar-Rey, L. K., Martínez-Díaz, G. P., Ramírez-Cadena, J., Idárraga-García, J., López-Herrera, N. R., Barragán, W., Paola Tique, Y., Fonseca, H. A., Jiménez, J. A., & Plazas-Ruiz, J. M. (2022). Neotectónica y paleosismología de la Falla de Algeciras, Huila, Colombia. In *Servicio Geológico Colombiano y Universidad Pedagógica y Tecnológica de Colombia*. https://doi.org/10.32685/9789585399389

González, O., Millán, Z., & Bezada, M. (2008). Pedogénesis de una cronosecuencia de suelos en la región de Yaritagua y Guama, estado Yaracuy-Venezuela. *Revista Geografica Venezolana*, *49*(2), 223–245.

Gramal-Aguilar, A., Carranco-Andino, F., Romero-Cóndor, C., Pulupa-Vela, R., Calderón-Romero, D., & Toainga-Oñate, S. (2021). Evidencias de canibalización de secuencias Cretácicas y Paleógenas de la Cuenca Oriente en la cuña orogénica de los Andes ecuatorianos. *Boletín de Geología*, *43*(3), 15–34. https://doi.org/10.18273/revbol.v43n3-2021001

Gutscher, M. A., Malavieille, J., Lallemand, S., & Collot, J. Y. (1999). Tectonic segmentation of the North Andean margin: Impact of the Carnegie Ridge collision. *Earth and Planetary Science Letters*, *168*(3–4), 255–270. https://doi.org/10.1016/S0012-821X(99)00060-6

Holbrook, J & Schumm, S. A. (1999). Geomorphic and sedimentary response of rivers to tectonic deformation: A brief review and critique of a tool for recognizing subtle epeirogenic deformation in modern and ancient settings. *Tectonophysics*, *305*(1–3), 287–306. https://doi.org/10.1016/S0040-1951(99)00011-6

Instituto Geofísico de la Escuela Politécnica Nacional (IGEPN). Instituto geofísico-EPN (2024, June 10). Seismic Catalog 2012-Present. Geophysical Institute - EPN. Retrieved from http://www.igepn.edu.ec

Jaillard, E., Caron, M., Dhondt, A., Ordoñez, M., Andrade, R., Bengtson, P., Bulot, L., Cappetta, H., Dávila, C., & Díaz, R. (1997). Síntesis estratigráfica y sedimentológica del Cretáceo y Paleógeno de la cuenca oriental del Ecuador. *Orstom-Petroproduccion Eds*, 164.

Jomard, H., Saqui, D., Baize, S., Alvarado, A., Bernard, B., Audin, L., Hidalgo, S., Pacheco, D., Ruiz, M., & Segovia, M. (2021). Interactions between active tectonics and gravitational deformation along the Billecocha fault system (Northern Ecuador): Insights from morphological and paleoseismological investigations. *Journal of South American Earth Sciences*, *111*(May). https://doi.org/10.1016/j.jsames.2021.103406

Kawakatsu, H., & Cadena, G. P. (1991). Focal mechanisms of the March 6, 1987 Ecuador earthquakes CMT inversion with a first motion constraint. Journal of Physics of the Earth, 39(4), 589-597.

Kendrick, E., Bevis, M., Smalley, R., Brooks, B., Vargas, R. B., Lauría, E., & Fortes, L. P. S. (2003). The Nazca–South America Euler vector and its rate of change. Journal of South American Earth Sciences, 16(2), 125-131. https://doi.org/10.1016/S0895-9811(03)00028-2

Lafuente, P., Rodríguez-Pascua, M. A., Simón, J. L., Arlegui, L. E., & Liesa, C. L. (2008). Sismitas En Depósitos Pliocenos Y Pleistocenos De La Fosa De Teruel. *Revista de La Sociedad Geológica de España*, *21*(3–4), 133–149.

Legrand, D., Baby, P., Bondoux, F., Dorbath, C., Bès de Berc, S., & Rivadeneira, M. (2005). The 1999–2000 seismic experiment of Macas swarm (Ecuador) in relation with rift inversion in Subandean foothills. Tectonophysics, 395(1-2), 67–80. https://doi.org/10.4000/books.ifea.3013

Le Heron, D.P., Etiene, J.L., 2005. A complex subglacial clastic dyke swarm, Solheimajokull, Southern Iceland. Sedimentary Geology, 181, 25-37. https://doi.org/10.1016/j.sedgeo.2005.06.012

Lluno, S., Conteron, H., Guzmán, O., Campos, C., & Cornejo, C. (2024). Paleoseismological study of the Porotoyacu Fault in the Amazonian Ecuadorian Piedmont. En G. Easton & G. González (Eds.),

Proceedings of the 12th International INQUA Meeting on Paleoseismology, Active Tectonics and Archaeoseismology (pp. 288–293). PATA Chile 2024. https://doi.org/10.34720/fc3d-mp19

Lowe, D. R. (1975). Water escape structures in coarse-grained sediments. *Sedimentology*, *22*(2), 157–204. https://doi.org/10.1111/j.1365-3091.1975.tb00290.x

Marco, S. & Agnon, A. (1995). Prehistoric earthquake deformations near Masada, Dead Sea graben. *Geology*, *23*(8), 695–698. https://doi.org/10.1130/0091-7613(1995)023<0695:PEDNMD>2.3.CO;2

Masana, E., Rodríguez-Pascua, M. A. & Martinez-Diaz, J. J. (2011). Los paleoterremotos: estudiando el pasado para entender el futuro. *Enseñanza de Las Ciencias de La Tierra*, *19.3*, 305–316.

McCalpin, James P & Nelson, A. R. (2009). Introduction to paleoseismology. In *International Geophysics* (1st ed., Vol. 95, pp. 1–27). Elsevier Inc. https://doi.org/10.1016/S0074-6142(09)95001-X

Montenat, C., Barrier, P., Ott, P., & Hibsch, C. (2007). Seismites : An attempt at critical analysis and classification. *Sedimentary Geology*, *196*(1–4), 5–30. https://doi.org/10.1016/j.sedgeo.2006.08.004

Moreno, X., Masana, E., Ruano, P., & Coll, M. (2007). Primeras evidencias de paleoterremotos en la falla de Carboneras : estudio paleosismológico en el segmento de La Serrata. *Geogaceta*, *41*, 135–138.

Moretti, M., & Sabato, L. (2007). Recognition of trigger mechanisms for soft-sediment deformation in the Pleistocene lacustrine deposits of the Sant'Arcangelo Basin (Southern Italy): Seismic shock vs. overloading. *Sedimentary Geology*, *196*(1–4), 31–45. https://doi.org/10.1016/j.sedgeo.2006.05.012

Moretti, M., Alfaro, P., Caselles, O., & Canas, J. A. (1999). Modelling seismites with a digital shaking table. *Tectonophysics*, *304*(4), 369–383. https://doi.org/10.1016/S0040-1951(98)00289-3

Moretti, M., Van Loon, T., 2014. Restrictions to the application of 'diagnostic' criteria for recognizing ancient seismites. J. Palaeogeogr. 3 (2), 162–173. https://doi.org/ 10.3724/SP.J.1261.2014.00050

Munsell, A. H. (1995). Munsell Rock Color Chart. Geinseheim. Munsell Color Company

Nocquet, J., Villegas-Lanza, J., Chlieh, M., Mothes, P., Rolandone, F., Jarrin, P., Cisneros, D., Alvarado, A., Audin, L., Bondoux, F., Martin, X., Font, Y., Régnier, M., Vallée, M., Tran, T., Beauval, C., Maguiña Mendoza, J., Martinez, W., Tavera, H. & Yepes, H. (2014). Movimiento de astillas continentales y subducción rastrera en el norte de los Andes. Nature Geoscience, 7(4), 287-291.

Obermeier, S. F. (1996). Use of liquefaction-induced features for paleoseismic analysis - An overview of how seismic liquefaction features can be distinguished from other features and how their regional distribution and properties of source sediment can be used to infer the location and strength of Holocene paleo-earthquakes. *Engineering Geology*, *44*(1–4), 1–76. https://doi.org/10.1016/s0013-7952(96)00040-3

Obermeier, S.F., (1989). The New Madrid earthquakes: an engineering-geologic interpretation of relict liquefaction features. U.S. Geological Survey Professional Paper, 1336-B, 114.

Obermeier, S. F. (1998a). Liquefaction evidence for strong earthquakes of Holocene and latest Pleistocene ages in the states of Indiana and Illinois, USA. *Engineering Geology*, *50*(3–4), 227–254. https://doi.org/10.1016/S0013-7952(98)00032-5

Obermeier, S.F., (1998b). Seismic Liquefaction Features: Examples from Paleoseismic Investigations in the Continental United States. U.S. Geological Survey, 358 G. Shanmugam Open-File Report, pp. 98-488. http://pubs.usgs.gov/of/ 1998/of98-488/.

Obermeier, S., Pond, E. C., Olson, S. M., Green, R. a, Stark, T. D., & Mitchell, J. K. (2001). Paleoliquefaction studies in continental settings: Geologic and geotechnical factors in interpretations and back-analysis. *US Geological Survey Open-File Report*, 1–29. https://doi.org/10.3133/ofr0129

Onorato, M. R., Perucca, L., Coronato, A., López, R., & Blanc, P. (2020). Evidencias morfotectónicas en el sistema de fallas Magallanes-Fagnano, borde transformante entre las placas Sudamericana y Scotia, isla Grande de Tierra del Fuego. Revista de la Asociación Geológica Argentina, 77, 47–61.

Perucca, L., Rothis, M., Bezerra, F. H., Vargas, N., & Lima, J. (2015). Late Quaternary evolution of the La Cantera Fault System (Central Precordillera, Argentina): A morphotectonic and paleoseismic analysis. Tectonophysics, 661, 200–209. https://doi.org/10.1016/j.tecto.2015.08.041

Peterson, G.L., 1966. Structural interpretation of sandstone dikes, Northwest Sacramento Valley, California. GSA Bulletin, 77, 833-842. https://doi.org/10.1130/0016-7606(1966)77[833:SIOSDN]2.0.CO;2

Pratt, W. T., Duque, P., & Ponce, M. (2005). An autochthonous geological model for the eastern Andes of Ecuador. *Tectonophysics*, *399*(1–4), 251–278. https://doi.org/10.1016/j.tecto.2004.12.025

Proyecto Multinacional Andino (2009). *Atlas de deformaciones cuaternarias de los Andes*. Servicio Nacional de Geología y Minería.

Quinde, P., & Reinoso, E. (2016, junio). Estudio de peligro sísmico de Ecuador y propuesta de espectros de diseño para la Ciudad de Cuenca. Revista de Ingeniería Sísmica, 1-26. https://doi.org/10.18867/ris.94.274

Rodríguez, E. E., Beck, S. L., Ruiz, M., Meltzer, A., Portner, D. E., Hernández, S., Segovia, M., Agurto-Detzel, H., & Charvis, P. (2024). Seismic imaging of the Northern Andean subduction zone from teleseismic tomography: a torn and fragmented Nazca slab. Geophysical Journal International, 236(1), 593–606. https://doi.org/10.1093/gji/ggad421

Rodríguez-Pascua, M. A. (2005). Paleoseismological studies in Spain: A review. Boletín Geológico y Minero, 116(3), 203–216.

Rodríguez-Pascua, M. A., Calvo, J. P., De Vicente, G., & Gómez-Gras, D. (2000). Soft-sediment deformation structures interpreted as seismites in lacustrine sediments of the Prebetic Zone, SE Spain, and their potential use as indicators of earthquake magnitudes during the Late Miocene. *Sedimentary Geology*, *135*(1–4), 117–135. https://doi.org/10.1016/S0037-0738(00)00067-1

Romero, C., Rivadeneira, M., Calderon, E., Naranjo, M., Meneses, M., Gramal, A., Toainga, S., 2019. Reconstruyendo el pasado del planeta: El registro estratigrafico ´ y sedimentologico ´ de la Formacion ´ Tena en la carretera Tiwintza – Puerto Morona.

Sagripanti. G & Villalba, D. (2009). Recurrencia De Fuertes Terremotos Asociados a Fallas De Intraplaca a La Latitud 33ºs , Falla Las Lagunas , Sampacho , Córdoba. Revista de La Asociación Geológica Argentina, 65(3), 417–428.

Schwertmann, U. & Taylor, R. M. (1989). Iron Oxides. In Minerals in Soil Environments, (2nd Edition) -SSSA Book Series, no. 1, pp. 379–438.

Seilacher, A., 1969. Fault-graded beds interpreted as seismites. Sedimentology 13 (1–2), 155–159.

Tamay, J., Galindo-Zaldívar, J., Martos, Y. M., & Soto, J. (2018). Gravity and magnetic anomalies of Ecuadorian margin: Implications in the deep structure of the subduction of Nazca Plate and Andes Cordillera. Journal of South American Earth Sciences, 85, 68–80. https://doi.org/10.1016/j.jsames.2018.04.020

Tejada, F., Rothis, M., Onorato, M. R., Blanc, P. A., Perucca, L., Audemard-M, F. A., & Vargas, N. (2021). Neotectonic and paleoseismic analysis of the Loma Negra Oriental fault, orogenic front of the Central Precordillera, Argentina. *Boletin de La Sociedad Geológica Mexicana*, *73*(2), 1–21. https://doi.org/10.18268/BSGM2021v73n2a080121

Topal, S & Özkul, M. (2014). Soft-sediment deformation structures interpreted as seismites in the kolankaya formation, Denizli basin (SW Turkey). *The Scientific World Journal*, *2014*. https://doi.org/10.1155/2014/352654

Torrent, J., Schwertmann, U., Fechter, H., & Alferez, F. (1983). Quantitative relationships between soil color and hematite content. *Soil Science*, *136*(6), 354–358.

Trenkamp, R., Kellogg, J. N., Freymueller, J. T., & Mora, H. P. (2002). Wide plate margin deformation, Southern Central America and Northwestern South America, CASA GPS observations. Journal of South American Earth Sciences, 15(2), 157–171. https://doi.org/10.1016/S0895-9811(02)00018-4

Tschopp, H.J., (1953). Oil explorations in the Oriente of Ecuador, 1938-1950. AAPG (Am. Assoc. Pet. Geol.) Bulletin. 37 (10), 2303–2347. https://doi.org/10.1306/5CEADD94- 16BB-11D7-8645000102C1865D.

Truswell, J.F., 1972. Sandstone sheets and related intrusions from Coffee Bay, South Africa. Journal of Sedimentary Research, 42, 578e583.

Turcotte, D. L., & Schubert, G. (2014). Geodynamics. Cambridge University Press.

Van Loon, A. J. & Brodzikowski, K. (1987). Problems and progress in the research on soft-sediment deformations. *Sedimentary Geology*, *50*(1–3), 167–193. https://doi.org/10.1016/0037-0738(87)90032-7

Wells, D. L. & Coppersmith, K. J. (1994). New empirical relationships among magnitude, rupture length, rupture width, rupture área, and surface displacement. *Bulletin - Seismological Society of America*, *84*(4), 974–1002. https://doi.org/10.1785/bssa0840040974

Wesnousky, S. G. (2008). Displacement and geometrical characteristics of earthquake surface rupture: Issues and implications for seismic-hazard analysis and the process of earthquake rupture.

Bulletin of the Seismological Society of America, *98*(4), 1609–1632. https://doi.org/10.1785/0120070111

Yeats, R. S., Sieh, K. y Allen, C. R. (1997). The geology of earthquakes. Oxford University Press. https://books.google.com.ec/books?id=_8bNwAEACAAJ

Yepes, H., Chatelain, J. L., Guillier, B., Alvarado, A., Egred, J., Ruiz, M., & Segovia, M. (1996). The Mw 6.8 Macas earthquake in the sub-Andean zone of Ecuador, October 3, 1995. Seismological Research Letters, 67(6), 27-32.

Yepes, H., Audin, L., Alvarado, A., Beauval, C., Aguilar, J., Font, Y., & Cotton, F. (2016). A new view for the geodynamics of Ecuador: Implication in seismogenic source definition and seismic hazard assessment. Tectonics, 35(5), 1249–1279. https://doi.org/10.1002/2015TC003941

ANEXO A: Resúmenes extendidos presentados en el Congreso Internacional REDU, desarrollado en Universidad Regional Amazónica IKIAM

CARTOGRAFÍA DE LA FALLA POROTOYACU EN EL BARRIO LAS VERÓNICAS: RESULTADOS PRELIMINARES

Henry Conteron [1*], Samira Lluno [1*], Corina Campos[2], Oswaldo Guzmán[2] **y** Anderson Guamán[3]

[1]Universidad Regional Amazónica Ikiam, Parroquia Muyuna, Kilómetro 7 vía a Alto Tena, s/n, Tena, Napo, Ecuador. Conteron86@gmail.com

[2]Grupo de investigación en Ciencias de la Tierra y Clima. Universidad Regional Amazónica Ikiam, Ecuador.

[3]Laboratorio de Geociencias. Universidad Regional Amazónica Ikiam, Parroquia Muyuna, Kilómetro 7 vía a Alto Tena, s/n, Tena, Napo, Ecuador

Resumen

En la zona oriental de Ecuador existe un sistema de fallas denominado Cutucú-Napo, donde se encuentra la falla denominada "Porotoyacu", que con 15 km de extensión atraviesa las ciudades de Tena y Archidona de la provincia de Napo. Estudios previos, a escala regional, han postulado cinemática transcurrente inversa para esta falla, pero el detalle geométrico de la estructura y el cartografiado detallado de la misma es desconocido, por lo que la amenaza que puede representar no ha sido completamente comprendida. Entonces, para abordar esta problemática, se está realizando un estudio con el objetivo de cartografiar la superficie y el subsuelo de la falla a nivel local y regional. Este estudio se está llevando a cabo en una sección específica de la falla Porotoyacu, ubicada en el barrio Las Verónicas. La investigación comenzó con la aplicación de fotogrametría aérea para crear un modelo digital de elevación de alta resolución del área de estudio. Posteriormente, se desarrolló un diseño sísmico y se aplicó la técnica de tomografía sísmica. Actualmente, los datos adquiridos a través de la tomografía sísmica están siendo procesados y analizados para obtener una imagen detallada de la estructura interna de la Tierra. En los próximos meses, se analizarán imágenes satelitales y modelos digitales de elevación a diferentes escalas (30 cm y 30 m). Este estudio promete proporcionar información valiosa sobre el estado actual de la falla Porotoyacu y sus implicaciones para la seguridad geológica.

Palabras clave: Falla Porotoyacu, Actividad sísmica, Tomografía sísmica, Cartografía, fotogrametría



ESTUDIO PALEOSISMOLOGICO DE LA FALLA POROTOYACU EN UNA AFLORAMIENTO DEL BARRIO "LAS VERÓNICAS": RESULTADOS PRELIMINARES

Samira Lluno [1*], Henry Conteron[1], Oswaldo Guzmán[2], Corina Campos[2], Anderson Guamán[3],

[1]Universidad Regional Amazónica Ikiam, Parroquia Muyuna, Kilómetro 7 vía a Alto Tena, s/n, Tena, Napo, Ecuador.

[2]Grupo de investigación en Ciencias de la Tierra y Clima. Universidad Regional Amazónica Ikiam, Tena, Ecuador. (Bhattacharya & Bandyopadhyay, 1998)

[3]Laboratorio de Geociencias. Universidad Regional Amazónica Ikiam, Parroquia Muyuna, Kilómetro 7 vía a Alto Tena, s/n, Tena, Napo, Ecuador

*Autor de correspondencia: samira.lluno@est.ikiam.edu.ec

Resumen

La Falla Porotoyacu se extiende por más de 15 km y atraviesa las ciudades de Tena y Archidona. A pesar de la cartografía, a escala regional de la falla, y la actividad símica instrumental de la misma, la amenaza que representa esta falla es en gran medida desconocida. En un esfuerzo por contribuir a su conocimiento, se está llevando a cabo un estudio paleosismológico en el sector del barrio Las Verónicas, ubicado al norte de la falla. En este contexto, se ha identificado un posible escarpe de falla, donde se ha realizado un corte antrópico que deja expuestas ciertas características de deformación en los estratos. El estudio se está desarrollando en varias etapas. Inicialmente, se identificó un afloramiento en el cual se lograron definir 9 unidades estratigráficas principales, donde se realizó un mallado de 1x1 metro a lo largo y ancho. Posteriormente, se procedió a un reconocimiento y delimitación detallada de todas las unidades y estructuras de deformación presentes, utilizando marcadores de referencia (tachuelas). Esto sirvió como base para la creación de representaciones gráficas minuciosas del afloramiento en hojas milimétricas. Reconociendo las deformaciones y geometrías presentes, se logró identificar zonas con diferentes evidencias sísmicas, como espejos de falla, saltos de falla, rupturas y desniveles a lo largo de los estratos. Finalmente, este proyecto resalta la importancia de la investigación geológica y paleosismológia en la identificación y comprensión de fallas geológicas, y subraya la necesidad continua de realizar estudios de este tipo para garantizar la seguridad de las comunidades en regiones

propensas a eventos sísmicos. Adicionalmente, se espera realizar un levantamiento topográfico de alta resolución, a escala milimétrica, y adquirir datos de símica de refracción, los cuales se utilizarán para definir la geometría en superficie y subsuelo de la falla.

Palabras clave: Falla Porotoyacu, Paleosismólogia, afloramiento, escarpe de falla, mallado, unidades estratigráficas, espejos de falla, saltos de falla.

ANEXO B: Resúmenes extendidos presentados en el Congreso Internacional PATAdays desarrollado en Chile

CARTOGRAPHY OF THE POROTOYACU FAULT IN A SOUTHERN SECTION OF THE ECUADORIAN AMAZON

Henry Conteron [1]
Samira Lluno [1]
Oswaldo Guzmán [2]
Sebastián Araujo [2]
Corina Campos [2]
Bryan Valencia [2]
Anderson Guamán [3]
Juan Villacrés [1]

[1] Universidad Regional Amazónica Ikiam, Tena, Napo, Ecuador

[2] Earth Sciences and Climate Research Group, Universidad Regional Amazónica Ikiam, Ecuador

[3] Geosciences Laboratory, Universidad Regional Amazónica Ikiam, Parroquia Muyuna, Napo, Ecuador

*Email: Conteron86@gmail.com

ABSTRACT

This study employs aerial photogrammetry followed by seismic tomography to achieve a detailed mapping of the Porotoyacu fault in the Ecuadorian Amazon. The study area, located south of the fault, covers 0.388 km². Initially, a high-resolution digital elevation model (22 cm/pixel) was used for detailed surface mapping. Subsequently, the fault geometry was identified at depth using seismostratigraphic and structural analysis of a 69-meter seismic profile extending to 25 meters deep. The results reveal that: 1) The fault trace extends in a north-south direction. 2) The Porotoyacu fault has an inverse geometry with a steep angle near the surface that flattens at depth. And, 3) The slope observed corresponds to the flank of an anticline.

KEY WORDS

Porotoyacu Fault, Seismic activity, Seismic tomography, Cartography, photogrammetry

INTRODUCTION

Seismicity in Ecuador is controlled by the subduction zone of the Nazca plate with the South American plates and the responsible faults are poorly known (fig. 1A) (Chunga et al., 2016). Ecuador has approximately 92 active surface faults (Eguez et al., 2003; Costa et al., 2020). These geological structures are part of several fault systems, among which the Napo-Cutucú fault System stands out. Located in the Eastern Sub-Andean Belt of Ecuador, this fault system represents a geological feature of the region. It is active throughout the northern Amazon region (Bès de Berc, 2003). Within this fault system is the Porotoyacu fault, an active surface structure. This fault has an approximate extension of 15 km crossing the Tena city, and a transcurrent-inverse kinematics (fig.

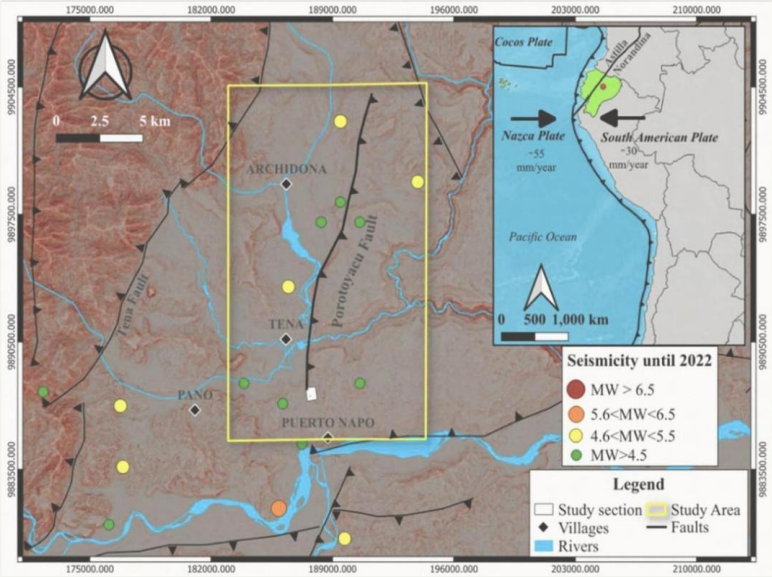

1B) (Costa et al., 2020). Evidence and ruptures associated with a specific fault have been conducted in a trench south of Tena. These findings, displaying SSE and SSW orientations, are directly linked to the Porotoyacu fault (Cornejo, 2020). This study aims to cartograph the Porotoyacu fault on a local scale and determine its subsurface geometry in a southern section of the Porotoyacu fault by employing aerial photogrammetry and seismic refraction tomography (Vp wave). This section is located in the vicinity of the fault trace and shows possible deformations (fig. 2A).

Fig. 1: Location of the study area (A) Geodynamics of Ecuador. The green polygon represents Ecuador within the broader geodynamic context of South America, where the Nazca Plate subducts beneath (Hasterok et al., 2022). The study area is delineated by a red dot. (B) Map of the Porotoyacu Fault. The topography of the study area is depicted on a Red Relief Image Map (RRIM), a technique developed by Chiba & Hasi (2016) using a Digital Elevation Model (DEM) from ALOS PALSAR DEM. The fault trace provided by the SARA Project is visible as a black line (Adapted from Costa et al., 2020). The Porotoyacu Fault area is highlighted within a yellow rectangle, while the white rectangle represents the specific study section where the proposed methodologies were performed. The colored dots indicate the seismic activity until 2022, classified by magnitude (MW) (IGPN, 2022).

METHODS

PHOTOGRAMMETRY: This process covered an area of 0.388 km² (fig. 3A) using a DJI Phantom 4 RTK drone. Due to limited equipment limitations, control points were not used in this study. The photogrammetric process was carried out using Agisoft Metashape software. A total of 432 images were processed, of which 429 were correctly oriented. A rotation angle of yaw, pitch, and roll was applied. for orientation, maximum precision was used and a generic preselection was applied. Stationary tie points were not excluded and guided matching was not used. Depth maps were generated using low-quality parameters and moderate filtering due to the capacity of the equipment. In addition, a dense point cloud was created with 8,892,697 points. for the classification of terrain points, a maximum angle of 7 degrees, a maximum distance of 0.1 m, and a cell size of 25 m were established (figure 3B). finally, a Digital Elevation Model (DEM) was generated with a size of 3,904 x 4,487 using the dense point cloud as the data source (fig. 2A).

SEISMIC TOMOGRAPHY: The survey collected data in the study area by following a slope with a 7-degree inclination (fig. 2A). 25 geophones were placed along a 70-meter seismic line, each at a distance of 3 meters and an approximate depth of 5 cm (fig. 2B). The geophones used had a frequency of 4.5 Hz and use a sampling time of 0.250 ms. We fired 25 shots at 3-meter intervals between geophones using the Geometrics ES-300 equipment. This seismic line was denoted AB. The seismic data was processed using modules from the Seisimager software. Initially, the Pickwin module was employed to visualize the initial signals recorded by the seismograph and to generate curves known as dromochrones through manual data selection (fig. 4A).

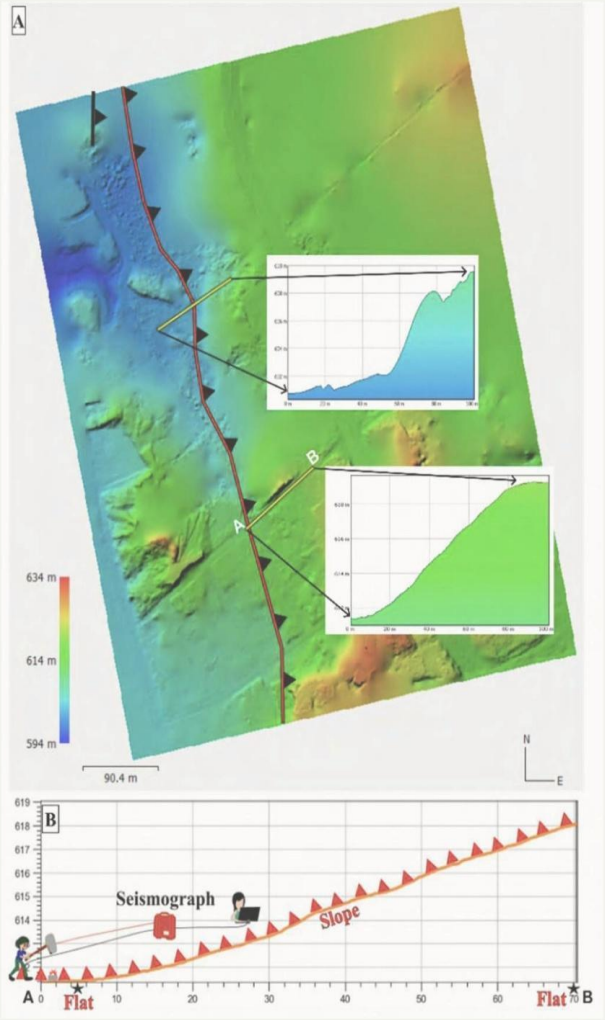

Fig. 2: Study Area. The Digital Elevation Model (DEM) illustrates elevation variations across the terrain, using a color gradient from dark blue (lower elevations) to red (higher elevations). The red line represents the trace of the Porotoyacu Fault identified in this study, while the black line indicates the fault trace proposed by the SARA Project. Insets show two topographic profiles that capture changes in elevation along the fault line, with red arrows denoting where the fault trace intersects the profiles. B) Seismic Line AB Design. This panel shows a schematic representation of the seismic line AB on the ground, laid out along a topographic profile. The red triangles symbolize the distribution of geophones along the seismic line, while the black stars mark the start and end points of the slope.



Fig. 3: Photogrammetric Analysis. A) Flight Zone. The area selected by the morphological expression of the fault. An important aspect to consider is that the density of vegetation in this area can affect the accuracy of the Digital Elevation Model (DEM). A red line representing seismic line AB was recorded. B) Classification of the point cloud. Obtained through photogrammetric processing using Agisoft Metashape software. Brown dots represent terrain, green dots indicate different levels of vegetation, and red dots indicate built structures such as houses and buildings.

Subsequently, the Plotrefa module was used to create a plot of the dromochrones and define the parameters of the a priori model (fig. 4B). Once the a priori model was obtained, tomographic inversion tests were performed. Octave software was used to confirm the final optimal tomographic model. (Araujo et al., 2023). Using matrix operations, data conversion was performed, facilitating the creation of the convergence plot (fig. 5B) and the regularization of the L-curve (fig. 5A). finally, the Geoplot module was used to visualize the seismic profile. We adjusted the corresponding parameters to optimize the visualization, resulting in a clearer and more detailed representation of the seismic data.

Fig. 4: Refraction seismic tomography process. A) Pickwin module. For example, in a shot for a seismic line of the experiment, the source indicates the position of each shot on the distance scale. Distance is plotted on the x-axis, while time is plotted on the y-axis. B) Plotrefa module. Illustrates the initial seismic tomography model with 10 layers, showing velocity variations from 0.3 km/sec at the surface to 2.5 km/sec at a depth of 25 meters over a depth range of 25 meters. The different colored dots represent the location of the geophones.

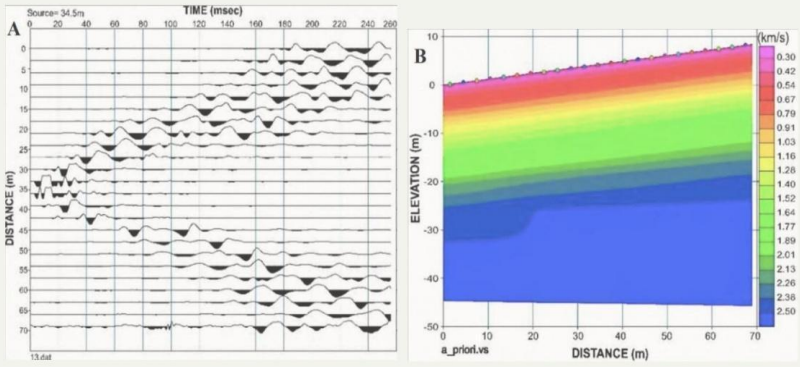

RESULTS

PHOTOGRAMMETRY: The Digital Elevation Model (DEM) obtained (figure 2A) reveals areas with notable elevation changes, starting at an average of 607 meters and reaching 620 meters within less than 100 meters, forming a slope with an approximately 7-degree inclination and a southwest orientation on average. Perpendicular topographic lines drawn across these changes depict an anticlinal feature, originating from compressive forces. Based on this observation, the Porotoyacu fault was traced in the DEM, spanning 700 meters in length. It exhibits non-linearity as it cuts through the area where residential structures are situated.

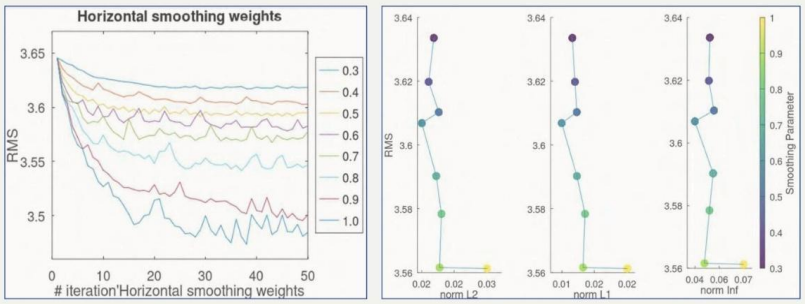

Fig. 5: Regularization process. A) L-Curve. It is based on the mean square error (RMS) and includes a vertical smoothing of 1 and a horizontal smoothing that varies from 0.3 to 1.0 for each line. 50 iterations were performed to obtain the optimal model. This process indicates that all start from the same value, so the final selected model is correct. B) The RMS convergence. It is displayed on the vertical axis, while the L2, L1, and Infinity norms are represented on the horizontal axis. These norms are used to adjust the optimal velocity model, based on the data observed in seismic refraction. It is worth noting that this model is inferred from the horizontal smoothing parameters, as indicated at the inflection point for AB at 0. 9 represented by black arrows.

SEISMIC TOMOGRAPHY: The seismic profile (fig. 6) shows that the seismostratigraphic units exhibit a coherent deformation pattern, suggesting that identical events and structural elements are responsible for deformation in all units. In the southwestern (SW) part of the seismic profile, the structures exhibit a concave-down geometry in the regions where deformation is most pronounced. Interestingly, the axial lines of these concavities are not vertically aligned between units. This unique deformation configuration is interpreted to be caused by faulting. In this context, a main fault has been identified, referred to as the Porotoyacu. This fault exhibits a reverse regimen and presents a notable characteristic: its angle intensifies starting from -16 meters in depth. In parallel, an antithetic fault has been detected. Unlike the Porotoyacu fault, this fault exhibits a normal régimen.

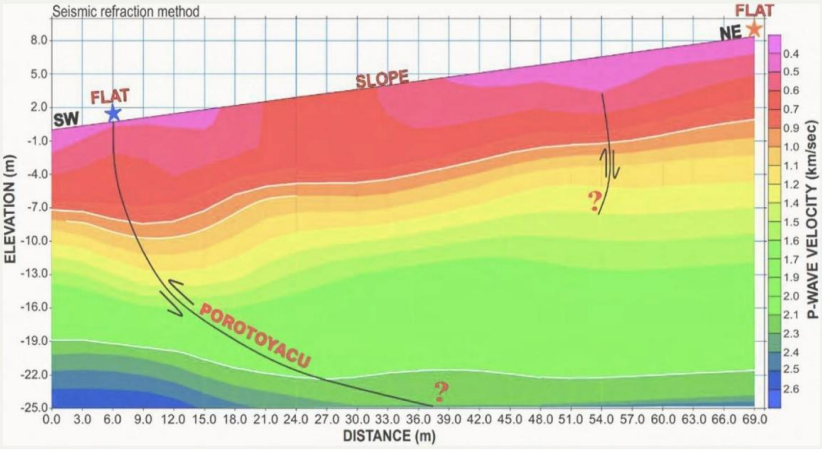

Fig. 6: Seismic refraction tomography. The 69-meter SW-NE seismic profile was obtained with a root mean square error (RMSE) of 3.50 ms. The black lines represent the Porotoyacu Fault and the antithetic fault. The white lines drawn along the profile denote deformations in all the seismostratigraphic units, which are represented by a color palette symbolizing the P-wave velocity (Vp). In addition, the blue star marks the beginning of the slope and the location of the surface fault trace.

CONCLUSIONS

The Digital Elevation Model (DEM) shows that the Porotoyacu fault trace extends in a north-south direction, intersecting the subsurface area where it was detected. Seismic tomography data further indicate that the fault hasa reverse geometry, characterized by a steep angle at the surface that gradually transitions to a low angle at depth. This westward-verging fault, which is opposed to the typical eastward tectonic transport observed in Ecuador, is identified as a Backthrust. Additionally, the seismic profile indicates that the slope corresponds to the flank of an anticline.

ACKNOWLEDGEMENTS

This study results from the research project CTC-006-2020 and OLLIN IGCP 669. I express my deep gratitude for their invaluable support. I want to express my sincere thanks to the Amazonian Regional University Ikiam for its contribution. My appreciation goes to the community of Las Verónicas, for their generosity in allowing the use of the area for the realization of this study. finally, I would like to thank my parents, whose unconditional support regarding mobility

REFERENCES

Araujo, S., Guzmán, O., Guamán, A., Espín, R., García, F., & Chulde, E. (2023). Seismic refraction tomography in San Luis, headward Coca River erosion zone. Journal Of Applied Geophysics, 212, 104981. https://doi.org/10.1016/j.jappgeo.2023.104981

Bès de Berc, S., Baby, P., Soula, J., Rosero, J., Souris, M., Christophoul, F., & Vega, J. (2004). The Mera-Upano Surface: Geomorphological Marker of Fluvial Incision and Tectonic Uplift in the Ecuadorian Sub-Andean Zone. Institut Français d'Études Andines. https://doi.org/10.4000/books.ifea.3009

Cornejo Bazurto, E.C. (2022). Analysis of Seismites and Paleoseismology as Indicators of the Magnitudes of Seismic Activity of the Santa Rosa Fault in the Amazonian Piedmont, Ecuador. Regional Amazonian University IKiam.

Costa, C., Alvarado, A., Audemard, F., Audin, L., Benavente, C., Bezerra, F.H., Cembrano, J., González, G., López, M., Minaya, E., Santibañez, I., Garcia, J., Arcila, M., Pagani, M., Pérez, I., Delgado, F., Paolini, M., Garro, H. (2020). Hazardous faults of South America; compilation and overview. Journal of South American Earth Sciences, 104, 102837. doi: 10.1016/j.jsames.2020.102837

Chiba, T., & Hasi, B. (2016). Ground surface visualization using red relief image map for a variety of map scales. ISPRS - International Archives of the Photogrammetry, Remote Sensing and Spatial Information Sciences, 393- 397.

Chunga, K., Quiñónez, M., Huaman, F., Besenzon, D., Mulas, M., Garcés, D., Larreta, E., Gorshkov, A., & Michetti, A. (2016). Earthquake and Tsunami Geology. 1st ed. Quito. Eguez, A., Alvarado, A., Yepes, H., Machette, M.N., Costa, C., Dart, R.L., Bradley, L. (2003). Database and map of Quaternary faults and folds of Ecuador and its offshore regions. US Geological Survey OpenFile Report, 03-289, 3, 289.

Hasterok, D., Halpin, J., Hand, M., Collins, A., Kreemer, C., Gard, M.G., Glorie, S., (2022) New maps of global geologic provinces and tectonic plates, Earth Science Reviews. Preprint available (EarthArXiv) https://doi.org/10.31223/X5TD1C

Instituto Geofísico de la Escuela Politécnica Nacional (IGEPN). (2024, June 10). Seismic Catalog 2012-Present. Geophysical Institute - EPN. Retrieved from http://www.igepn.edu.ec

PALEOSEISMOLOGICAL STUDY OF THE POROTOYACU FAULT IN THE AMAZON ECUADORIAN PIEDMONT

Samira Lluno [1]
Henry Conteron [1]
Oswaldo Guzmán [2]
Corina Campos [2]
Carolina Cornejo [3]

[1] Universidad Regional Amazónica Ikiam, Parroquia Muyuna, Kilometer 7 via Alto Tena, s/n, Tena, Napo, Ecuador. Email:

[2] Earth Sciences and Climate Research Group. Universidad Regional Amazónica Ikiam, Tena, Ecuador

[3] Universidad Técnica de Manabí. Maestría en Prevención y Gestión de Riesgos de la Facultad de posgrado de la Universidad Técnica de Manabí. Portoviejo, Ecuador.

*Email: samira.lluno@est.ikiam.edu.ec

ABSTRACT

The tectonics activity in the Amazon has not been studied in depth. An example of this is the Porotoyacu fault through populations in the Amazon region. A paleoseismological study is being carried out in the south of the city of Tena. To decipher the paleoseismicity engraved in outcrop i.e. calculate the number and magnitude of seismic events and identify the structure of deformation or seismites. On the outcrop have recognized two paleo-ruptures. The first with normal kinematics with two events with magnitudes between Mw~6.7 and 6.8 and surface wave magnitude of Ms=6.9. The second is reverse with an only event of magnitude 613<Mw<6.52 and Ms=6.24. In addition, between the structure of deformation identify their load cast, flame structures, dikes, and pseudonodules originating from earthquake M>5. finally, these deformation structures in the overlying units indicate direct geologic evidence of Quaternary seismic activity of the Porotoyacu fault.

KEY WORDS
Porotoyacu Fault, Paleoseismology, outcrop, seismites, magnitude

INTRODUCTION

Ecuador is in a tectonic active regimen by the convergent of the Nazca plate and Sudamericana plate. Resulting in 92 Quaternary faults identified as superficial with aerial photographs in the map of the quaternary fault of Ecuador (Eguez, et al., 2003). Despite this, earthquakes are generally of magnitude 4.5 or lower at the Ecuador (IG-EPN, 2024). But existing registrations of atypical events with □□ > 6 located in Napo province (Council, 1991) implying that high seismic events may occur in the Amazonia. Another example is the study by (Baby, Rivadeneira, & Barragán, 2004) in 1995 that registered an earthquake □□ = 7.0 correlated to the system of faults Cutucú-Napo.

The system Cutucú-Napo is part of the Oriente Basin, and it's formed by the uplift of Napo to NO and the mountain range Cutucú to SO (Baby, Rivadeneira, & Barragán, 2004). This study also states that the surface structures of the Cutucú- Napo system are inverted normal to reverse faults. Until 2020, the study of South America Risk Assessment Project (SARA) (Costa, et al., 2020) establishing the presence of the Porotoyacu fault as part of a system of faults Cutucú-Napo.

In addition to knowing the location of the trace of Porotoyacu fault through the city of Tena and Archidona figure. 1) there is no more precise information about its seismic activity. Therefore, to study seismic activity use Paleoseismology such as the study of prehistoric earthquakes by the number of events and their magnitude engraved in the stratigraphy geological (McCalpin & Nelson, 2009). In conjunction with the identification of structures of deformation or seismites are product of the liquefaction (Masana, Rodrigues-Pascua, & Martinez-Diaz, 2011) mainly allows us to interpret the magnitude of seismic events.

Fig. 1: Ubication of the study area: A) Regional location of the study area: In the Ecuadorian territory base map from ESRI. The red line in the limit represents the contact of Nazca and South America plates. The numerous red lines represent geologic faults that cross the country. The green rectangle delimits the study area. B) Ubication of study are in Napo Province (DEM-Geoportal): The blue star represents the outcrop where the paleoseismological study is performed. The big red line in the center represents the Porotoyacu Fault with its kinematics of Project SARA (Costa, et al., 2020), the black circles represent the cities. The map was made with arc map tools.

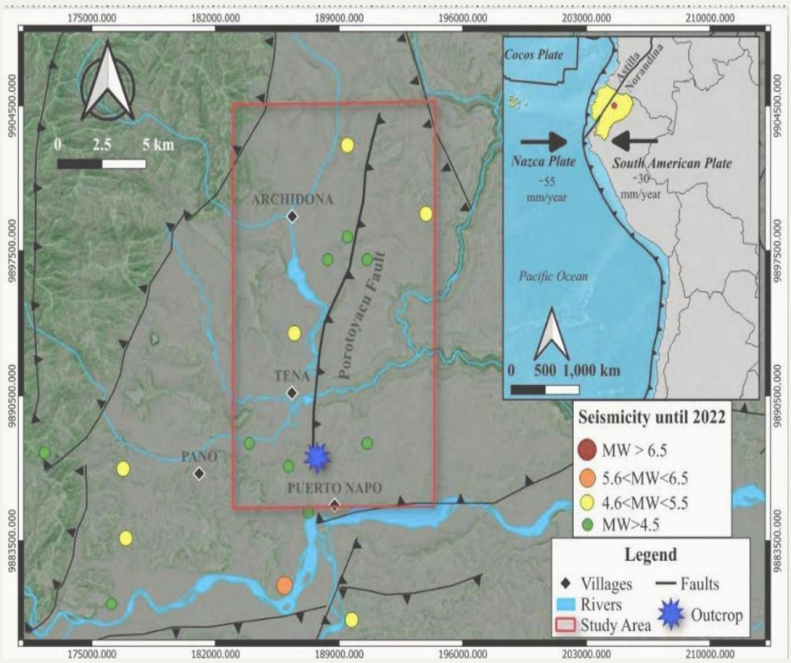

The paleoseismological studies in Ecuador have been focused on the Ecuadorian Sierra, as in the case of the Pallatanga fault (Baize, et al., 2015) study where have been excavated various trenches through of lengths of the trace to extract more information about the behavior of this fault. On the other hand, the Amazonia in Ecuador only has one paleoseismological study realized by (Cornejo, 2022) about the Porotoyacu fault in another outcrop located South of the trace.

Approximately 24 seismic events with M 2.5~6.3 detected instrumentally between 1927-2022 have been reported in the study area (IGEPN, 2022) representing mild to moderate seismicity.

The objectives of this work are to provide information and understand the geological threat posed by the Porotoyacu fault. It is necessary to relate all the seismic events possibly recorded in the geologic record with their respective magnitude and identification of structures of deformation that could be evidence of recent tectonic activity of the Porotoyacu fault. for this reason, a paleoseismological study was carried out in an outcrop located 0.43 Km from north of the fault trace (figure. 1).

Geomorphology of the site

The study site has identified a possible scarp fault (>70 m) with direction SW-NE (figure 2) that coincides with the SSW-NE regional orientation of the Porotoyacu fault. In field is observed an unevenness of 7° of inclination between two plain surfaces with elevation of 609 m in the initial point (Ip), the scarp fault (Sf) with 611 m and final point (fp) 615 m, this type of topographic deformation is direct evidence of vertical displacement of Porotoyacu fault by seismicity. this topographic anomaly repeats itself several kilometers beyond the study site, ruling out anthropogenic with the help of orthophotographs a possible trace is established as shown in (figure 2). Also, to confirm the presence of the fault there is an outcrop that exposes various characteristics of the deformation, such as displacement between layers, fault mirrors or rupture planes with stretch marks, etc. All these characteristics could be related to the presence of the Porotoyacu fault.



Fig. 2: Possible fault scarp market with the red line and green box pointed to the outcrop next to the fault scarp. The black line is trace of Porotoyacu fault that produce this geomorphological indicator. The arrows point to raised and depressed side.

REFERENCES

Allen, J. (1982). Sedimentary Structures. Elsevier, 1-633. Audermand, F., & Santis, F. (1991). Survey of Liquefaction Structures Induced by Recent Moderate Earthquakes. Bulletin, 5-16. doi:10.1007/BF02602705

Baby, P., Rivadeneira, M., & Barragán, R. (2004). La cuenca Oriente: Geologia y Petroleo. (I. IFEA, Ed.) Travaux de l'Institut Français d'Etudes Andines.

Baize, S., Audin, L., Winter, T., Alvarado, A., Pilatasig, L., Taipe, M., . . . Yepes, H. (2015). Paleoseismology and tectonic geomorphology of the Pallatanga fault (Central Ecuador), a major structure of the South American crust, Elsevier, 237, 14-28.

Cornejo, C. (2020). Analisis de sismitas y paleosismologia como indicadores de amgnitudes de la actividad sismica de la falla Santa Rosa, en el piedemonte amazonico, Ecuador. Universidad Amazonica Ikiam, Tena.

Costa, C., Alvarado, A., Audermand, F., Audin, L., Benavente, C., Bezerra, H., Perez, I. (2020). Hazardous faults

of South America; compilation and overview. Journal of South American Earth Sciences, Volume 104, 102837. Obtenido de https://doi.org/10.1016/j.jsames.2020.102837.

Council, N. R. (1991). The March 5, 1987, Ecuador earthquakes: Mass wasting and socioeconomic effects. Ecuador: National Academic Express.

Eguez, A., Alvarado, A., Yepes, H., Machette, M., Costa, C., & Dart, R. (2003). Database and Map of Quaternary faults and folds of Ecuador and its offshore regions. USGS, Volumen 104. doi:10.3133/ofr03289

RESULT / DISCUSS

In the study zone, has been identifying paleo- ruptures in two zones of outcrop and various structures of deformation interpreted as seismites. for this reason, be calculated the events determined with vertical displacement obtained in each rupture as used in the formulas by (Wells & Coppersmith, 1994), (Bonilla, Mark, & Lienkaemper, 1884) .

Paleo-rupture with their events and magnitudes

With the observation in field, has been identify two mainly ruptures (figures 3,4) where has estimated the surface wave magnitude(M_s) and magnitude moment (M_w). In he first rupture (R1) has been identify two events with vertical displacement of 0.70 m in the U3 and other with 1.46 affect U1-U2. The last result is the accumulated, then, really this event has a vertical displacement of 0.76 m. To the second rupture (R2) find only an event with a vertical displacement of 0.11 m in the U6-U7. In addition, R1 has a kinematics normal and R2 kinematics reverse. Thus, has been calculated the moment magnitude with the proposal (Wells & Coppersmith, 1994) both to normal faults (N), reverse (R) and undefined faults (All) and the surface wave magnitude of Bonilla (1884).

To R1 with a scenario of normal type, we obtain a M_w = 6.91 and M_s = 6.70 by first event. To second event M_w = 6.88 and M_s = 6.68 . To R2 with the second scenario with reverse type faulting for the first and only event, we have a M_w = 6.24 and M_s = 6.51. finally, to undefined faults for the rupture 1 (R1) we calculated a magnitude of 6.83 for first event and 6.80 for the second event. To rupture 2 (R2) we have a magnitude of 6.13 for the only event.

Fig.3: Photomosaic of outcrop, where are present various fault rupture planes and structures of deformation.

Fig.4: Digitalization of outcrop with stratigraphic units, rupture planes, seismites, the black points are structural data of rupture planes.



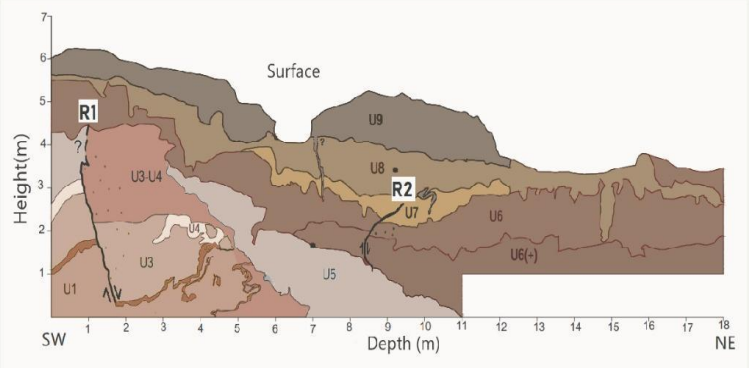

Seismites and estimated paleoseismic magnitude.

According to studies by (Shmuel & Amotz, 1995), (Audermand & Santis, 1991) seismic events with magnitude M>5 can generate processes like liquefaction and generatethe structure of deformation. The study site, consist in sedimentary deposits of claystone and siltstone, which allow the formation of ductile deformations such as the following.

Load cast: Generally, these structures are synform and are associated with antiforms (flame structure) such as (figure.5) where, penetration is visualized of overlying united (U7) to the underlying (U6) with concave shape (Geraint, 2003). This structure is present in various zones on the outcrop. The U7 consists of gravel with a siltstone matrix enter U6 with >10 cm of length.

Pseudonodules: The author (Allen, 1982) mentions in his article that this structure consists of isolated masses belonging united superior which is involved in the underlying. Pseudonodules are originated by the earthquake of M6.5 (Kuenen, 1958). Pseudonodules are present inside U1 with a length >12 cm and a height of 10 cm. Also, they are at the top of U5 with a diameter of 1 cm as shown in (figura.6 a) y b).

Fig. 5: Load cast and flame structure seismites observed between the top of U6 and base of U7.

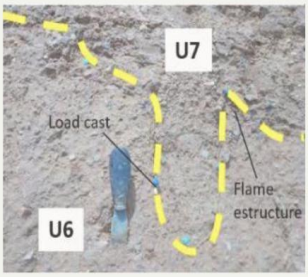

flame structure: Based on the study by (Topal & Özkul, 2014) are formed where the overlying sediments are depressing into underlying sediment and forming a flame-like structure. As mentioned above, these structures always are accompanied by load cast such as (figure. 5) in a field measuring approximately 5 cm in U7.

Dike: This type of structure has its origin in earthquakes of magnitude 5 to 8 (Audermand & Santis, 1991). Usually, the size of the dike is variable from 30 cm to 1 m (Topal & Özkul, 2014). The example in (figure 7) shows units formed by gravels with silty matrix that undergo a penetration process starting in U8, which cracks the lower unit (U6). forming a dike of more than 2 m in length.

Fig. 6: a) Pseudonodules seismites observed in U1. b) Pseudonodules seismites between the top U5 and base of U6.

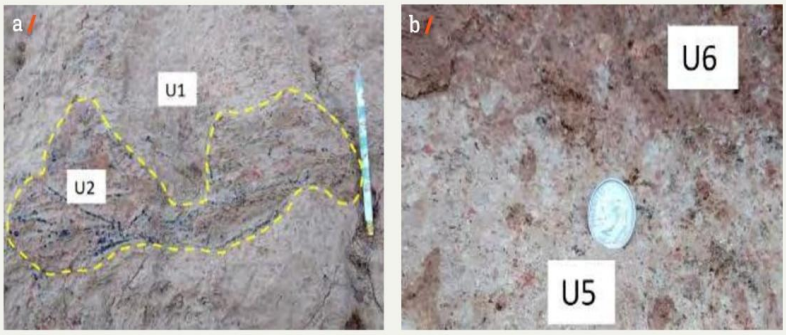

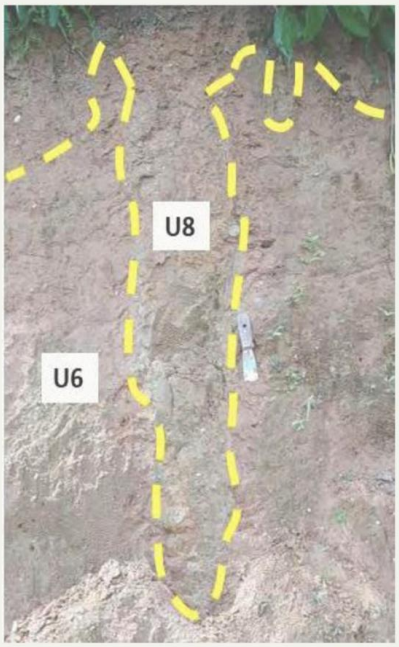

Fig.7: Dikes seismites observed between the top of unit 6 and the base of unit 8

CONCLUSION

The analysis in the field indicated SW and NE Orientations from the scarp fault reflecting the same orientation of the Porotoyacu fault. In the outcrop are observer kinematics normal (R1) and reverse (R2) faulting. The magnitude calculates to R1 and R2 (6.50< (6.50 < □□ < 6.70) and a (6.24 < □□ < 6.91) .These types of displacement indicated a magnitudes (Mw>5) showing liquefaction processes originated by ruptures. Despite the paleo-rupture planes in the stratigraphic units, they do not cut the superficial units but, the seismites as dykes, load cast belong to superficial units. Therefore, Porotoyacu is an active fault, as shown by this geological evidence produced in the Quaternary. It is estimated that these ruptures and seismites if they are related with the Porotoyacu fault.

ACKNOWLEDGMENTS

I am grateful to the CTC-006-2020 project of investigation and OLLIN IGCP 669 that supports my topic of thesis. and Tutors. To the University Ikiam by the support in my career and president of the Las Veronicas neighborhood that allows us to realize the study. To Congress PATAdays 2024 for the opportunity to share my knowledge. finally, thanks to Cornejo. C for their help and patience with the interpretation of seismites.

Geraint, O. (2003). Load structures: Gravity-driven sediment mobilization in the shallow subsurface. Geological Society Special Publications, Vol.216, 21-34. doi:10.1144/GSL.SP.2003.216.01.03

Kuenen, P. (1958). Experiments in Geology. Trans. Geol. Soc. of Glasgow, 1-37.

Masana, E., Rodrigues-Pascua, M., & Martinez-Diaz, J. (2011). Los paleoterremotos: estudiando el pasado para entender el futuro. Enseñanza de las Ciencias de la Tierra, 305'316.

McCalpin, J., & Nelson, A. (2009). Introduction to Paleoseismology (Vol. Vol.95). International Geophysics.

Shmuel, A., & Amotz, M. (1995). Prehistoric earthquake deformations near Masada, Dead Sea Graben. Geology, 695-698. doi:10.1130/0091-7613(1995)023<0695:PEDNMD>2. 3.CO;2

Topal, S., & Özkul, M. (2014). Soft-Sediment Deformation Structures Interpreted as Seismites in the Kolankaya Formation, Denizli Basin (SW Turkey). (K. Nemeth, Ed.) The Scientific World Journal, 13 pages.

Wells, D., & Coppersmith, K. (1994). New Empirical Relationships among Magnitude, Rupture Length, Rupture Width, Rupture Area, and Surface Displacement. Bulletin of the Seismological Society of America, Vol. 84(No. 4), 974-1002. Obtenido de